

1 Atmospheric methane: Comparison between methane's record in 2006-2022  
2 and during glacial terminations.

3

4

5 Euan G. Nisbet<sup>1</sup>, Martin R. Manning<sup>2</sup>, Ed J. Dlugokencky<sup>3</sup>, Sylvia Englund Michel<sup>4</sup>, Xin Lan<sup>3,5</sup>,  
6 Thomas Röckmann<sup>6</sup>, Hugo A.C. Denier van der Gon<sup>7</sup>, Jochen Schmitt<sup>8</sup>, Paul I. Palmer<sup>9</sup>,  
7 Michael N. Dyonisius<sup>10</sup>, Youmi Oh<sup>3</sup>, Rebecca E. Fisher<sup>1</sup>, David Lowry<sup>1</sup>, James L. France<sup>1,11</sup>,  
8 James W.C. White<sup>12</sup>, Gordon Brailsford<sup>13</sup>, Tony Bromley<sup>13</sup>.

9

10 1. Dept. of Earth Science, Royal Holloway, Univ. of London, United Kingdom

11 2. School of Geography, Environment and Earth Sciences, Victoria Univ. of Wellington, New Zealand.

12 3. NOAA Global Monitoring Laboratory, 325 Broadway, Boulder CO 80305-3328, USA

13 4. Institute of Arctic and Alpine Research, University of Colorado Boulder, USA

14 5. Cooperative Institute for Research in Environmental Sciences, University of Colorado Boulder, USA.

15 6. Institute for Marine and Atmospheric research Utrecht (IMAU), Utrecht University, 3584 CC Utrecht, The  
16 Netherlands.

17 7. TNO, Department of Climate, Air and Sustainability, Utrecht, the Netherlands

18 8. Climate and Environmental Physics and Oeschger Centre for Climate Change Research, University of Bern,  
19 3012 Bern, Switzerland.

20 9. School of GeoSciences, Univ. of Edinburgh, United Kingdom

21 10. Physics of Ice, Climate and Earth, Niels Bohr Institute, 2200 Copenhagen, Denmark.

22 11. Environmental Defense Fund, 41 Eastcheap, London, United Kingdom

23 12. College of Arts and Sciences, University of North Carolina, Chapel Hill, NC, USA.

24 13. National Institute of Water & Atmospheric Research Ltd (NIWA), 301 Evans Bay Parade Hataitai Wellington  
25 New Zealand

26

27 Corresponding author: Euan Nisbet ([e.nisbet@rhul.ac.uk](mailto:e.nisbet@rhul.ac.uk))

28

29

30 *The air is getting hotter. There's a rumbling in the skies.*

31 *I've been wading through the high muddy water, With the heat rising in my eyes.*

32 Bob Dylan: Trying to get to Heaven before they close the door.

33

34 **Key points**

35 The rapid growth in the atmospheric methane burden that began in late 2006 is very  
36 different from methane's past observational record. Recent studies point to strongly  
37 increased emissions from wetlands, especially in the tropics. This increase is comparable in  
38 scale and speed to glacial/interglacial terminations when the global climate system suddenly  
39 reorganised.

40

41

## 42 **Abstract**

43 Atmospheric methane's rapid growth from late 2006 is unprecedented in the observational  
44 record. Analyses of atmospheric methane data attribute a large fraction of this atmospheric  
45 growth to increased natural emissions over the tropics, which appear to be responding to  
46 changes in anthropogenic climate forcing. Isotopically lighter measurements of  $\delta^{13}\text{C}_{\text{CH}_4}$  are  
47 consistent with the recent atmospheric methane growth being mainly driven by an increase  
48 in emissions from microbial sources, particularly wetlands. The global methane budget is  
49 currently in disequilibrium and new inputs are as yet poorly quantified. Although microbial  
50 emissions from agriculture and waste sources have increased between 2006-2022 by  
51 perhaps 35-40 Tg/yr, approximately another 35-45 Tg/yr of the recent net growth in  
52 methane emissions may have been driven by natural biogenic processes, especially wetland  
53 feedbacks to climate change. A model comparison shows that recent changes may be  
54 comparable or greater in scale and speed than methane's growth and isotopic shift during  
55 past glacial/interglacial termination events. It remains possible that methane's current  
56 growth is within the range of Holocene variability, but it is also possible that methane's  
57 recent growth and isotopic shift may indicate a large-scale reorganisation of the natural  
58 climate and biosphere is under way.

59

## 60 **Plain language summary**

61 Atmospheric methane's unprecedented current growth, which in part may be driven by  
62 surging wetland emissions, has strong similarities to ice core methane records during glacial-  
63 interglacial 'termination' events during global reorganisations of the planetary climate  
64 system. Here we compare current and termination-event methane records to test the  
65 hypothesis that a termination-scale change may currently be in progress.

66

## 67 **Keywords**

68 Atmospheric methane growth driven by biogenic sources. Sudden global climate change.  
69 Glacial/interglacial comparison.

70

## 71 **Main Text**

72

### 73 **1. Introduction**

74 In the past, rapid changes in atmospheric methane have signalled rapid global climate shifts.  
75 Does atmospheric methane's recent growth, sustained from the end of 2006 through 2022  
76 and continuing, similarly signal a major global climate shift?

77 In the modern air, the global methane burden – the total amount of methane in the air –  
78 includes both emissions from human activities such as methane from fossil fuel use,  
79 agriculture and waste, as well as natural biogenic inputs. Both agricultural and natural  
80 emissions are subject to feedbacks from the sensitivity of the biosphere to changes in  
81 climate. Summing global biospheric change from measurement data across the planet is a  
82 complex task with large uncertainties, but provided direct anthropogenic forcing can be  
83 deducted (a difficult and complex task), the remaining non-anthropogenic growth in  
84 biogenic methane emissions provides a direct measure of change.

85 Unlike  $\text{CO}_2$ , whose annual cycle is strongly influenced by the spring growth and autumn leaf  
86 fall of deciduous plants in the temperate northern hemisphere, the natural methane cycle

87 reflects change across a much wider latitudinal spectrum, tropical, temperate and Arctic.  
88 Natural biogenic sources include tropical and boreal wetlands, ruminants, termites, Arctic  
89 bogs and permafrost, as well as forest and grassland fires, while anthropogenic biogenic  
90 methane comes from agriculture and waste, especially food waste disposal. Aquatic  
91 ecosystems, both natural and anthropogenic, contribute up to half the total emission  
92 (Rosentreter et al. 2021).

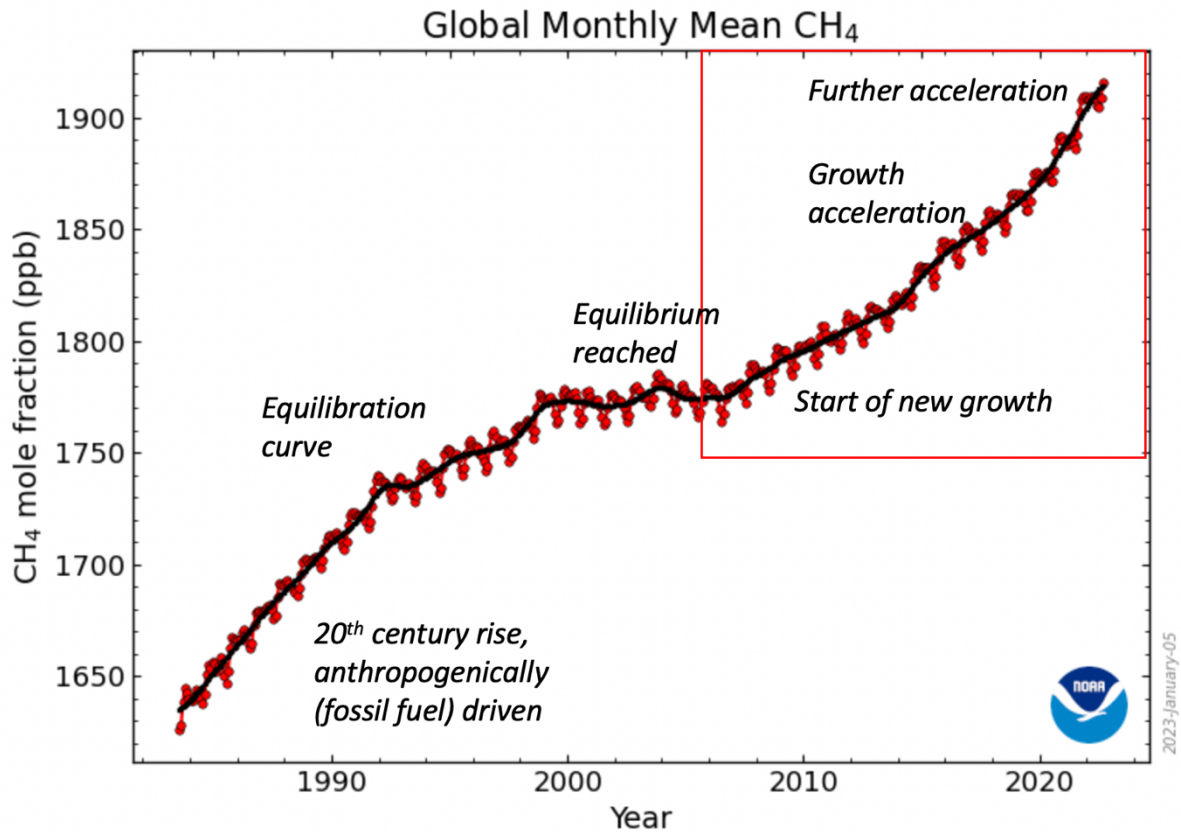
93 Starting in 2006 the atmospheric methane burden has grown strongly (Dlugokencky et al.  
94 2011, Nisbet et al., 2014, Schaefer et al., 2016, Mikaloff-Fletcher and Schaefer 2019),  
95 accompanied by a sustained negative shift in the carbon isotope delta value ( $\delta^{13}\text{C}_{\text{CH}_4}$ ). This  
96 shift indicates present-day atmospheric growth is primarily driven by biogenic emissions  
97 (Nisbet et al. 2016, 2019; Lan et al. 2021a,b, 2022; Basu et al 2022) and not primarily from  
98 increased fossil fuel emissions, nor by greatly stronger sink processes. Note that we  
99 distinguish between the atmospheric '*burden*' – the total mass of methane in the air  
100 expressed in Tg; '*emissions*' or fluxes, in Tg/yr; and '*emissions growth*' in Tg/yr per year. 1 ppb  
101 of methane, as an average mass fraction of the global atmosphere, has a mass of about  
102 2.77Tg.

103 Methane's dominant sink is the atmospheric hydroxyl radical [OH], especially in the tropical  
104 mid-troposphere, with minor sinks including reaction with atomic chlorine in the marine  
105 boundary layer and bacterial methanotrophy in upland and forest soils. The formation and  
106 distribution of [OH] is changing as the climatological tropics widen with expansion of the  
107 Hadley cells (Nicely et al. 2018). While it remains unclear how much of the observed tropical  
108 expansion is within the range of natural variability (Grise et al. 2019) the present rate of  
109 increase is exceptional in the long-term record.

110 The following sections review recent work on the complex and often contradictory puzzle of  
111 methane's post-2006 growth. That synthesis is then compared with past events in the  
112 glacial paleoclimatological record, where is strong evidence (Möller et al. 2013) that fast  
113 methane rises during rapid glacial to interglacial shifts in the global climate are driven by  
114 feedbacks involving tropical wetlands that respond rapidly to warming.

115 *Figure 1. Global monthly mean of atmospheric CH<sub>4</sub>, NOAA network. Note convex*  
116 *equilibration curve to 2006; concave acceleration curve from 2007. The convex curve from*  
117 *the 1980s to early 2000s is consistent with relaxation to a source-sink steady state*  
118 *(Dlugokencky et al., 2003), but then the start of a renewed growth became apparent in*  
119 *2007, and the slope of the new concave curve steepened in 2013 (acceleration of growth),*  
120 *followed by further acceleration in 2020. Modified from Lan et al. (2022).*

121



122

123 *1.1 Feedbacks*

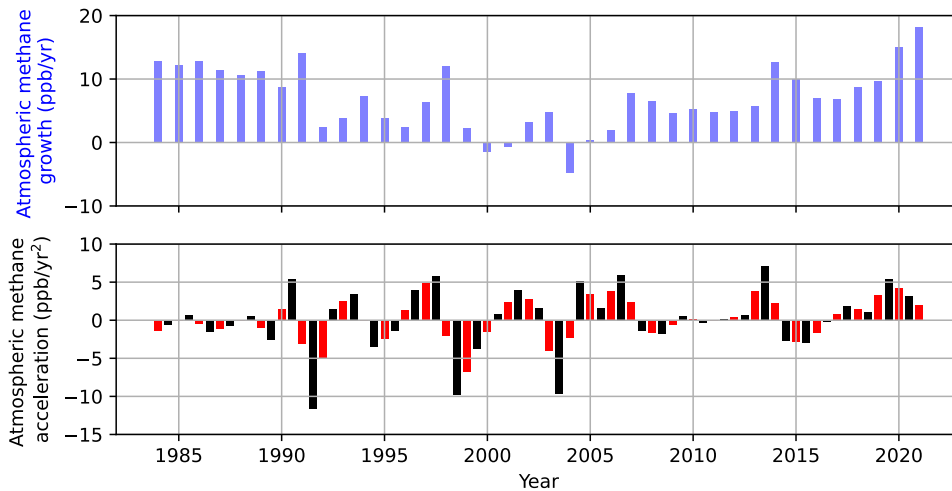
124 Anthropogenic methane emissions have dramatically added to the primary forcing of the  
 125 climate (Saunio et al., 2020), but the extent of the feedback response of methane  
 126 emissions as climate has become warmer and wetter remains uncertain (Dean et al, 2018).  
 127 For methane in particular, it is difficult to separate primary emissions (e.g. gas industry and  
 128 coal mine leaks), natural feedbacks (e.g. increased wetland emissions) and changing  
 129 anthropogenic biogenic emissions from farming, sewage, and landfills. As fertiliser  
 130 production, especially fixed nitrogen, has grown, the productivity of neighbouring wetlands  
 131 may have risen, driven by nitrogen runoff. Rising CO<sub>2</sub> also acts as a fertiliser, globally  
 132 promoting C3 plant growth (trees and bushes) (Haverd et al. 2020, Graven et al. 2013,  
 133 Matthews, 2007, Möller et al. 2013), though this impact is eventually limited by supply of  
 134 other nutrients such as fixed nitrogen and phosphorous (Wang et al, 2020).

135 Considering the interlinkages between climate and methane productivity, Dean et al. (2018)  
 136 concluded that wetlands will form the majority of the methane climate feedback up to the  
 137 year 2100. Higher primary productivity, in response to warmth, precipitation and  
 138 inundation, supplies and enhances microbial activity in anaerobic environments.  
 139 Methanogenic processes may respond more quickly to change than methanotrophic  
 140 processes (Wen *et al*, 2018). We may have entered a new era of increased natural methane  
 141 emissions from wetlands (Rosentreter et al. 2021), driven by multiple feedback factors,  
 142 including increased rainfall and temperatures, higher rainfall in key areas (Lunt et al 2021),  
 143 and higher ecosystem production, aided by agricultural impacts. If present-day feedback  
 144 responses are indeed strong, then the biogenic component of methane's very strong current

145 growth may be an integrative signal responding to, indicative of, and feeding global-scale  
 146 change.

147 Any modern global-scale climate change, by cause and starting point, must be  
 148 fundamentally different from past changes in the palaeoclimate record. Nevertheless, there  
 149 are strong analogies between methane's current growth and ice core methane records  
 150 during glacial-interglacial 'terminations'. In these events, the methane record tracked  
 151 planetary-scale meteorological reorganisations of the climate system (Broecker & Denton,  
 152 1990; Cheng et al. 2009; Denton et al. 2010). Thus, the question arises (Nisbet 2022, 2023):  
 153 Is methane's modern growth (Fig. 2) also a signal that a planetary-scale climate  
 154 reorganisation is underway?

155 *Figure 2. Annual mean growth (blue bars; ppb/yr) and acceleration in half-year intervals*  
 156 *(red, black bars; ppb/yr<sup>2</sup>) of atmospheric methane inferred from NOAA data, 1984-2022*  
 157 *(NOAA 2023a). Red bars denote the gradient of the growth rate calculated using second-*  
 158 *order accurate central differences of the interior points and first-order accurate one-side*  
 159 *differences of the end points. Black bars denote the difference in atmospheric growth*  
 160 *between successive years.*



161

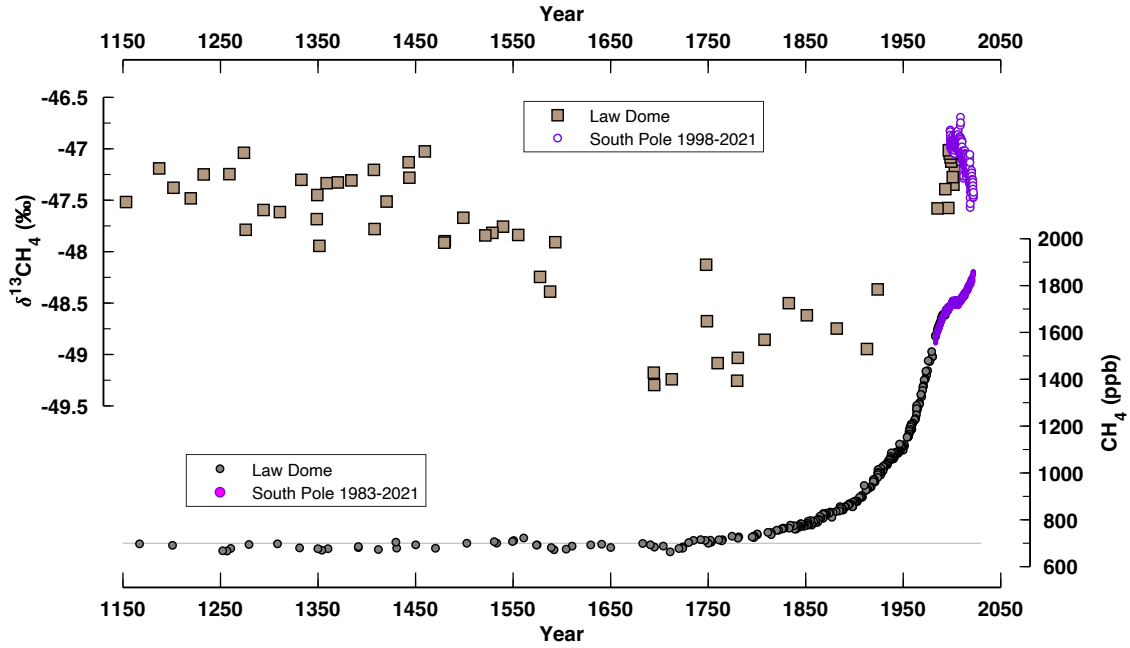
162

163 *Figure 3. Past records of  $\delta^{13}C_{CH_4}$ .*

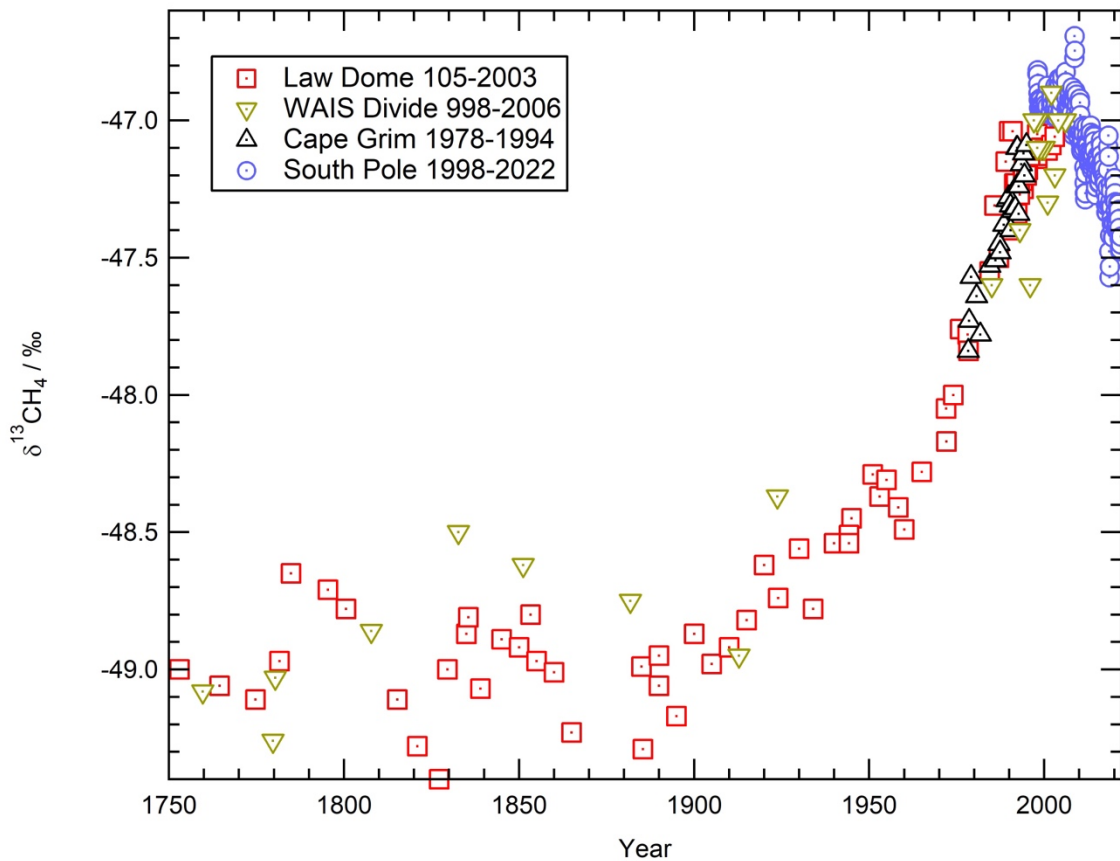
164 *3a. Methane and  $\delta^{13}C_{CH_4}$  record back to the year 1150 CE, showing the background evolution*  
 165 *of both CH<sub>4</sub> and  $\delta^{13}C_{CH_4}$  before the budget was disturbed by human interferences (i.e.*  
 166 *before ca. 1500 -1600 AD), to indicate historic variability due to changes in climate and*  
 167 *wetland emissions on multidecadal or longer time scales. Note the CH<sub>4</sub> background is*  
 168 *essentially flat over pre-industrial time, but there is a notable negative trend of about 2‰*  
 169 *between 1500-1650 that is gradually reversed as coal-fired industrialisation begins. For*  
 170 *longer record see Sapart et al. (2012).*

171 *3b. Post-1750  $\delta^{13}C_{CH_4}$  record from South Pole and ice core measurements, showing recent*  
 172 *record in more detail. Note long +ve trend in  $\delta^{13}C_{CH_4}$ , driven by fossil fuel emissions, and*  
 173 *sustained reversal of trend since 2007.*

174 *Data from Law Dome: Ferretti et al. 2005; see also Rubino et al. 2019; WAIS Divide:*  
 175 *Mischeler et al 2009; Sapart et al. 2012 and from NOAA*  
 176 *[https://gml.noaa.gov/aftp/data/trace\\_gases/ch4c13/flask/surface/](https://gml.noaa.gov/aftp/data/trace_gases/ch4c13/flask/surface/)).*



177



178

179 **2. Methane growth, pre-industrial period to present**

180 There has been strong centennial-scale variation in methane's recent historic record (Fig. 3).  
 181 From Antarctic ice core measurements, Ferretti et al. (2005), Sapart et al. (2012) and  
 182 Mischler et al (2009) found that  $\delta^{13}\text{C}_{\text{CH}_4}$  was about -47‰ around 800 CE, but then showed a

183 strong depletion trend from about 900 CE to 1700 CE, until  $\delta^{13}\text{C}_{\text{CH}_4}$  was about -49‰. Prior to  
184 the onset of industrialisation, in the medieval years from the 12th to the 19th centuries CE,  
185 methane rose by around 100 ppb, accompanied by a negative trend in  $\delta^{13}\text{C}_{\text{CH}_4}$  from -47.5‰  
186 to -49‰ (Fig. 3). Ferretti et al. (2005) interpreted this medieval 2‰ depletion as evidence  
187 for a major drop in anthropogenic biomass burning emissions between 800-1700 CE, for  
188 example a reduction in deliberate and intense North American grassland burning.  $\text{CH}_4$  was  
189 rising during this period, implying the reduction in biomass burning emissions must have  
190 been more than balanced by other sources. This interpretation is supported by  $\text{CO}$  evidence  
191 from ice cores. Agricultural methane emissions may have helped strengthen the negative  
192 trend (Mischler et al. 2009). But that historic depletion rate was about 0.0025‰ per year,  
193 totalling less than 0.04‰ over 15 years, very different from what has taken place in the 15  
194 years 2007-2022.

195 Starting around the years 1750 to 1800 (Fig. 3b), with the onset of coal-fired and then oil  
196 and gas-powered industrialisation, the  $\delta^{13}\text{C}_{\text{CH}_4}$  trend rapidly shifted positive (Etheridge et al.  
197 1998, Ferretti et al. 2005, Mischler et al. 2009, Sapart et al. 2012). That exceptionally rapid  
198 positive shift accompanying fossil-fuel industrialisation from the years 1800-2007 was +2‰  
199 in 250 years, or about 0.01‰ per year, interpreted as evidence that the rise was primarily  
200 driven by fossil fuel emissions, first mainly from coal, then with methane emissions as a by-  
201 product of oil extraction and use, and more recently from the gas industry too.

202 In contrast, the ongoing 2007-2022 reverse negative shift in  $\delta^{13}\text{C}_{\text{CH}_4}$  has been -0.55‰ in 15  
203 years: a rate of negative shift four times faster than the positive rise during industrialisation,  
204 and more than tenfold the rate of the medieval depletion trend. However, it should be  
205 noted that many biogenic sources, especially in extra-tropical wetlands, have greater  
206 leverage on atmospheric  $\delta^{13}\text{C}_{\text{CH}_4}$  than fossil fuel emissions which are closer in source  
207 signature to the bulk atmospheric value.

208 Sustained accurate methane measurement began in the late 1970s and by 1983 NOAA led a  
209 co-operative global network collecting flask samples of air from remote sites. Between 1984  
210 and 1990 the growth rate was over 10 ppb/yr, accompanied by a continuing positive shift in  
211  $\delta^{13}\text{C}_{\text{CH}_4}$  (Quay et al. 1988, Etheridge et al. 1998, Ferretti et al. 2005), but in the early 1990s  
212 Steele et al. (1992) first recognised a slowing-down of growth and predicted stabilisation  
213 around 2006. This was confirmed by Dlugokencky et al. (1994, 1998, 2003) and Lowe et al.  
214 (1994) as the budget equilibrated and the growth rate in fossil fuel emissions slowed. After  
215 some years of equilibrium in the early 2000s, the return of growth in the atmospheric  
216 methane burden became apparent from late 2006 and into 2007 (Figure 3).

217 Methane's recent growth is wholly different from the late 20<sup>th</sup> century pattern. Unlike the  
218 convex, equilibrating trend of the late 20<sup>th</sup> century, growth since the end of 2006 has been  
219 on a concave, accelerating trend with the highest growth rates on record in 2020 and 2021  
220 (Dlugokencky et al. 2011, Nisbet et al., 2014, 2016, 2019, 2021, Lan et al. 2021a,b, 2022,  
221 2023; Fig. 1). Moreover, methane's post-2006 isotopic record is isotopically quite unlike the  
222 record of the 'fossil-fuel' industrial 19<sup>th</sup> and 20<sup>th</sup> centuries. The long trend towards more  
223 positive  $\delta^{13}\text{C}_{\text{CH}_4}$ , indicative of fossil fuel emissions, has unexpectedly reversed, replaced by  
224 sustained strong trend to more negative  $\delta^{13}\text{C}_{\text{CH}_4}$ . The trend is not a subtle statistical drift but  
225 rather it is a strong planet-wide shift far outside any plausible statistical variability.

226 In 2006, the global mean of  $\text{CH}_4$  in the marine background air was 1775 ppb, rising to 1912  
227 ppb in 2022, a total rise of 137 ppb (about 379 Tg) in the methane burden. In 2021 alone,

228 growth was around 18 ppb or about 50 Tg. Rapid growth continues with an increase in 2022  
229 of 14 ppb.

230 Synchronous with the onset of sustained sharp growth in CH<sub>4</sub> has been the isotopic reversal,  
231 initiating a sustained strong negative trend in  $\delta^{13}\text{C}_{\text{CH}_4}$  (Fig. 3; also Nisbet et al. 2019, Lan et  
232 al. 2021a,b).  $\delta^{13}\text{C}_{\text{CH}_4}$  values in Arctic air declined from -47.3‰ in 2006 towards -48‰ in mid-  
233 2022. At the South Pole (Fig. 4),  $\delta^{13}\text{C}_{\text{CH}_4}$  values were about -46.9‰ in 2006, sinking towards -  
234 47.4‰ in 2022 (Michel et al. 2022). These trends were constructed from detailed individual  
235 flask records (e.g. see Figure SI 1 showing the flask-by-flask record from Ascension).

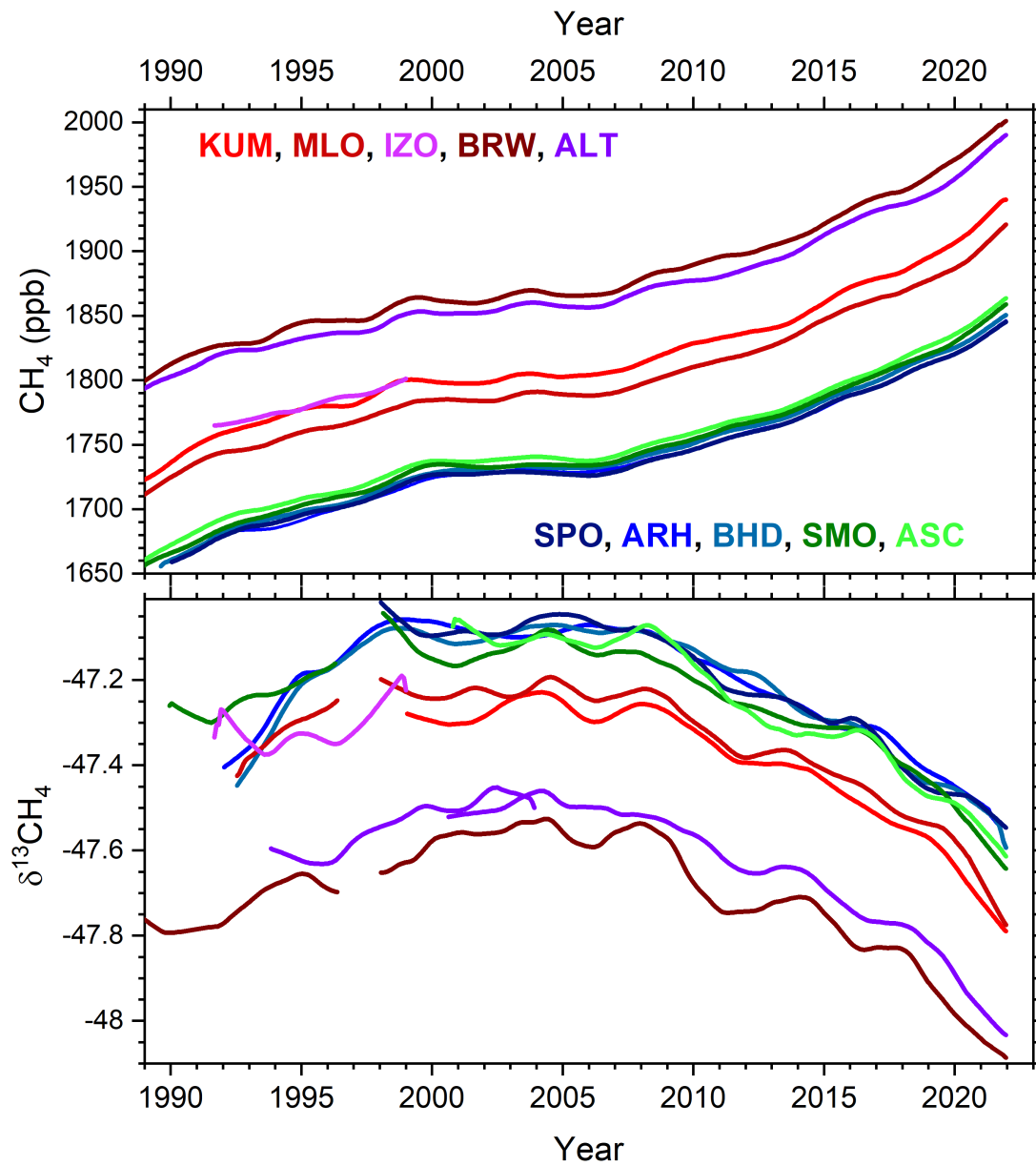
236 As seen in Figure 4, the last 30 years have had two phases for an increase in CH<sub>4</sub> mole  
237 fraction but with these having strong opposite and global trends in  $\delta^{13}\text{C}_{\text{CH}_4}$ . Longer term  
238 records from ice-core and firn air show that this 'turnover' in  $\delta^{13}\text{C}_{\text{CH}_4}$ , has reversed a  
239 centuries-long trend towards 'heavier' (more <sup>13</sup>C-rich) methane that ended around 1998,  
240 then a few years of stability, and onset of the current trend towards 'lighter' (less <sup>13</sup>C-rich)  
241 values that began in late 2006 and has been sustained ever since. Globally, the negative  
242  $\delta^{13}\text{C}_{\text{CH}_4}$  shift over 2006-2022 has been about -0.55‰, from the maximum (most positive)  
243 record in March 2008 to the more recent 2022 (Lan et al 2021a,b and update 2023).  
244

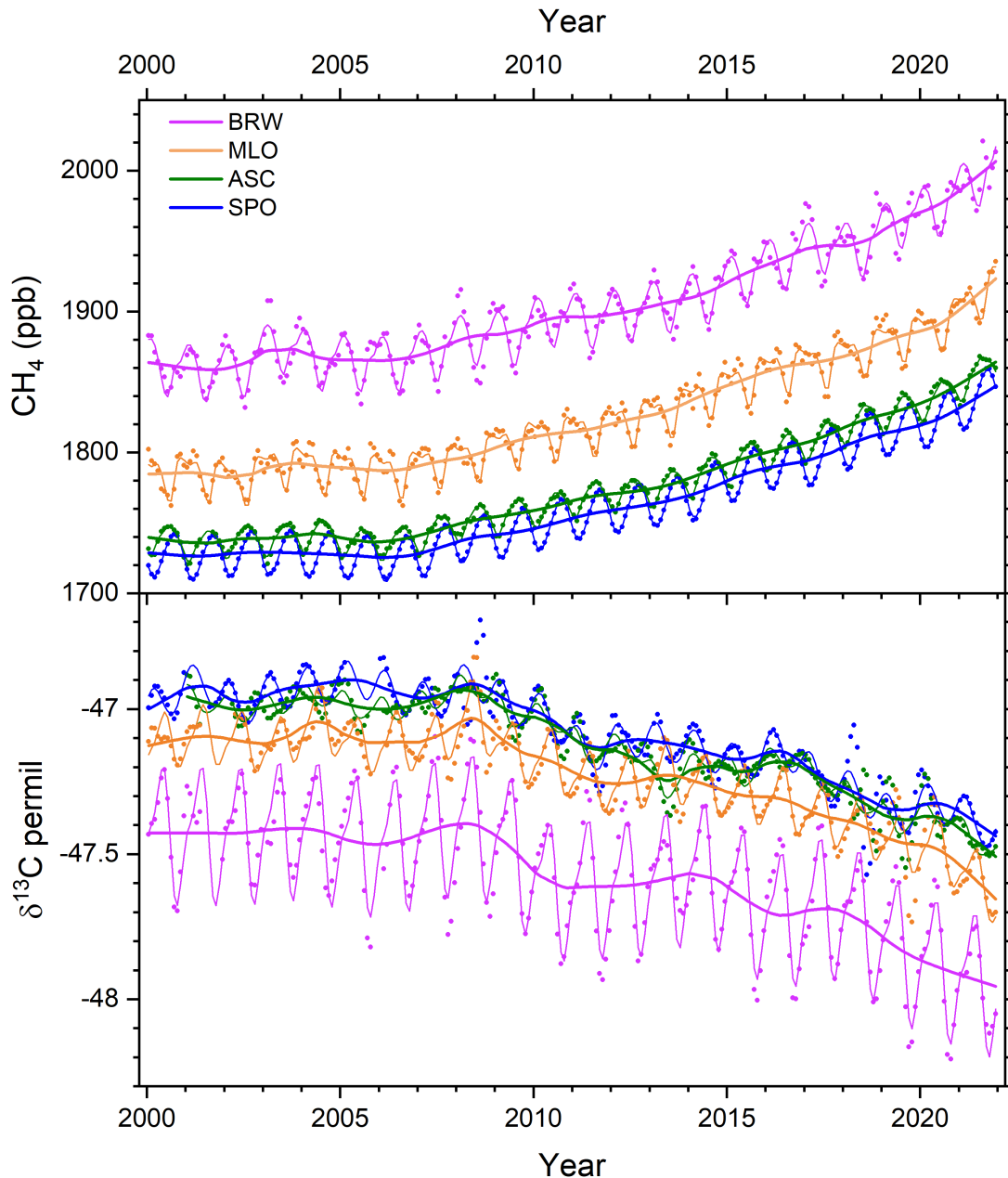
245 *Figure 4. Trends in methane mixing ratio (top panels) and  $\delta^{13}\text{C}_{\text{CH}_4}$  (lower panels)*

246 *Figure 4a) Trends in methane mixing ratio (top panel) and  $\delta^{13}\text{C}_{\text{CH}_4}$  (lower panel) for five long*  
247 *term monitoring sites in each hemisphere. In the Southern Hemisphere the measurement*  
248 *stations are: NOAA's SPO – South Pole (90°S), SMO – Samoa (14°S), and ASC – Ascension*  
249 *(8°S); and NIWA's ARH – Arrival Heights, McMurdo, Antarctica (78°S) and BHD – Baring*  
250 *Head, NZ (41°S). In the Northern Hemisphere they are: NOAA's KUM – Cape Kumukahi*  
251 *(20°N), MLO – Mauna Loa (20°N), BRW – Barrow, Alaska (71°N), ALT – Alert, Canada (83°N),*  
252 *and University of Heidelberg's IZO – Izana (28°N). Early  $\delta^{13}\text{C}_{\text{CH}_4}$  data for SMO, MLO and BRW*  
253 *are from Quay et al (1991) and for IZO from Levin et al., (2012).*

254 *Figure 4b) Detailed patterns showing seasonality for four selected sites, BRW and MLO in the*  
255 *Northern Hemisphere, and ASC and SPO in the Southern Hemisphere. NOAA data.*

256 *NOAA data from [https://gml.noaa.gov/aftp/data/trace\\_gases/ch4c13/flask/surface/](https://gml.noaa.gov/aftp/data/trace_gases/ch4c13/flask/surface/).*  
257 *NIWA data in the World Data Center for Greenhouse Gases <https://gaw.kishou.go.jp/>. For*  
258 *further details see Supplementary Information. Intercomparison follows Umezawa et al.*  
259 *(2018). SPO and MLO are at 2810 and 3397 m elevation respectively but the other points are*  
260 *close to sea level. Details of the data from these sites are shown in supplementary material*  
261 *while this figure summarises the similar patterns seen globally.*

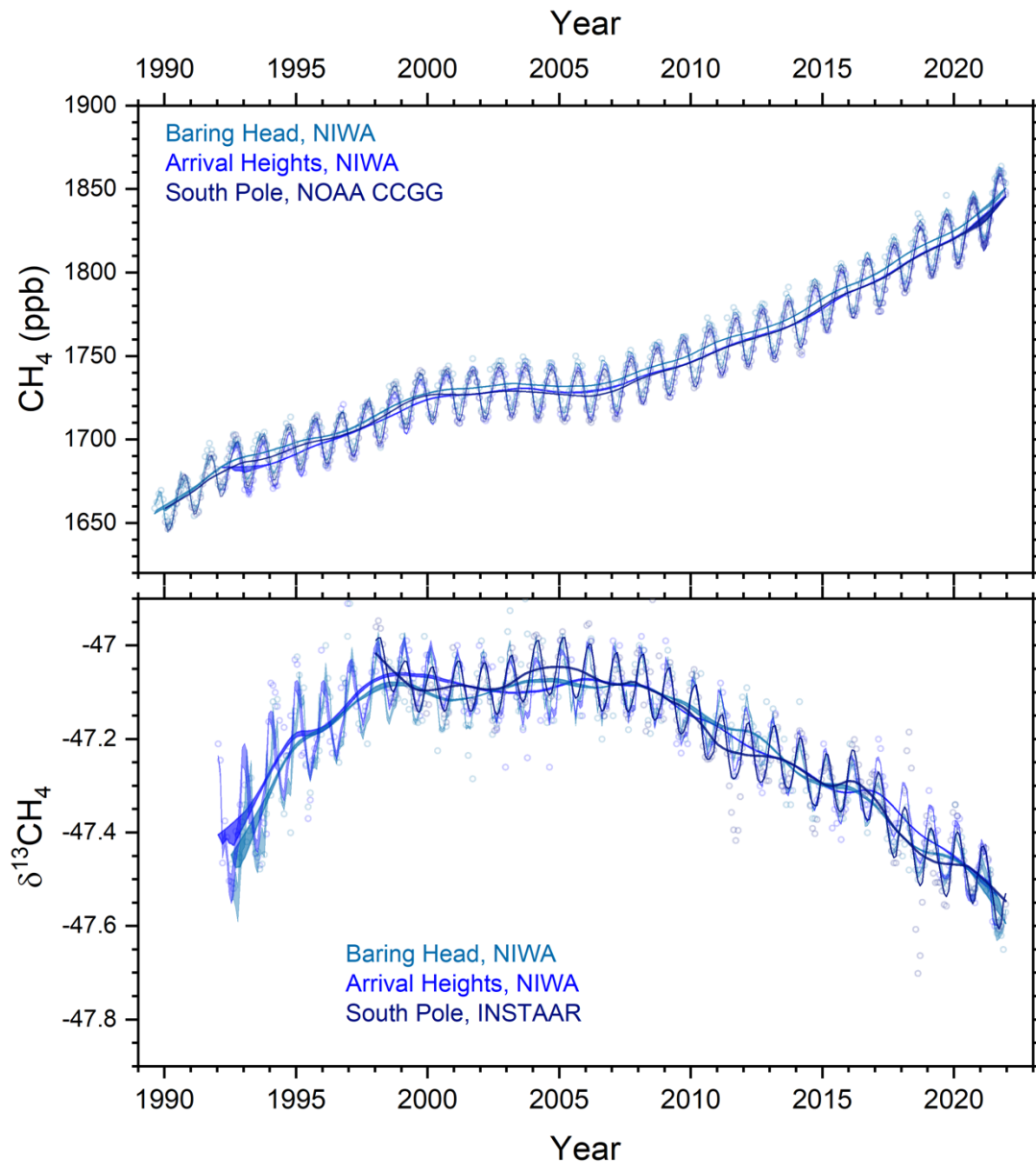




263

264 Figure 5 shows in detail the 'turnover' and seasonality in the remote (i.e. global)  $\delta^{13}\text{C}_{\text{CH}_4}$   
 265 trend. The centuries-long trend towards 'heavier' (more  $^{13}\text{C}$ -rich) methane ended around  
 266 1998 (e.g. see Dlugokencky et al. 1994). Then came a few years of stability. The onset of the  
 267 trend towards 'lighter' (less  $^{13}\text{C}$ -rich) values began in late 2006 and has been sustained ever  
 268 since. Globally, the negative  $\delta^{13}\text{C}_{\text{CH}_4}$  shift over 2006-2022 has been about  $-0.55\text{‰}$ , from the  
 269 maximum (most positive) record in March 2008 to 2022 (Lan et al 2021a,b and update  
 270 2023).

271 *Fig. 5 Remote Southern Hemisphere Isotopic Trend since the 1980s. Data from NIWA New*  
 272 *Zealand (Baring Head (41°S), Arrival Heights (78°S) and NOAA/INSTAAR measurements (SPO*  
 273 *90°S). See Fig. 4 for data sources; intercomparison after Umezawa et al. (2018).*  
 274 *[https://gml.noaa.gov/aftp/data/trace\\_gases/ch4c13/flask/surface/](https://gml.noaa.gov/aftp/data/trace_gases/ch4c13/flask/surface/).*



275

276

### 3. Methane sources and sinks; isotopic impacts.

277

278

279

280

281

282

283

284

285

286

287

The bulk source of global methane emissions has  $\delta^{13}\text{C}_{\text{CH}_4} \cong -53\text{‰}$  for all sources (Dlugokencky et al. 2011, Nisbet et al. 2019, Sherwood et al. 2017). Oh et al. (2022) estimated a mean global wetland  $\delta^{13}\text{C}_{\text{CH}_4}$  signature of  $-61.3 \pm 0.7\text{‰}$ . This reflects a mix between northern high-latitude C3 plant wetlands (mean  $-67.8\text{‰}$ ) and tropical C4-rich wetlands (mean  $-56.7\text{‰}$ )(Quay et al, 1988, Dlugokencky et al. 2011; Sherwood et al. 2017, 2021, Ganesan et al. 2018, MOYA/ZWAMPS Team (2021), Menoud et al., 2022). Note the means and precisions cited here are from partial and perhaps unrepresentative sampling: real world averages may be several ‰ different. In addition to the global C3/C4 plant distribution, the distribution of hydrogenotrophic / acetoclastic methanogens and vegetation-specific CH<sub>4</sub> transport all contribute to the  $\delta^{13}\text{C}_{\text{CH}_4}$  variability of wetland emissions (Ganesan et al. 2018). France et al. (2021) found methane from South American

288 and African southern outer tropical (seasonal) wetlands had  $\delta^{13}\text{C}_{\text{CH}_4}$   $-60 \pm 5\text{‰}$  while  
289 equatorial wetlands emitted methane with  $\delta^{13}\text{C}_{\text{CH}_4}$   $-52 \pm 2\text{‰}$ . Similarly, Oh et al. (2022) found  
290 tropical wetland emissions are enriched by about 11‰ relative to boreal wetlands.

291 Agricultural emissions, like wetland emissions, vary with latitude and C3/C4 proportions in  
292 ruminant diets (Menoud et al. 2022, and tropical measurements are scarce. For rice fields,  
293 France et al. (2021) found  $\delta^{13}\text{C}_{\text{CH}_4}$   $-61 \pm 4\text{‰}$ . Farmed ruminant emissions vary with diet, with  
294 a global average  $\delta^{13}\text{C}_{\text{CH}_4}$  perhaps around  $-65\text{‰}$  (e.g. Chang et al. 2019), but data are scarce  
295 from tropical ruminants where C4 fodder can dominate; for example, for Kenyan pastured  
296 cattle,  $\delta^{13}\text{C}_{\text{CH}_4}$  is around  $-57\text{‰}$  (MOYA/ZWAMPS Team 2021). Fossil fuel emissions have  
297  $\delta^{13}\text{C}_{\text{CH}_4}$  globally roughly between  $-43\text{‰}$  and  $-45\text{‰}$  (Lan et al. 2021a). However,  $\delta^{13}\text{C}_{\text{CH}_4}$   
298 values range widely from highly positive values (e.g.  $-25\text{‰}$  for some gasfields) to very  
299 negative (as light as  $-70\text{‰}$  in some cases). Howarth (2019) suggested that about a third of  
300 growth in methane emissions from all sources globally over the past decade came from  
301 shale gas production in North America. Nevertheless, Milkov et al. (2020), Basu et al. (2022)  
302 and Zhang et al. (2023) showed this to be unlikely.

303 The steady-state lifetime for atmospheric methane is between 9 and 10 years (Ehhalt 1974;  
304 Dlugokencky et al. 2011; Nisbet et al. 2019; Lan et al. 2021a). Methane's perturbation  
305 lifetime, which accounts for atmospheric chemistry relaxation times and is more relevant for  
306 climate impacts of emission reductions, is approximately 12 years (Prather et al. 2012,  
307 Myhre et al. 2013). Methane's main sinks, atmospheric hydroxyl [OH], Cl, and soil  
308 methanotrophy, are all subject to interannual variability as well as to the growth in the  
309 methane burden. Nicely et al. (2018) found the expected decline in [OH] caused by methane  
310 growth was largely offset by positive trends in tropospheric [OH] responding to changes in  
311 water vapour,  $\text{NO}_x$ , and  $\text{O}_3$ . Methane's sinks all respond to climate change. Yin et al. (2021)  
312 showed that the longer-term impact of [OH] changes was modest, a conclusion updated by  
313 Basu et al (2022). Similarly, Thompson et al. (2018) and Drinkwater et al. (2023) also found  
314 the impact of changes in the atmospheric sink did not appear to be a key driver of  
315 methane's strong and sustained growth. However, in some years specific events can have  
316 large impacts on methane growth. In particular, [OH] fluctuations can make a major  
317 contribution to methane growth in hot El Niño years (Zhao et al. 2020), especially when  
318 there are enhanced CO emissions from biomass burning. Such effects smooth out during a  
319 full El Niño /Southern Oscillation (ENSO) cycle, as CO emissions from biomass burning  
320 decrease again in subsequent cool, regionally-wet La Niña years.

321 Sources and sinks show interannual variability and may have been affected by covid lock-  
322 downs in 2020 (Laughner et al. 2021), though that transient impact is unlikely to have been  
323 sustained significantly into 2021 and 2022. For the unusual year 2020, when anthropogenic  
324 emissions of air pollution were much affected by COVID lockdowns (e.g. Cooper et al.  
325 2022), the growth in methane was driven both by a decline in [OH], and by increased wetland  
326 emissions (Peng et al. 2022), especially in the tropical and sub-tropical Northern Hemisphere  
327 and in western Siberia and central Canada. Using analysis of GOSAT retrievals, Qu et al  
328 (2022) concluded 14% of growth was from [OH] changes. Likewise, Feng et al (2023) also  
329 found an [OH] reduction comparable to Peng et al.'s results, but concluded that most of the  
330 observed increase in atmospheric methane during 2020 and 2021 was caused by increased  
331 emissions, especially in Eastern Africa. The full causes of methane's remarkable growth in  
332 2021 and 2022, when covid lockdowns were less severe, are still being debated but it is

333 notable that over the period 2020-2022 the methane growth histogram matches the very  
 334 unusual 'triple-dip' 3-year La Niña event (NOAA 2023b).

335 Methane's minor sinks are destruction by atmospheric chlorine (Hossaini et al. 2016),  
 336 oxidation by soil methanotrophs, and upward transport into the stratosphere where  
 337 methane is destroyed (and isotopically fractionated) by photooxidation. Methane  
 338 destruction by chlorine is particularly interesting: although it only accounts for ~2.5% of the  
 339 total methane sink (but with larger regional-scale effects (Hossaini et al. 2016)), it is highly  
 340 fractionating for C and H isotopes (Strode et al. 2020). All these sinks will have interannual  
 341 variability, especially in the ENSO cycle, and will also be subject to changing feedbacks to  
 342 long-term climate warming.

343 All biological methane sources, both purely 'natural' and anthropogenic, respond to climate  
 344 change and the rapid strong positive feedbacks make methane an excellent integrating  
 345 indicator of large-scale wetland ecosystem change. Increased warmth and moisture in the  
 346 'wet tropics' are likely to increase plant growth and thus ruminant productivity, and also  
 347 microbial activity in manure and wetlands. In the boreal and Arctic realms warmth is also  
 348 likely to increase wetland emissions. Moreover, as mentioned above (section 1.1), CO<sub>2</sub> acts  
 349 as a potent fertiliser for C3 plants, increasing plant productivity (Lobell and Field, 2008;  
 350 Uddin et al. 2018; Haverd et al 2020) and thus supply of organic matter to eventual  
 351 anaerobic decay, though it is possible this impact is eventually limited by supply of other  
 352 nutrients, primarily fixed nitrogen and phosphorus (Wang et al. 2020).

353 **Table 1: Simplified comparison of some recent assessments of wetland emissions and**  
 354 **their growth.**

355 **a) Examples of some estimated outer tropical wetland emissions**

<i>Location</i>	<i>Latitude, area</i>	<i>Emissions Tg/yr</i>	<i>Reference</i>
Bangweulu, Upper Congo basin, Zambia	11°S, >10000 km <sup>2</sup>	1 to 3	Shaw et al, 2021
Pantanal, Brazil	Around 17°S, around 150000 km <sup>2</sup>	2 to 3.3	Gloor et al., 2021
Llanos de Moxos, Bolivia	Around 12-15°S, Around 70000 km <sup>2</sup>	3.6	France et al, 2022
<i>Freshwater wetlands</i>	<i>Global</i>	138-165	Rosentreter et al 2021
<i>East Africa</i>	<i>Regional</i>	Mar-May 2018 6Tg Oct-Dec 2019 9Tg	Lunt et al. 2021
<i>South Sudan</i>	<i>Regional</i>	7.4 ± 3.2 Tg	Pandey et al. 2021

356 **b) Global emissions growth (all sources) in the single years 2020 and 2021**

Period	Emissions growth in year (Tg)	Reference
2020	27	Feng et al. 2023
2021	21	Feng et al. 2023
2020	25-37 (48% from Africa)	Qu et al.

357 **c) Global wetland-only emissions growth in the single years 2020 and 2021**

Period	Emissions growth in year (Tg)	Reference
2020	14-26	Zhang et al. 2023
2021	13-23	Zhang et al. 2023
2020	6 - 7	Peng et al. 2022
2019-2020	22-32 (of which 15 in Africa)	Qu et al. 2022

358 **d) Global emissions in the years from the onset of growth prior to 2020**

Reference	Period	Growth in biogenic emissions Tg/yr	Estimated emissions growth acceleration Tg/yr/yr
Basu et al. 2021	2007-2012	26	4
Basu et al. 2021	2013-2017	32	
Zhang et al. 2023	2007-2021	8 - 10	1.3 -1.4
Oh et al. 2022	2006-2016	28 assumed scenario	

359

360 *Table 1 Note: numbers given here are for comparison purposes only. See cited sources for*  
 361 *original details. Numbers here highly simplified, rounded off from the disparate results in the*  
 362 *many cited studies, and are very approximate with large uncertainties.*

363 **4. The wetland hypothesis**

364 The wetland hypothesis is that biogenic emissions, particularly from wetlands, are growing  
 365 rapidly and are the dominant cause of recent growth (Lunt et al. 2019, Nisbet et al. 2016,  
 366 2019, Lan et al. 2021a,b, Basu et al. 2022, Oh et al, 2022, Zhang et al. 2023). Aquatic  
 367 ecosystems are enormously important in the global methane budget (Rosentreter et al.  
 368 2021). Dean et al. (2018) found wetland emission growth can be primarily ascribed to  
 369 climate change feedbacks. Table 1 provides a highly simplified comparison of results from  
 370 recent studies in a very active and complex field.

371 The 'wetland hypothesis' has been supported by powerful evidence that increased wetland  
 372 emissions, especially in the tropics, drove methane's exceptional growth in 2020 (Lunt et al.  
 373 2019, 2021, Qu et al. 2022, Feng et al. 2022, 2023; Peng et al. 2022). The isotopic evidence is  
 374 strong. Using a process-based biogeochemistry model, Oh et al. (2022) concluded the spatial  
 375 distribution of wetland  $\delta^{13}\text{C}_{\text{CH}_4}$  emissions is consistent with the observed latitudinal gradient  
 376 in  $\delta^{13}\text{C}_{\text{CH}_4}$ , implying the growth in microbial emissions has been the dominant driver for  
 377 methane's post-2006 rise and concurrent negative trend in  $\delta^{13}\text{C}_{\text{CH}_4}$ . The causes of increased  
 378 wetland emissions likely include increased rainfall and inundation in drainage basins  
 379 (Pandey et al. 2017, Lunt et al. 2019, 2021, Feng et al. 2022), and also overall warm  
 380 temperatures in the post-2006 period, as plant and microbial productivities rise with  
 381 temperature, provided water and nutrients are available.

382 Methane's remarkable growth in 2020-2022 has been synchronous with an unusual La  
 383 Niña event (Hasan et al. 2022) with a 'triple-dip' 3-year period (McPhaden et al. 2023) that  
 384 has brought sustained seasons of exceptional rainfall to the important regions in the moist  
 385 tropics. However, emissions from aquatic systems are highly variable (Rosentreter et al.  
 386 2021), and inherently difficult to parameterize (Ringeval et al., 2014).

387 Because cloud cover is typically deep and persistent during wet seasons over key emitting  
 388 regions, it is difficult to study tropical wetland emissions in rainy season using satellite  
 389 remote sensing directly overhead, but the long atmospheric lifetime of methane allows for  
 390 these emissions to be quantified via observations collected downwind. Feng et al. (2022)  
 391 used satellite observations to infer that over 80% of the observed growth in the global  
 392 methane burden between 2010-2019 came from tropical terrestrial emissions. Separately,  
 393 Feng et al. (2023) estimated that 66 % of methane's global increase in 2020 was due to  
 394 increased emissions, particularly from the tropics. They found evidence for growing  
 395 microbial sources over the tropics with a very large increase ( $14\pm 3$  Tg) in recent (2020)

396 emissions from northern hemisphere Eastern Africa (e.g. the Nile Sudd – see Lunt et al.  
397 2019), while emissions decreased in China and India.

398 These results are supported by the findings of Qu et al. (2022) from GOSAT retrievals, that  
399 82% of methane growth from 2019 to 2020 was driven by increased emissions, with a large  
400 contribution from African wetlands. Similarly, Drinkwater et al. (preprint submitted 2023)  
401 found methane recent growth (2004-2020) has been driven by a progressive increase in  
402 emissions, with emissions from tropical and sub-tropical sources (30°N to 30°S, i.e. including  
403 the monsoonal climate belt) accelerating by 3.8 Tg/yr/yr. They concluded methane's growth  
404 was primarily driven by biogenic emissions, especially from regions with large wetlands,  
405 with increases in annual emissions over the period of about 17 Tg from Northern  
406 Hemisphere Africa, and 21 Tg from Tropical South America, though Chinese annual  
407 emissions also increased very strongly (27 Tg).

408 Anthropogenic impacts can also increase wetland emissions. Although widespread drainage  
409 of wetlands is also taking place, tropical wetlands in Africa can host large cattle populations  
410 (own observations). Indirect anthropogenic forcing factors include CO<sub>2</sub> fertilisation (Holden  
411 et al. 2013, Haverd et al 2020), run-off to wetlands from nitrogen fertiliser application  
412 (Ackerman et al 2018), sulphate deposition (Gauci et al. 2005) in regions like southern Africa  
413 and China with large coal-industry emissions, and perhaps also the complex impacts of  
414 human predation on wetland fauna. The fertilising impact of run-off from arable croplands  
415 into nearby wetlands by nitrogen fertilisers (Fowler et al. 2013) may be important. However,  
416 most boreal wetlands are far from farming drainage, while in many parts of the tropics,  
417 although fertiliser application in arable lands around wetlands is increasing rapidly (e.g.  
418 Uganda), the use of fertilisers is still very low compared to farming in northern temperate  
419 regions (Dangal et al, 2019; FAO 2017, IFAsat 2022).

420 In particular, CO<sub>2</sub> fertilisation of C3 plants may be important. There is evidence (Möller et al.  
421 2013) for CO<sub>2</sub> fertilisation impact in past transitions: the strong correlation between  $\delta^{13}\text{C}_{\text{CH}_4}$   
422 and CO<sub>2</sub> in the ice core record of the past 160 ka is much better than the correlation  
423 between  $\delta^{13}\text{C}_{\text{CH}_4}$  and CH<sub>4</sub>. This suggests CO<sub>2</sub> fertilisation was an active feedback in past  
424 changes by increasing plant productivity and hence microbial methane emissions during the  
425 initiation of interglacial episodes, with isotopic impacts favouring C3 plants (more negative  
426  $\delta^{13}\text{C}_{\text{CH}_4}$ ) over C4 grasses. Thus the glacial/interglacial  $\delta^{13}\text{C}_{\text{CH}_4}$  record may reflect *in situ* shifts  
427 in plant populations and productivity as well as shifts in the geographic loci of emission.  
428 However, on the modern planet this impact is difficult to assess. It is also likely that nitrogen  
429 cycle constraints and phosphorus availability may be progressively limiting the effect of CO<sub>2</sub>  
430 fertilisation (Wang, S. et al. 2020, Huntingford et al, 2022).

431 Wetland models have large uncertainties (Chang et al. 2023) and tropical wetland emissions  
432 may be much larger than hitherto inferred in land surface models of wetland methane  
433 sources (Shaw et al. 2022; Zhang et al. 2023; Nisbet 2023). Recent tropical wetland field  
434 campaigns that included both low-flying aircraft and on-ground sampling have shown that  
435 emissions from some wetlands are very substantial indeed. For example, overflying the  
436 Llanos de Moxos wetlands in Bolivian Amazonia in March 2019 (late wet season), France et  
437 al. (2022) found extremely large methane enhancements (500 ppb over background). These  
438 were inferred to have come from very high surface fluxes of methane. Annual emissions  
439 were estimated around 3.6 Tg/yr from the Llanos de Moxos wetlands. Further south, in the  
440 Pantanal wetlands of Brazil and Bolivia in the South American seasonal outer tropics, Gloor  
441 et al. (2021) used a planetary boundary layer budgeting technique to estimate the

442 Pantanal's total regional emissions of 2.0 to 2.8 Tg/yr, while their Bayesian inversion using  
443 an atmospheric transport model found even higher emissions of  $\sim 3.3$  Tg/yr.

444 At about the same southern outer tropical (seasonal) latitude in Africa, from an aircraft  
445 campaign in February 2019 (mid-wet season) in the Upper Congo Bangweulu wetlands of  
446 Zambia, Shaw et al. (2022) derived very large emissions of 1.2 to 3.0 Tg/yr. Bangweulu is  
447 only part of the Upper Congo's extensive suite of wetlands. Emissions from Zambezi basin  
448 wetlands were also significant (Shaw et al. 2022). This work suggests total emissions from  
449 wetlands in the Congo and Zambezi basins may be very large. Interestingly the regional  
450  $\delta^{13}\text{C}_{\text{CH}_4}$  isotopic signatures of emissions of outer (single rainy season) tropical C4/C3  
451 wetlands in Zambia and Bolivian Amazonia were very similar, around  $-59\text{‰}$  to  $-60\text{‰}$  (France  
452 et al. 2021, MOYA team et al. 2021), presumably reflecting the similarity of the seasonal  
453 outer tropical C4/C3 vegetation mix.

454 Unfortunately, on-ground or low-level aircraft/UAV *in situ* monitoring of major tropical  
455 wetlands is inadequate (Ringeval et al. 2014, Nisbet 2023), so it is not possible to use *in-situ*  
456 monitoring to confirm year-on-year changes. From satellite observations, Lunt et al. (2021)  
457 found strong XCH<sub>4</sub> enhancements in East Africa consistent with large positive seasonal  
458 precipitation anomalies. Zonal observations from remote stations of the NOAA network  
459 (Nisbet et al. 2016, 2019) broadly support the findings of increased wetland emissions.  
460 Interannual rainfall and temperature variability can be very large (Lunt et al 2021, Peng et  
461 al., 2022, Palmer et al. 2023), depending on shifts in the position and intensity of the Inter-  
462 Tropical Convergence Zone (ITCZ). Thus expansion and intensification of the tropical Hadley  
463 cell circulation can have dramatic impacts on methane emissions.

464 To turn to bottom-up assessments, Zhang et al. (2023), applying climate data from  
465 meteorological stations and reanalysis in a land surface wetland model, found that climate  
466 change impacts increased annual wetland emissions by 8-10 Tg/yr in 2007-2021 compared  
467 to the 2000-2006 level. Specifically, they also found huge positive anomalies of 14-26 Tg in  
468 2020 and 13-23 Tg in 2021, and that tropical methane emissions contributed a large part of  
469 methane's growth in those two years. For the single year between 2019 and 2020, the  
470 bottom-up estimate of Peng et al. (2022) found an increase in wetland emissions of  $6.0 \pm 2.3$   
471 Tg. Their top-down 3D atmospheric inversion gave a global increase in surface emissions of  
472  $6.9 \pm 2.1$  Tg/yr between 2019 and 2020, which they also mostly attributed to increased  
473 wetland emissions. These very large increments are consistent with the hypothesis that  
474 growth has been supercharged by precipitation in the unusual 2020-2022 La Niña "triple  
475 dip" event (NOAA 2023b, McPhaden et al. 2023), though it should be noted that earlier  
476 intense La Niña events did not coincide with years of especially extreme methane growth.

477

478 **Table 2: Anthropogenic methane emissions in the years 2000, 2010 and 2020 and decadal**  
479 **growth rate in the last two decades.** Data from EDGARv7.0 (EDGAR, 2023, Crippa et al.,  
480 2021)

481

IPCC sector	Emission Tg yr <sup>-1</sup> CH <sub>4</sub>			Growth rate (Tg CH <sub>4</sub> yr <sup>-2</sup> )		
	Year	2000	2010	2020	2000_2010	2010_2020
1 Energy		103.51	123.98	137.42	2.05	1.34
2 Industrial processes and product use		0.19	0.33	0.49	0.01	0.02
3 Agriculture, forestry and other land use		137.41	151.93	162.47	1.45	1.05
3A1 Enteric Fermentation		91.70	101.69	111.03	1.00	0.93
3A2 Manure Management		10.87	11.69	12.54	0.08	0.08

3C1 Biomass Burning	1.35	1.71	1.96	0.04	0.03
3C7 Rice Cultivations	33.49	36.84	36.94	0.33	0.01
4 Waste	62.72	70.60	83.58	0.79	1.30
4A Solid Waste Disposal	29.64	30.65	35.65	0.10	0.50
4B Biological Treatment of Solid Waste	0.17	0.23	0.28	0.01	0.01
4C Incineration and Open Burning of Waste	1.14	1.32	1.55	0.02	0.02
4D Wastewater Treatment and Discharge	31.76	38.40	46.10	0.66	0.77
5 Other	0.15	0.15	0.15	0.00	0.00
Total anthropogenic	303.98	346.99	384.11	4.30	3.71
Total 'microbial anthropogenic' (excluding FF etc)*	197.98	219.98	243.18	<b>2.2</b>	<b>2.3</b>

\* excludes Energy (1), Biomass burning (3C1), and Incineration and open burning of waste (4C).

482

483

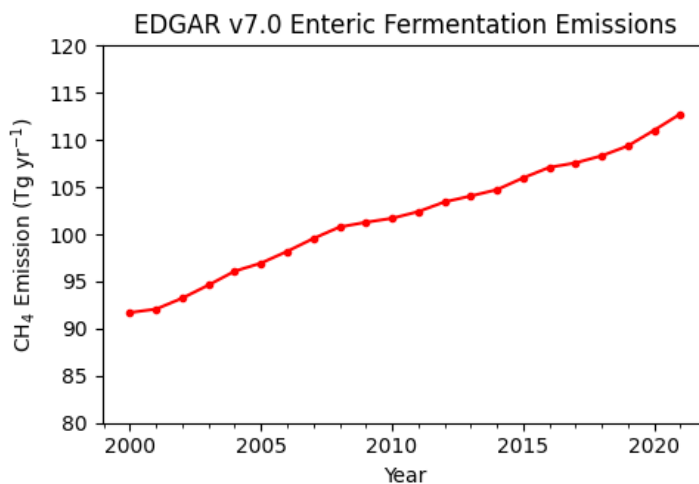
484

## 5. Agricultural, biomass burning, and waste emissions

485 Agriculture is a major source of biogenic methane emissions, from cattle breath ( $\delta^{13}\text{C}_{\text{CH}_4}$   
 486 slightly more negative than the bulk methane burden), wetland rice cultivation, and biomass  
 487 burning ( $\delta^{13}\text{C}_{\text{CH}_4}$  much more positive than the burden)(for isotopic signatures of sources see  
 488 Dlugokencky et al., 2011, Nisbet et al. 2016, 2019, MOYA/ZWAMPS Team 2021).

489 Livestock emissions are growing but the rate of growth is difficult to quantify. Zhang et al.  
 490 (2022) estimated, with uncertainty around 20%, that methane emissions from global  
 491 livestock populations were around 105 Tg in 2000, 121 Tg in 2011, and 132 Tg in 2019,  
 492 growing by 27 Tg from 2000-2019, or 1.4 Tg/yr/yr. Using an inversion framework to verify  
 493 methane emissions from satellite-based observations, Worden et al. (2023) reported a  
 494 growth rate of livestock emissions of 0.25 to 1.3 Tg/yr/yr. The growth rate they estimated  
 495 was similar to EDGAR results, although Worden et al. (2023) considered the EDGAR  
 496 assessment had underestimated livestock emissions. From 2000-2020, the EDGAR (2023)  
 497 assessment finds an increase in emissions from enteric fermentation of 20 to 21 Tg, (Fig. 6),  
 498 with another 2 Tg increase from animal manure (EDGAR 2023) but no significant  
 499 acceleration in the rate of increase in the past decade. Our assessment (Fig. 6) of growth in  
 500 ruminant emissions from enteric fermentation, estimated from the EDGAR (2023) database,  
 501 is nearly 1 Tg/yr/yr for 2000-2020 (Table 2), somewhat less than the Zhang et al. (2022)  
 502 estimate but within the very wide uncertainties.

503 *Figure 6. Estimated growth in methane emissions from enteric fermentation (ruminants),*  
 504 *from EDGAR (2023). See Table 2. Recent (2010-2021) growth rate about 1 Tg/yr/yr.*



505

506 The densest cattle populations are in South Asia, tropical Africa and tropical South America.  
 507 Livestock population growth will be facilitated by increased grazing and browsing  
 508 productivity in a warmer wetter climate. However, it is not clear how much agricultural  
 509 expansion in the tropics has increased total land surface methane emission. Africa and more  
 510 recently South America are undergoing a widespread transition from a complex 'natural'  
 511 ecology of diverse ruminants and pseudo-ruminants to a now human-dominated pastoral  
 512 system of cattle, goats and sheep (e.g. see Zhang et al. 2022).

513 In the 'natural' African ecology, ruminants from browsing giraffe to grazing buffalo exploit all  
 514 parts of the floral variety. In contrast, in cattle-dominated monocultures, where most or all  
 515 natural ruminants are eliminated, food production specifically for the very rapidly growing  
 516 human populations will have increased, but the total body mass per unit area of the  
 517 ruminants that are producing methane may not be larger (e.g. see data in Taylor and Walker  
 518 (1978). Moreover, much tropical cattle manure falls on dry pastures in aerobic conditions  
 519 not supportive of methanogens, although it should be noted that in some parts of Africa  
 520 cattle are kept overnight in 'bomas' (corrals) where manure collects under urine and  
 521 methane emissions can be significant (Leitner et al. 2023). Thus the overall net change in  
 522 methane emissions from replacing an original productive and diverse natural ecology with  
 523 anthropogenic cattle or maize monocultures is unclear.

524 Biomass burning emissions come from incomplete combustion. The amount of  
 525 burning varies from year to year, which has significant impact on emissions (Worden et al.  
 526 2017). In the tropics, biomass fires are closely linked to changes in the Inter-Tropical  
 527 Convergence Zone and the ENSO cycle. Grassland fires (mainly C4 plants in the tropics) are  
 528 widespread in dry winters after good rainy seasons, often covering very large areas. Crop  
 529 waste fires also occur mainly in dry season, varying with precipitation in the previous wet  
 530 season. These fires, particularly of <sup>13</sup>C-rich tropical C4 crop plants like maize, sugarcane, and  
 531 millet, emit isotopically heavy methane.

532 Burning of tropical C3 woodland and forest also occurs, especially in clearing land. Tracking  
 533 biomass burning is difficult: satellite observation quantifies burnt area but it is more difficult  
 534 to assess fuel load and intensity of fire (especially important in crop waste fires). Barker et  
 535 al. (2020) found high variability in emissions measured in flights over active fires, with  
 536 methane emissions of  $1.8 \pm 0.19$  g/kg of fuel over outer-tropical Senegal, but  $3.1 \pm 0.35$  g/kg  
 537 over equatorial Uganda. Boreal biomass burning, in contrast, is mainly wildfire in northern  
 538 C3 forests, highly dependent on summer temperatures, and more easily assessed by remote  
 539 sensing.

540 'Biogenic' CO is mainly produced by biomass burning, but the CO record in the 2000-2010  
 541 decade is affected by Europe's decade of 'dieselisation' favouring diesel-fuel passenger cars,  
 542 which are low emitters of CO. Contrasting the period 2001–2007 to the 2008–2014, Worden  
 543 et al (2017) concluded biomass burning emissions of methane decreased by 3.7 ( $\pm 1.4$ ) Tg  
 544 CH<sub>4</sub> per year, and this drop may have contributed to the standstill in methane growth in the  
 545 early years of the 21<sup>st</sup> century. For the periods 2007-2012 and 2013-2017, inversions of both  
 546 mixing ratio and isotopic data suggest overall global pyrogenic emissions dropped slightly or  
 547 showed little change, (Zhang et al. 2021, comparison in Basu et al. 2022).

548 Much agricultural growth comes from expansion of farmed land area, displacing natural  
 549 ruminants from grasslands or cutting forest and draining wetlands and burning peatlands.  
 550 Thus, for tropical agricultural emissions it is difficult to allocate proportions of 'feedback-

551 driven' and 'technology-driven' emissions growth. The impact on crop yields and ruminant  
552 fodder supply of indirect factors such as CO<sub>2</sub> fertilisation and sulphate deposition, is not  
553 easily quantified.

554 Bottom-up (EDGAR 2023) inventories suggest anthropogenic emissions from wastewater,  
555 solid waste, and landfills are increasing worldwide. Despite successful efforts to reduce  
556 waste emissions in Europe and other regions, the rapid growth of tropical cities is driving  
557 increased urban waste disposal and these emissions are very poorly quantified (Nisbet et al.  
558 2020). Waste disposal in tropical cities is increasing in large poorly-managed landfills (Nisbet  
559 et al. 2020), but food waste comes from local agriculture, so waste emissions are linked to  
560 local agricultural productivity. In the EDGAR v7.0 inventory (EDGAR 2023) the estimated  
561 growth of annual solid waste and landfill emissions from 2006 to 2021 is about 5.7 Tg, while  
562 methane from wastewater has increased by about 11 Tg/yr over the same period.

563 The 'climate feedback' proportion of growth in emissions of methane from tropical  
564 agricultural and waste disposal is uncertain. Growth in ruminant and landfill biogenic  
565 emissions depends both on global change feedbacks (more productivity in a warmer,  
566 wetter, CO<sub>2</sub>-rich environment) and also on 'direct-action' factors increasing agricultural  
567 productivity such as nitrogen fertiliser application and genetic modification of seeds.

568 Overall, including solid and liquid waste, manure handling and enteric fermentation in  
569 agricultural ruminants, EDGAR inventory data (Table 2) suggest microbial methane  
570 emissions from anthropogenic activities rose each year by about 2.3 Tg/yr, or an increase of  
571 about 35 Tg from the end of 2006 to 2020. Although there is wide uncertainty on these  
572 bottom-up estimates, they appear broadly consistent with top-down estimates.  
573 Importantly, there is no evidence in the data for a sudden acceleration in the growth of  
574 agricultural and waste emissions post-2006.

## 575 **6. Inference: increased natural emissions are a major cause of recent** 576 **methane growth.**

577 Quantifying emissions from 'natural' sources as they respond to climate change is difficult.  
578 Ongoing experimental measurement of methane fluxes from wetlands is minimal, especially  
579 in Africa. An alternative is to use isotopic information to assess global total (i.e. natural and  
580 anthropogenic) biogenic emissions and then subtract bottom-up estimates of emissions  
581 from biogenic sources under anthropogenic control, with the caveat that these too respond  
582 to climate warming.

583 Studying the period 1999-2016, Basu et al. (2022) estimated methane's 2008-2014 rise was  
584 driven by global emissions growth of  $27.1 \pm 0.6$  Tg yr<sup>-1</sup> or, nearly 4 Tg/yr/yr. They found the  
585 negative shift in  $\delta^{13}\text{C}_{\text{CH}_4}$  can be balanced by assuming about 15%, or 50 Tg, of the recent rise  
586 is from growth in fossil fuel emissions (i.e. with  $\delta^{13}\text{C}_{\text{CH}_4}$  more positive than the methane  
587 already in the air). Comparing the period 2007-2012 with the period 2013-2017, Basu et al.  
588 (2022) found an increase in biogenic emissions of  $32.3 \pm 3.2$  Tg/yr. After 2017 and especially  
589 in 2020-2023, the burden grew more rapidly.

590 Similarly, looking at the surge in growth in 2019-2020, using a global inverse analysis of  
591 GOSAT satellite observations, Qu et al. (2022) found the imbalance between sources and  
592 sinks of methane increased by 31 Tg in the year 2019-20. They found that half the growth in  
593 methane emissions in 2019-2020 took place in Africa, especially East Africa, most likely from  
594 wetlands, with strong emissions growth in Canada also. For the year 2020, Qu et al. (2022)

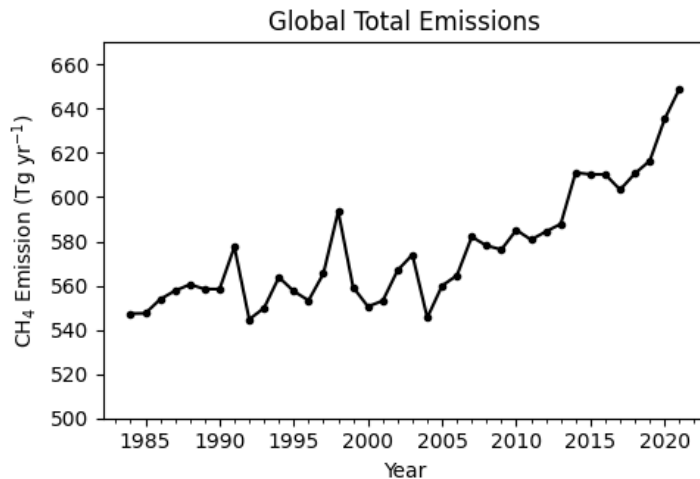
595 attributed 86±18% of the growth surge to increased emissions, especially from wetlands in  
 596 Africa (15 Tg/yr) and Canada and Alaska (4.8 Tg/yr), although there was also evidence for  
 597 14% of the growth coming from a decrease in methane's [OH] sink, to which also Stevenson  
 598 et al. (2022) attribute part of methane's growth in 2020. Overall, Qu et al. (2022) found total  
 599 emissions grew by 25–37 Tg/yr in 2019-2020. If their estimate that about 86% of growth  
 600 was biogenic is accepted, then the growth in biogenic emissions in 2019-2020 was as large  
 601 as 22-32 Tg.

602 Drinkwater et al. (2023), over the period 2004-2020, used *in situ* data to estimate a global  
 603 annual emission increase of 93 Tg/yr over the period (620 Tg/yr minus 527 Tg/yr), with 83%  
 604 of that increase occurring since 2011 when the global growth first began to accelerate.  
 605 Assuming 2.3 Tg/yr/yr of growth is from anthropogenic microbial sources, increased  
 606 wetland emissions will be responsible for the balance of emissions growth, of 2 to 2.5  
 607 Tg/yr/yr (with very wide uncertainty). Note also that the acceleration of methane's rise from  
 608 2020 implies the growth rate of emissions was much higher in 2020-2022.

609 More broadly, accepting the estimates of Basu et al. (2021) and Qu et al. (2022), and  
 610 extrapolating to end-2022, a very rough guess is that about 70-80 Tg/yr of the global  
 611 emission increase between 2006 and end-2022 came from specifically microbial sources,  
 612 both natural and anthropogenic. As detailed above, microbial emissions from anthropogenic  
 613 agricultural and waste sources have probably increased between 2006-2020 by about 35  
 614 Tg/yr (assuming linear growth, Fig. 6 and Table 2). If this is correct, the remaining recent net  
 615 growth in methane emissions is not likely to be primarily attributable to agricultural  
 616 expansion but has been driven by 'natural' biogenic processes, especially wetland feedbacks  
 617 to climate change.

618 Fig. 7 updates estimated emissions into the 2020s, using the methodology of Lan et al  
 619 (2021a) and Basu et al. (2022). Subtracting (say) 35 Tg for growth over this period in  
 620 anthropogenic emissions from agriculture and waste, the growth in 'natural' biogenic  
 621 emissions may have been 35-45 Tg. More generally, if total biogenic emissions continue to  
 622 accelerate at the same rate as in the period 2006-2022 (a very large assumption), then by  
 623 the year 2037, 30 years after the start of growth, specifically biogenic emissions might have  
 624 grown by perhaps 150 Tg/yr.

625 *Figure 7. Global methane emissions, estimated and updated using the top-down*  
 626 *methodology of Lan et al. (2021a) and Basu et al. (2022). For further details, see*  
 627 *supplementary information in Lan et al. 2021a, Fig S2b, red curve, updated.*



628

629

## 7. Glacial Terminations

630 During the past half-million years, several "termination" events have marked rapid changes  
 631 of global climate from cold glacial to warmer inter-glacial conditions. Terminations were  
 632 rapid major reorganisations of the Earth's climate systems, with degassing of upwelling  
 633 oceans and revival of a warmer biosphere (Broecker and van Donk, 1970; Raymo 1997;  
 634 Cheng et al. 2009; Denton et al. 2010; Lang and Wolff 2011, Schmitt et al. 2012). They are  
 635 characterised by very large-scale shifts of global and regional weather circulation patterns,  
 636 for example from glacial climates toward a more La Niña-like state (Cheng et al 2020).

637 Broecker and Denton (1990) interpreted 'terminations' in the broadest terms, as global-  
 638 scale climate reorganisations, which were synchronous with sharp changes in the methane  
 639 burden. likely driven by wetland emissions (Nisbet 1990, Nisbet and Chappellaz 2009). The  
 640 modern palaeoclimate understanding of a recognised 'Termination', named in Roman  
 641 numerals from I (youngest) to IX (nearly 800 ka ago) refers to specific transitions from glacial  
 642 to interglacial periods that took place about every 100 ka. In the finer detail of the glacial  
 643 record are Dansgaard-Oeschger (D-O) events, which were abrupt warming events, with  
 644 sharp temperature rises over decadal timescales, followed by slow relaxation over  
 645 millennia. These D-O events were very rapid, with decadal progression (Erhardt et al. 2019).  
 646 While Dansgaard-Oeschger events occurred within glacials and were likely linked to rapid  
 647 changes in sea ice cover (Boers et al. 2018), the numbered Terminations marked global-  
 648 scale climate changes.

649 Although full terminations took several millennia before the new warmer interglacial  
 650 climate was established, the transitions typically included brief abrupt phases when  
 651 methane growth and climate warming was very rapid indeed. It is likely that the new  
 652 warmer weather patterns became established within a few centuries or less (Severinghaus  
 653 et al. 1998), although it took millennia for the great ice domes to melt and, by their  
 654 shrinking, to change boreal albedo and replace ice with wetlands and forest, thus  
 655 completing the full climate transition of the termination.

656 Sudden methane growth is the bellwether of these changes (Möller et al. 2013, Bock et al.  
 657 2017). Methane emissions are very responsive to climate (Nisbet 1990, Petrenko et al. 2009,  
 658 Nisbet & Chappellaz 2009). Methane's growth record during glacial-interglacial Terminations  
 659 V to I (Fig. 8 and Table 3) is preserved in bubbles in ice cores (Spahni et al. 2005, Wolff et al.

660 2009, Möller et al. 2013, Bock et al. 2017). The methane record correlates with monsoonal  
661 patterns as observed in oxygen isotope records in stalagmites (Cheng et al. 2009).

662 During Termination IA ending the Younger Dryas, methane rose abruptly by ~250ppb, with  
663 essentially synchronous high-latitude and low-latitude climate change (Capron et al. 2021).  
664 Ice core data imply emissions increases as large as 6 to 21 Tg/year  
665 causing methane growth rates as high as 6 ppb/yr (Rhodes et al. 2015). It is likely methane's  
666 rapid growth was primarily driven by rising tropical emissions, responding to abrupt changes  
667 in tropical rainfall (Schaefer et al., 2006; Möller et al. 2013, Bock et al. 2017, Riddell-Young  
668 et al. 2023).

669 Feedback loops in the methane budget rapidly respond to global-scale climate change. It is  
670 likely that both warming and climate shifts such as intensification of ENSO events would  
671 have especially driven emissions in the tropics where both wetlands and regional land  
672 vegetation respond quickly to increased warmth and rainfall, wetland productivity  
673 increasing synchronously with parallel expansion of methane-emitting (Clauss et al. 2020)  
674 populations of ruminants (buffalo, antelope) and pseudo-ruminants (hippoipotamoi).

675 Figure 8 shows the changes in methane and  $\delta^{13}\text{C}_{\text{CH}_4}$  in selected past terminations, showing  
676 data updated from Bock et al. 2017; see also Möller et al. (2013). Initially, at the start of a  
677 typical termination, there was a gradual rise in methane and  $\text{CO}_2$ . This rise was accompanied  
678 by a negative shift in  $\delta^{13}\text{C}_{\text{CH}_4}$ , which covaried with  $\text{CO}_2$ , as was characteristic during glacials,  
679 and with  $\text{CH}_4$ . This gradual phase lasted a few thousand years.

680 In typical terminations the brief abrupt phase, with sharp growth in methane, In typical  
681 terminations the brief abrupt phase with its sharp growth in methane by several 100 ppb  
682 did not leave a significant imprint in the  $\delta^{13}\text{C}_{\text{CH}_4}$  record (Schaefer et al. 2006; Möller et al.  
683 2013, Bock et al. 2017) indicated with arrows in Fig. 8. This pattern is consistent with the  
684 interpretation that methane emissions growth was dominated by equatorial wetland which  
685 has  $\delta^{13}\text{C}_{\text{CH}_4}$  close to the global bulk source (Brownlow et al. 2017, Ganesan et al, 2019,  
686 Nisbet et al. 2021a,b, France et al. 2021, Oh et al. 2022). Methane's sharp growth in the  
687 abrupt phase is thus best explained by a rapid increase in emissions from tropical wetlands  
688 emitting methane with  $\delta^{13}\text{C}_{\text{CH}_4}$  close to that of the bulk atmosphere (i.e. especially in the  
689 equatorial zone) (Bock et al. 2017).

690 Switching on tropical wetlands was likely associated with a rapid shift in the ITCZ that  
691 coincided with resumption of a strong Atlantic Meridional Overturning Circulation (AMOC)  
692 at the start of interglacial climate conditions, initiating a warmer northern hemisphere and  
693 generally stable climate with subdued millennial-scale variability. The AMOC 'flip' is denoted  
694 in Fig. 8 by vertical dashed lines, and essentially marked the crux of the termination,  
695 although it took millennia for sea level to rise as the great ice domes in Canada and  
696 Scandinavia melted. During the 'flip' phase, there was typically a rapid increase of about 200  
697 ppb in methane mixing ratio, but only a relatively small change in  $\delta^{13}\text{C}_{\text{CH}_4}$ .

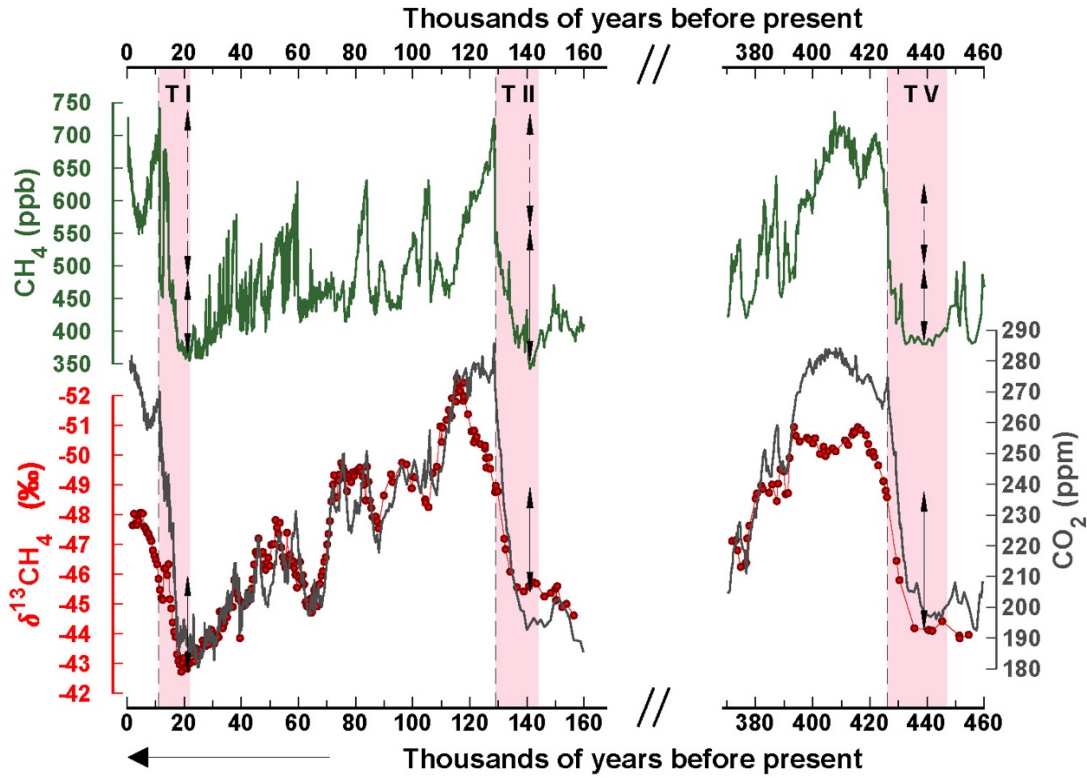
698 AMOC changes and consequential meridional heat transport anomalies have been a feature  
699 of past episodes of abrupt global climate shifts (Cheng et al. (2007). For example, Riveiros et  
700 al. (2013), and Rhodes et al. (2015) showed that AMOC slowdown is capable of producing  
701 atmospheric responses that extend throughout the Northern Hemisphere and into the  
702 tropics, with strong coupling between the two regions. Though very different from today's  
703 changes, the 32 ppb rise in atmospheric methane during the HS 1 event reported by Rhodes

704 et al. (2015) has interesting parallels with modern shifts, including both weakening of AMOC  
 705 and southern expansion of the ITCZ and Hadley cell. However, there are also large  
 706 differences: in HS1 there was boreal cooling as the ITCZ moved southward; in the present  
 707 event the north is warming strongly.

708 Although there are many possible explanations of this sequence of events, the pattern is  
 709 consistent with a wider scenario beginning with initial modest Hadley cell expansion during  
 710 interdecadal variation, bringing about more methane emission from wetter outer tropical  
 711 swamps ( $\delta^{13}\text{C}_{\text{CH}_4}$  perhaps very roughly  $-60\text{‰}$  in cool conditions). Then in response, changes  
 712 in AMOC, the Walker circulation and the Indian Ocean Dipole (Abram et al. 2020, Brierley et  
 713 al. 2023), may have brought about intensification of equatorial rainfall and consequent  
 714 rapid growth in equatorial wetland emissions, initiating methane's abrupt rise.

715 Thus in this scenario of the abrupt phase of a glacial termination, the growth of wetlands  
 716 under strong equatorial rainfall will rapidly increase the atmospheric methane burden but  
 717 be accompanied by only subdued initial leverage on  $\delta^{13}\text{C}_{\text{CH}_4}$ . Then, as the boreal realm  
 718 warms, northern methane sources with more negative  $\delta^{13}\text{C}_{\text{CH}_4}$  begin to contribute. Note  
 719 that in an end-glacial scenario the presence of large ice domes over Canada and Scandinavia  
 720 inhibited development of boreal vegetation: in these areas boreal wetlands were not  
 721 functioning until millennia later when the ice melted. Today, the boreal and Arctic wetlands,  
 722 which emit methane with markedly negative  $\delta^{13}\text{C}_{\text{CH}_4}$ , are very productive and are  
 723 experiencing strong warming (Previdi, et al. 2021).

724 *Figure 8. Ice core records from Terminations I, II and V. Modified from Bock et al. 2017 and*  
 725 *updated. Note synchronicity of CH<sub>4</sub> rise with negative shift in  $\delta^{13}\text{C}_{\text{CH}_4}$  (plotted upwards on y-*  
 726 *axis). Solid arrows denote the CH<sub>4</sub> from the start of a Termination to the point of the growth*  
 727 *flip. Dashed arrows mark the corresponding CH<sub>4</sub> change in the abrupt flip. CO<sub>2</sub> record is*  
 728 *from Bereiter et al. (2015) and CH<sub>4</sub> from Loulergue et al. (2008) with updates from Bock et*  
 729 *al. (2017).*



730

731

732 **Table 3: Synopsis of Termination changes**

733 *Summarised here from methane records detailed in Section 7, particularly Bock et al. 2017.*

734 *Assumes 1 ppb is equivalent to 2.77 Tg methane.*

735

Event	Approximate Date (ka BP) of abrupt phase	Change over whole termination ppb (approx.)	CH <sub>4</sub> Change over whole termination Tg (approx.)	Maximum Growth rate ppb/yr (approximate)	δ <sup>13</sup> C <sub>CH<sub>4</sub></sub> shift over whole termination (approximate)
<b>PAST</b>					
Termination IA	11.64	250	700-	> 2.5	-3.5‰
Termination IB	14.65	150	400-450	> 2	
Termination II	131	350	900-1000	> 2.5	-4.5‰
Termination III	250	300	800-850		
Termination IV	345	400	1100		
Termination V	430	350	900-1000		-5‰
<b>MODERN</b>					
Modern	2006-2022-?	135	374 318 (biogenic 85% component)	~ 9 (Between 6 and 18 ppb)	-0.7‰
Model to 2035	2006 to 2035	573	1584	10	-1.1‰ (roughly equivalent to -4.4‰ if injected into much smaller glacial burden)

736

737 Over full terminations, negative drops in  $\delta^{13}\text{C}_{\text{CH}_4}$  ranged between -5‰ to -3‰ (Bock et al.  
 738 2017). For example, in Termination V,  $\delta^{13}\text{C}_{\text{CH}_4}$  dropped from about -44‰ to -49‰, while in  
 739 Termination II there was a similar negative shift (Bock et al. 2017). Again, at the start of the  
 740 Preboreal Holocene  $\delta^{13}\text{C}_{\text{CH}_4}$  shifted from about -43‰ in full glacial conditions, to about -  
 741 46.3‰ (Fischer et al. 2008, Melton et al. 2012; Bock et al. 2017).

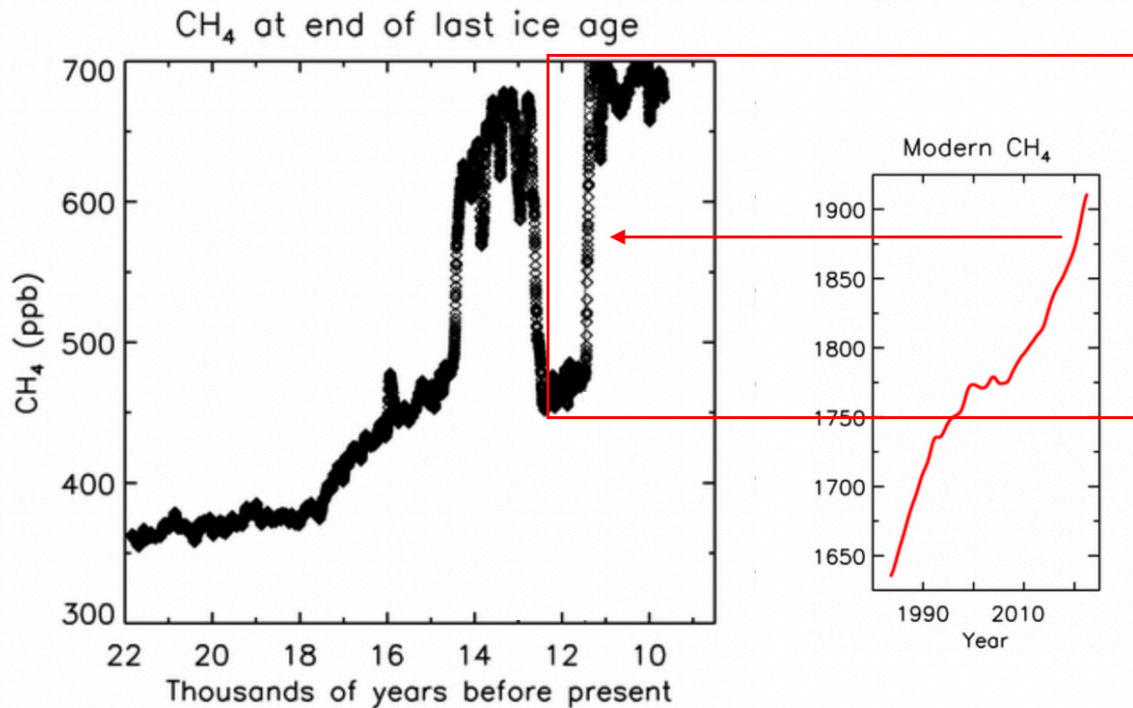
742 To consider the older events first, the abrupt phase of Termination II took place between  
 743  $130.9 \pm 0.9$  and  $130.7 \pm 0.9$  ka ago (Moseley et al., 2015), with contemporary strengthening  
 744 of the monsoon. In Terminations II and III the methane burden rose by roughly 500-600Tg in  
 745 sudden growth events. During similar abrupt rises in Terminations IV and V, methane rose  
 746 from about 400ppb to 700ppb, or more, increasing the methane burden by 800-900Tg.

747 The most recent termination was in multiple phases (Fig.9 left panel). In the abrupt part of  
 748 Termination 1B, which ended the last major glaciation, the Greenland Summit climate  
 749 rapidly warmed by  $9 \pm 3^\circ\text{C}$ , and 20-30 years later methane rose abruptly (Severinghaus and  
 750 Brook, 1999). Methane rose quickly over the sixty years between 14,655 and 14,595 BP,  
 751 with especially rapid growth in the decade from 14,655 - 14,645 BP (Severinghaus and Brook  
 752 1999). This change initiated the Bølling–Allerød interstadial, until 12.87 thousand years BP,  
 753 when the Younger Dryas began, with sudden cooling of the North Atlantic realm linked to a  
 754 drop in methane to 450-500 ppb. Then, ending the Younger Dryas, the abrupt warming  
 755 event of Termination 1A took place between  $\sim 11,700$  and 11,610 B.P, with the fastest  
 756 change about 11.64 thousand years ago (indicated by vertical line in Fig. 8). About 0-30  
 757 years after this warming began, methane rose sharply to above 700 ppb (Severinghaus et al  
 758 1998; Cheng et al. 2020). In all, methane rose as much as 250 ppb in little over a century, an  
 759 increase of about 700 Tg in the burden.

760 *Figure 9. Comparison between Methane's record during Termination 1 and methane's*  
 761 *growth since 1980s. Note – these plots are not to the same time scale.*

762 *Left panel: Methane record during Termination 1. Prior to about 17ka before the present,*  
 763 *methane was below 400 ppb (from various sources: see text). Methane rose in Termination*  
 764 *1B, especially in the abrupt phase about 14.65 kyr ago. The Younger Dryas. 12 ka ago, saw a*  
 765 *return to cold conditions, especially in the northern North Atlantic, abruptly ended in*  
 766 *Termination 1A, 11.64 kyr ago, date shown by vertical line.*

767 *Right panel: modern methane record. Growth prior to 2006 shows convex equilibration*  
 768 *trend; growth from 2006 shows concave (accelerating) trend (NOAA data). Note time scales*  
 769 *not the same.*



770

771 There is evidence for strong growth in tropical (30°S to 30°N) methane emissions during  
 772 Termination 1 (Riddell-Young et al. submitted 2023, Baumgartner et al 2012), as tropical  
 773 wetlands responded to an abrupt expansion of tropical rain belts. Methane output may  
 774 have risen from perhaps 60 Tg/yr during glaciation to 120 Tg/yr or more in the post-  
 775 termination Holocene. That global increase of 60 Tg across the whole event can be  
 776 compared to the present-day estimate derived above that 'natural emissions' have  
 777 increased by about 35-45 Tg since 2006. Riddell-Young et al. (submitted 2023) and  
 778 Baumgartner et al. (2012) also found evidence for a supplementary role of emissions from  
 779 boreal methane sources, findings prescient of the present-day results of Qu et al. (2022).  
 780 Similar patterns are also inferred from the weak inter-polar gradient for methane in  
 781 Termination 1B which suggests methane growth was driven by a major tropical input  
 782 (Severinghaus and Brook 1999).

783 In addition to termination events, examples of rapid changes in atmospheric methane, in  
 784 which methane rose by 32-53 ppb, are also recorded in Heinrich events during glacial  
 785 periods. Though not analogous to present-day conditions, the rapid methane changes are  
 786 instructive as they show how responsive methane emissions are to climate shifts. Heinrich  
 787 events are marked by layers of ice-rafted debris in the North Atlantic seabed record, that  
 788 must have been dropped by armadas of icebergs breaking off the ice sheets over Greenland  
 789 and North America. Studying the HS1 event (16.15 kyr BP), which occurred near the end of  
 790 the last major glacial period, Rhodes et al. (2015) inferred a marked southerly shift in the  
 791 Inter-Tropical Convergence Zone had taken place in response to Northern Hemisphere  
 792 cooling and greater sea-ice cover, causing a major expansion in southern hemisphere  
 793 wetlands, which in turn drove a rapid increase in methane emissions by 29 Tg/yr.

794 To conclude, the methane and  $\delta^{13}\text{C}_{\text{CH}_4}$  records of glacial/interglacial events are consistent  
 795 with the hypothesis that the abrupt phase of methane growth was driven by a very rapid  
 796 biogenic response, mainly from tropical wetlands.

797 **8. Meteorological Changes**

798 Meteorologically, past termination events may have originated in specific regional locations  
 799 and then spread globally. For example, in the North Atlantic realm, the rapid meteorological  
 800 changes in the most studied abrupt termination event, the end of the Younger Dryas (T1A),  
 801 may have been a consequence of a set of changes originating in the tropics and then  
 802 spreading to include the North Atlantic, the Asian Monsoon and the Westerlies (Cheng et al.  
 803 2020). Moreover, model experiments typically show a spin-up time before any change has  
 804 impact on the global methane budget: thus for a methane signal to have become  
 805 identifiable in the period 2007-2022, the changes triggering the necessary spin up would  
 806 have been perhaps a decade or more ago.

807 If the post-2006 methane growth represents more than multi-decadal variability and is  
 808 indeed the start of a major long-term reorganisation of the planetary climate system, then  
 809 two questions arise: Can such global-scale modern meteorological changes be identified,  
 810 given that both short-term change and sustained regional multi-decadal variability are  
 811 characteristic of the Holocene climate (Wanner et al, 2008)? Are there today any direct signs  
 812 of incipient global-scale meteorological reorganisation?

813 Recent meteorological changes, though different in style and regional impact, may indeed  
 814 be similar in speed and planetary scale to global changes during termination events. During  
 815 2006-2020 the total Earth system has experienced a remarkable heating of  $0.76 \pm 0.2 \text{ Wm}^{-2}$   
 816 with about 89% of the heat stored in the ocean, 6% on land, 4% in the cryosphere and 1% in  
 817 the atmosphere (von Schuckmann et al. 2023). Even a small increase in the partitioning of  
 818 this heat into the air will have dramatic impact on global weather.

819 Arguably the most profound global-scale evidence for present-day climate warming comes  
 820 from the heat content of the upper part of the oceans (von Schuckmann et al. 2023), which  
 821 not only has a sustained and strong warming trend, but the rate of warming is accelerating  
 822 (Cheng et al 2023). Warming has been particularly anomalous in the South Atlantic, in the  
 823 North Atlantic offshore North America and in the Indian Ocean offshore Southern Africa.  
 824 Ocean heat produces evaporation and thus precipitation: wetlands will respond. The 'triple-  
 825 dip' La Niña of the first years of this decade must be a factor (McPhaden et al. 2023), while  
 826 multi-centennial variability of internal origin may also be important.

827 In recent years, there has been marked weakening of the Atlantic Meridional Overturning  
 828 Circulation (AMOC), in particular since 2005 (WMO 2023, Bonnet et al, 2021). Concurrently,  
 829 changes in the Walker circulation (El Niño /Southern Oscillation, ENSO) and the Indian  
 830 Ocean dipole have had profound impacts on tropical precipitation and temperature on land.  
 831 Hadley cell expansion has shifted the zone of tropical cyclones (Sharmila and Walsh 2018),  
 832 with poleward shifts in extra-tropical storm tracks and jets, and upper tropospheric  
 833 warming. As during glacial/interglacial transitions, and particularly in the abrupt 'flip' phase,  
 834 the Hadley circulation is expanding again today and the extension of the subtropical edge of  
 835 the Hadley circulation has already had impact on a wide range of extratropical biological  
 836 productivity (e.g. Pandey et al. 2017, Osland et al 2021). The poleward shifts of the  
 837 planetary circulation and the concurrent expansion of tropical weather systems are now  
 838 becoming well-documented (Staten et al. 2020, Grise et al. 2019, Voight et al. 2021,  
 839 Studholme et al. 2022).

840 Tropical weather systems are tightly interlinked (Cai et al. 2019, McPhaden et al. 2023), with  
 841 widespread major recent changes. Geng et al (2022) have suggested that increased ENSO  
 842 changes may emerge much sooner than hitherto expected, while Wang et al. (2019)

843 presented evidence for major shifts in the origination and strength of El Niño events, finding  
844 more frequent occurrence of extreme events since the 1970s and changes in ENSO onset  
845 from originating in the eastern Pacific to the western Pacific. McPhaden et al. (2023), Hasan  
846 et al. (2022) and Jo et al. (2021) suggested linkage between the Indian Ocean Dipole and  
847 Atlantic and Pacific conditions. Sun et al. (2022) present evidence for substantial increases in  
848 early onset of monsoon weather and positive Indian Ocean Dipole events, with dramatic  
849 impacts on regional flooding. For example, catastrophic rains and floods in East Africa in  
850 2019 came from a remarkable concatenation of meteorological factors, including record  
851 levels of the Dipole Mode Index, ENSO effects, anomalous zonal winds over the central  
852 Indian Ocean, very warm sea surface temperatures in the eastern Atlantic and Indian  
853 Oceans, and unusual zonal circulation (Nicholson et al 2022).

854 There have been recent large-scale shifts in the Indian Ocean Dipole (IOD) and unusual  
855 ENSO changes (Pandey et al. 2017). These weather changes have profound impacts on  
856 methane emissions. Feng et al. (2022) attributed much of the change in methane emissions  
857 over tropical South America and tropical Africa to IOD and ENSO shifts. Dramatic changes  
858 may be affecting the Indian Ocean Dipole, which plays a major role in controlling rainfall  
859 over the wetlands of east sub-Saharan Africa (Feng et al, 2022), with recent trends towards  
860 more frequent and intense positive events (Abram et al. 2020). During strong La Niña  
861 episodes, rainfall can deeply fill wetlands, while during El Niño episodes various parts of  
862 Amazonia and East Africa have experienced changes likely related to climate warming, with  
863 longer dry- and shorter wet-seasons in some places, and fires spreading to areas that have  
864 not burned for millennia; the opposite taking place in other regions. In particular, rains in  
865 Eastern Africa have strong links to the ENSO cycle and are dependent on changes in the  
866 Walker circulation (Nicholson 2015) and Indian Ocean dipole, together with the strength of  
867 pulses of the Madden-Julien oscillation.

868 Polar climates are also changing rapidly (Łupikasza & Cielecka-Nowak, 2020) especially with  
869 Arctic amplification of warming (Previdi et al. 2021). Arctic sea ice is in very rapid retreat  
870 (Kim et al. 2023). Arctic amplification may be linked to a negative Northern Hemisphere  
871 Annular Mode, large scale circulation changes, and increased durations of weather patterns  
872 and extreme precipitation over the Northern Hemisphere (Liu et al. 2021). Weather patterns  
873 are shifting in continental interiors (IPCC 2021 their Fig. 8.11), with regional warming across  
874 Siberia (Wang et al 2022). Regional climate warming has had significant impact on plant  
875 productivity, promoting the greening of the tundra (Berner et al. 2020). Boreal and Arctic  
876 warming have had marked effects on temperature and precipitation over large swampy  
877 areas, for example in western Siberia (Gorbatenko et al 2020), presumably by increasing  
878 supplies of organic detritus and thus methanogen productivity.

879 These profound ongoing global-scale changes in the modern ocean and atmospheric  
880 circulation patterns have many parallels in past termination events (see Section 7 and Fig.  
881 8), though with the caveat that the modern world is profoundly different, especially in the  
882 absence of the major meteorological impacts of the large ice domes over Canada and  
883 Scandinavia. Thus any global-scale meteorological changes that occur in the next few  
884 decades will clearly be very different from the glacial/interglacial transitions. Yet perhaps  
885 there are analogies too, particularly in the paleoclimatological evidence that the global  
886 climate system can reorganise very rapidly indeed, over as short a time period as a few  
887 decades.

888 A further caveat: although the present-day meteorological changes are widespread and  
889 profound, clearly on an inter-hemispheric scale, and likely involving multiple interlinked  
890 teleconnections, they may yet still be within the multi-decadal or centennial spectrum of  
891 Holocene variability. Many major meteorological circulation patterns have only recently  
892 been identified and their record of change compared to the recent historic past remains  
893 poorly documented, although the IPCC (2021) Summary for Policymakers commented that  
894 evidence of observed change has strengthened since the previous assessment report. It is  
895 not clear that current climate extremes, though large, abrupt, and ongoing, and with potent  
896 impact on methane emissions (Feng et al 2022), are great enough in sum to be evidence for  
897 an ongoing global-scale meteorological reorganisation. A grand-scale meteorological  
898 progression of the type identified by Cheng et al. (2020) would be hard to identify from  
899 weather data while it took place, and likely only recognisable in retrospect. The evidence  
900 remains unclear.

901 Moreover, apart from the measurement of heat stored in the oceans (Cheng et al. 2023, von  
902 Schuckmann et al. 2023), it is difficult to quantify the total sum of change, nor to quantify  
903 the collective impact on global climate. But equally it is plausible that the multiplicity of  
904 recent events, their abruptness, and their power are circumstantial signs a major  
905 reorganisation of the global climate system has already begun. Like the heat of the oceans,  
906 the biogenic methane signal may be a telling summation, a bellwether that signals the onset  
907 of permanent global change, the end of the Holocene.

908 To summarise the results in Sections 1-8: In the period 2007-2022, methane's growth rate  
909 has been very high, with an overall concave (accelerating) trend and a significant negative  
910 shift in  $\delta^{13}\text{C}_{\text{CH}_4}$ . If the estimates given above of the growth in agricultural emission are  
911 accepted, then much of the new emissions that are driving this growth come from wetlands  
912 and other natural sources, as found by Basu et al (2022), Qu et al. (2022), Feng et al. (2022,  
913 2023), Peng et al (2022) and Rosentreter et al. (2021). If the "85% biogenic" estimate (Basu  
914 et al. 2022) continues to apply in the year 2022, growth from specifically biogenic emissions  
915 alone (i.e. growth from climate change feedbacks, both wetland and agricultural and waste)  
916 may have been 15 ppb, implying the present-day 'non-fossil fuel' growth trend by itself is  
917 significantly faster than the maximum growth rates in the ice core records (Table 2).

## 918 **9. Modelling**

### 919 **9.1 Modelling Methodology**

920 Is methane's growth since late 2006 now becoming comparable in scale and in cause to  
921 methane's growth during a termination event?

922 To address this question, modelling focussed on the question: what would happen to the  
923 methane burden and its  $\delta^{13}\text{C}_{\text{CH}_4}$  during the abrupt phase of a termination event, if the  
924 abrupt growth took place today? This is not a model to replicate the palaeoclimate record  
925 but to elucidate modern trends. Thus the model is set up with a modern distribution of  
926 wetlands, including both tropical and boreal wetlands (which were largely absent in glacial  
927 periods). The model is designed to match century-scale trends over a conceptual abrupt  
928 growth phase and to follow major emission variations.

929 A modified version of the model used in Nisbet et al. (2019) was used. The model is a  
930 running budget model with 4 semi-hemispheres and exchange rates between them  
931 consistent with the observed interhemispheric rate of mixing. Methane removal uses [OH]

932 destruction from Spivakovsky et al. (2000) with kinetic isotope exchange from Cantrell et al  
 933 (1990), Cl removal from Hossaini et al. (2016), and soil removal from Curry (2007). The  
 934 model was designed to examine changes in methane mole fraction and in methane's  
 935 isotopic content, averaged over four semi-hemispheric regions (30–90°S, 0–30°S, 0–30°N,  
 936 and 30–90°N), with exchange rates between them consistent with the interhemispheric  
 937 transport time. Fitting methane's carbon isotopic record is central to the modelling because  
 938 of the powerful insights  $\delta^{13}\text{C}_{\text{CH}_4}$  provides into changing methane sources (Craig et al. 1988).

939 We first modelled an abrupt ('flip') phase patterned on a the abrupt phase of a 'typical'  
 940 termination event, to understand its dynamics. Then, having characterized the abrupt phase  
 941 of a typical event, we used the model to match the current (21<sup>st</sup> century) growth record. The  
 942 model tracks the impact of a sharp increase in biogenic methane, to test whether it is  
 943 comparable to the sudden changes in a typical termination.

#### 944 **9.1.1 – Termination event model – changes in methane burden and $\delta^{13}\text{C}_{\text{CH}_4}$**

945 We simulated modern-type emissions growing over a time period of 30 years, into a  
 946 putative model of methane's glacial-like atmospheric burden to see if a 'termination-like'  
 947 pattern developed, not just replicating the growth in methane burden but also to  
 948 investigate the  $\delta^{13}\text{C}_{\text{CH}_4}$  isotopic consequences.

949 Biogenic sources used in each semi-hemisphere for the “Ice-age” and “Termination 1”  
 950 periods are scaled down from a modern scenario fitting recent  $\text{CH}_4$  and  $\delta^{13}\text{C}_{\text{CH}_4}$  data (Nisbet  
 951 et al 2019) and are not from glacial-period biosphere reconstructions, but the fossil fuel  
 952 contribution, taken as 30% of the total source at present (Lowe et al. 1988; Lassey et al.  
 953 2007), was omitted. Relative to the total, the distribution of  $\text{CH}_4$  sources by semi-  
 954 hemisphere was: 12.4% in 30-90°S (HSH); 27.7% in 0-30°S (LSH); 31.1% in 0-30°N (LNH) and  
 955 28.8% in 30-90°N (HNH). The analysis of geographic spread was not expected to be very  
 956 sensitive to the latitudinal distribution of fossil methane sources but the omitted recent  
 957 fossil fraction was taken as being distributed 20% : 40% : 40% in LSH : LNH : HNH. Omitting  
 958 the fossil fuel emissions source leaves a distribution for the other sources as: 17.7% in HSH;  
 959 31.0% in LSH; 27.3% in LNH; and 24.0% in HNH.

960 These proportions according to latitudinal zone applied to a global total source consistent  
 961 with sources scaled to give a global mean  $\text{CH}_4$  mixing ratio of 700 ppb for "post-transition"  
 962 and 400 ppb for 'initial' conditions. The initial scenario also reduced the 30-90°N (HNH)  
 963 region source further because cold temperatures restricted land plants and especially  
 964 wetland areas. Global average results are not particularly sensitive to how much the HNH  
 965 region is reduced relative to the global total source, but results are shown for the HNH  
 966 region source being reduced from 24% to 16% of the total with the other 8% distributed  
 967 equally over LNH and LSH.

968 The isotopic signatures of the “Initial” (i.e. pre-transition) sources (S), here termed  $\delta^{13}\text{C}_\text{S}$ , are  
 969 taken as having  $\delta^{13}\text{C}_\text{S}$  4‰ heavier than present sources, and the source pulse of increased  
 970 emission leading into the transition is taken as having  $\delta^{13}\text{C}_\text{S} = -59\text{‰}$ , a value typical of  
 971 modern outer (seasonal) tropical wetlands (France et al. 2021, MOYA/ZWAMPS Team 2021).  
 972 The transition between the "interglacial" and "glacial" states of the global methane budget  
 973 is done with a constant rate of change in the source, and its  $\delta^{13}\text{C}_{\text{CH}_4}$ , over 30 years. Mixing  
 974 ratio, source emissions,  $\text{Src}$  (Tg/yr), source signatures for  $\delta^{13}\text{C}_\text{S}$ , and atmospheric  $\delta^{13}\text{C}_{\text{CH}_4}$ ,  
 975 here termed  $\delta^{13}\text{C}_\text{M}$ , are summarised in Table 4.

976 **Table 4: Source emissions,  $\delta^{13}\text{C}_s$ , mixing ratios and atmospheric  $\delta^{13}\text{C}_M$  in modelled 'Initial'**  
 977 **(pre-transition) to post-transition ('Post') values**

	Source Tg/yr (running annual average)					Source $\delta^{13}\text{C}_s$ ‰				
	30-90°S	0-30°S	0-30°N	30-90°N	Global	30-90°S	0-30°S	0-30°N	30-90°N	Global
Initial	23.6	46.7	41.8	21.4	133.5	-49.8	-50.8	-51.7	-56.4	-51.8
Post	30.9	78.2	79.6	45.1	233.7	-53.8	-54.3	-54.8	-57.5	-55.0
	Mixing ratio ppb (running annual average)					Atmospheric $\delta^{13}\text{C}_M$ ‰				
	30-90°S	0-30°S	0-30°N	30-90°N	Global	30-90°S	0-30°S	0-30°N	30-90°N	Global
Initial	408.6	403.5	396.7	393.8	400.7	-44.7	-44.7	-44.7	-44.82	-44.75
Post	694.2	695.1	698.9	699.9	697.0	-47.9	-47.9	-48.0	-48.0	-48.0

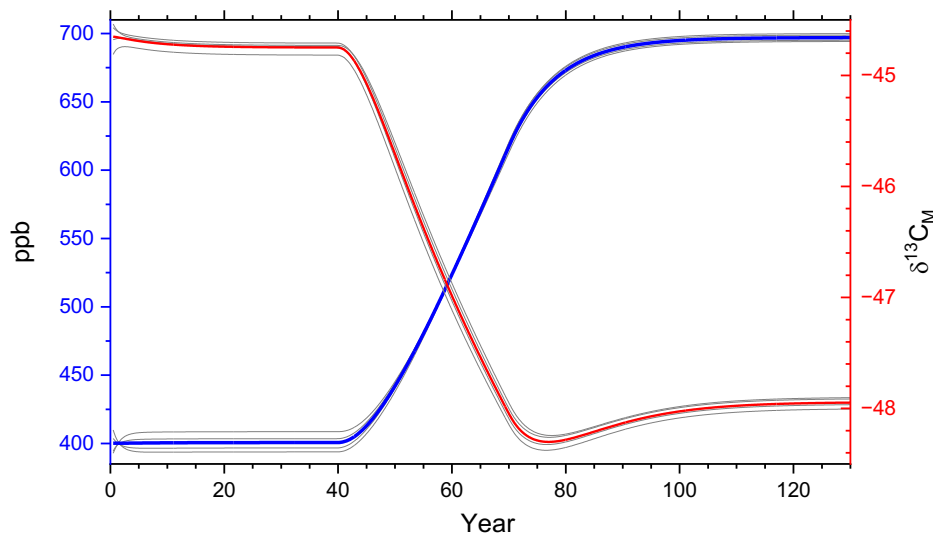
978

979 **9.1.2 Modelling Results.**

980 Plots of the changes in methane mixing ratio and  $\delta^{13}\text{C}_{\text{CH}_4}$  in the modelled 'Source-jump'  
 981 *Scenario* (Table 4), are shown in Figures 10a and 10b. This sequence of events is broadly  
 982 similar to the real records of the methane burden in typical glacial terminations. The  
 983 isotopic results reflect the very rapid growth of emissions from all latitude zones, both  
 984 tropical and boreal. The isotopic results show the 'Tans effect' (Tans 1997), with changes in  
 985  $\delta^{13}\text{C}_M$  overshooting followed by a slow recovery – i.e. with  $\delta^{13}\text{C}_M$  taking longer to equilibrate  
 986 than the mixing ratio. Inter-hemispheric spatial gradients take time to adjust after major  
 987 changes in emissions and Tans (1997) pointed out that the timescale for the  $\delta^{13}\text{C}_{\text{CH}_4}$  ratio is  
 988 also longer than for methane's abundance so provides complementary information.

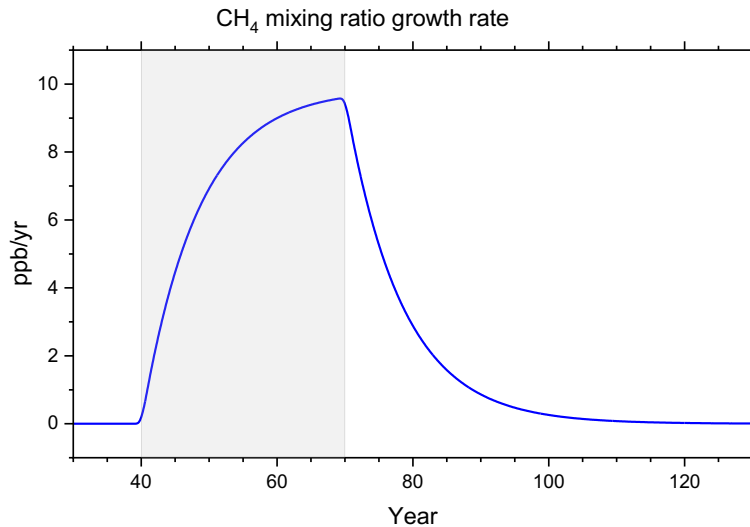
989 In glacial terminations, the boreal wetlands took longer to deglciate and hence the  
 990 dominance of tropical emissions with  $\delta^{13}\text{C}_{\text{CH}_4}$  close to the bulk atmospheric source led to a  
 991 brief hiatus in  $\delta^{13}\text{C}_{\text{CH}_4}$  while the burden grew. In the model, unlike the real past record, the  
 992 abrupt growth of boreal sources produces a significant negative shift in  $\delta^{13}\text{C}_{\text{CH}_4}$ .

993 *Figure 10a. Methane mole fraction ( $\delta^{13}\text{C}_M$ ) in ppb and  $\delta^{13}\text{C}_{\text{CH}_4}$  from the 4-box running budget*  
 994 *analysis with a 30-yr transition from 'Initial' to 'Post' sources. Blue is the global average mole*



995 *fraction and thin lines are for the four semihemispheres. The latitudinal distribution of the*  
 996 *CH<sub>4</sub> mole fraction reverses from being lowest in 30-90°N to being the highest there. Red is*  
 997 *the global average  $\delta^{13}C_M$  and thin lines show values for each semihemisphere and this*  
 998 *change in  $\delta^{13}C_{CH_4}$  is uniform across all semihemispheres.*

999 *Figure 10b. Growth rate (ppb/yr) of the global average CH<sub>4</sub> mixing ratio in Fig. 8a.*



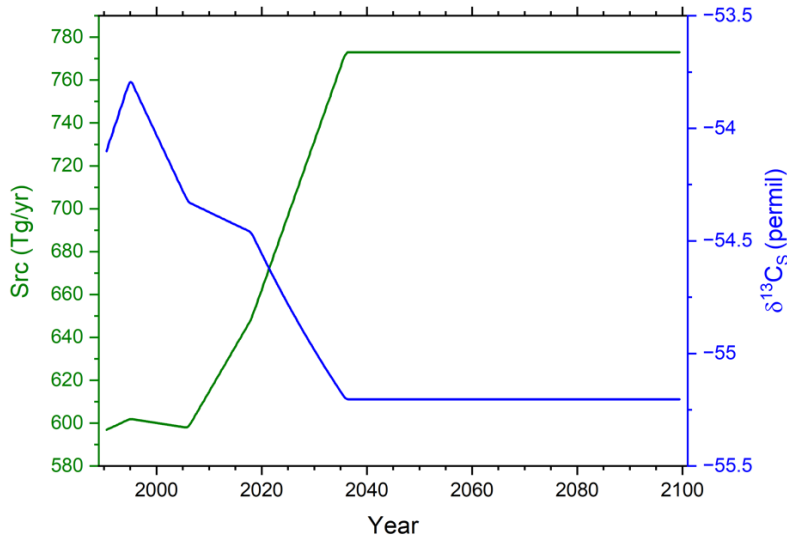
1000 **9.2. Present-day scenario: Modelling methane's modern growth and predicting the**  
 1001 **near future**

1002 To predict the impact if current trends continue for a full span of 30 years, from end-2006 to  
 1003 2037. the second model experiment focussed on matching the current growth in methane  
 1004 emissions and then projecting into the future until the change is assumed to be completed  
 1005 after 2036. This is an optimistic scenario that assumes good progress in the Global Methane  
 1006 Pledge to reduce methane emissions from purely abiogenic (fossil fuel) sources, and that  
 1007 biogenic emission growth then slows in a stable future climate.

1008 **9.2.1 – Modern event methane growth model – changes in methane burden and  $\delta^{13}C_{CH_4}$**

1009 The 'modern-day' model run is for a 30-year period 2007-2037, together with initialising  
 1010 years and years of post-change stability in emissions budgets. After the 30-year period,  
 1011 emissions stabilise. In this model, sources are fitted to observations with a simple piecewise  
 1012 linear fit of both source emissions, *Src* (Tg/yr) and  $\delta^{13}C_S$  up to 2022 (Fig. 11). Then the  
 1013 projections in Figs 11a and 11b that go beyond 2022 extend the source flux growth that was  
 1014 fitted to the most recent data, and continue for the rest of a 30 year transition period. The  
 1015 isotopic signature  $\delta^{13}C_S$  is determined by assigning a constant  $\delta^{13}C$  lighter than the current  
 1016 average  $\delta^{13}C_S$  to the *Src* increase.

1017 *Fig. 11. 'Modern-day' model for a 30 year transition period 2007-2037 assuming a change*  
 1018 *from earlier global climate state ending in late 2006 to new stable climate state beginning in*  
 1019 *2037. Source flux (*Src*) and source isotopic signature  $\delta^{13}C_S$ , modelled to fit to measurement*  
 1020 *data (see Fig. 11a) up to 2022, thereafter projected to end of 30 year period, after which *Src**  
 1021 *and  $\delta^{13}C_S$  remain constant.*

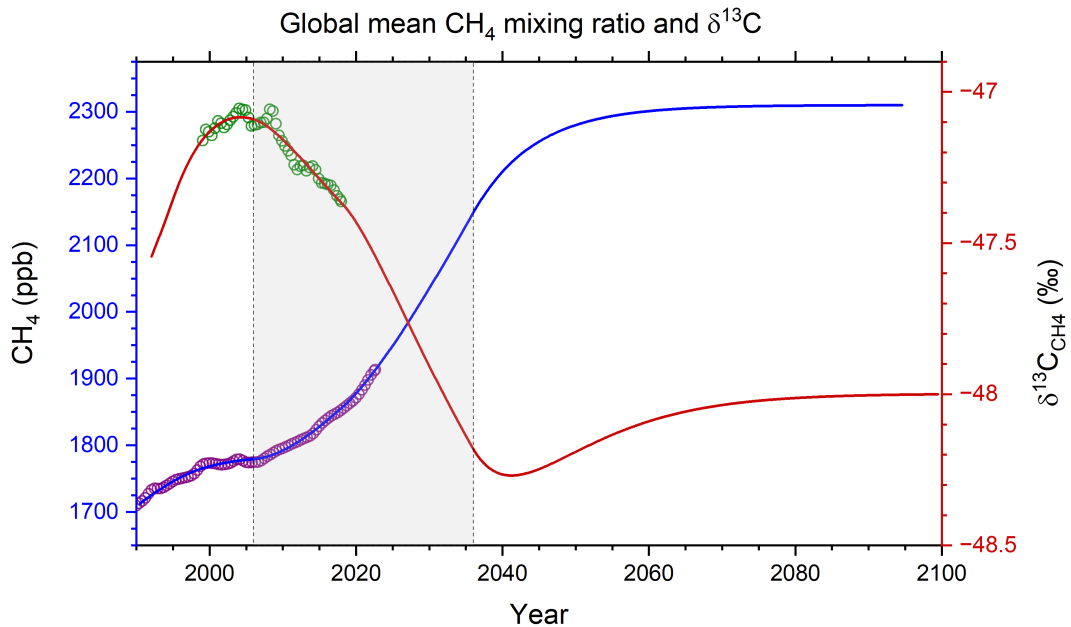


1022

1023 For the *Present-day Scenario*, Figure 12a shows NOAA methane mixing ratio and  
 1024 atmospheric  $\delta^{13}\text{C}_{\text{CH}_4}$  data together with an extrapolated extension of the running budget  
 1025 analysis in Nisbet et al. (2019). The fit-to-data follows a smoothed version of the observed  
 1026 mixing ratio, shown in Figure 12a, with a maximum growth of 14.5 ppb/yr in 2022 (Figure  
 1027 12b), when the observed rate was actually about 14 ppb, following an 18 ppb rise in 2021.  
 1028 This fit-to-data is up to August 2022 for the observed mixing ratio and  $\delta^{13}\text{C}_{\text{CH}_4}$   
 1029 measurements, and then extrapolated to 2037, for a full 30-year period of emissions  
 1030 growth. The scenario has an overall mean growth rate over 30 years of 10.5 ppb/yr.

1031 *Figure 12a. Change in global mean mixing ratio (blue) and  $\delta^{13}\text{C}_{\text{CH}_4}$  (red) together with NOAA*  
 1032 *data to August 2022 and  $\delta^{13}\text{C}_M$  data (green) to 2018. Compare with Fig. 10a.*

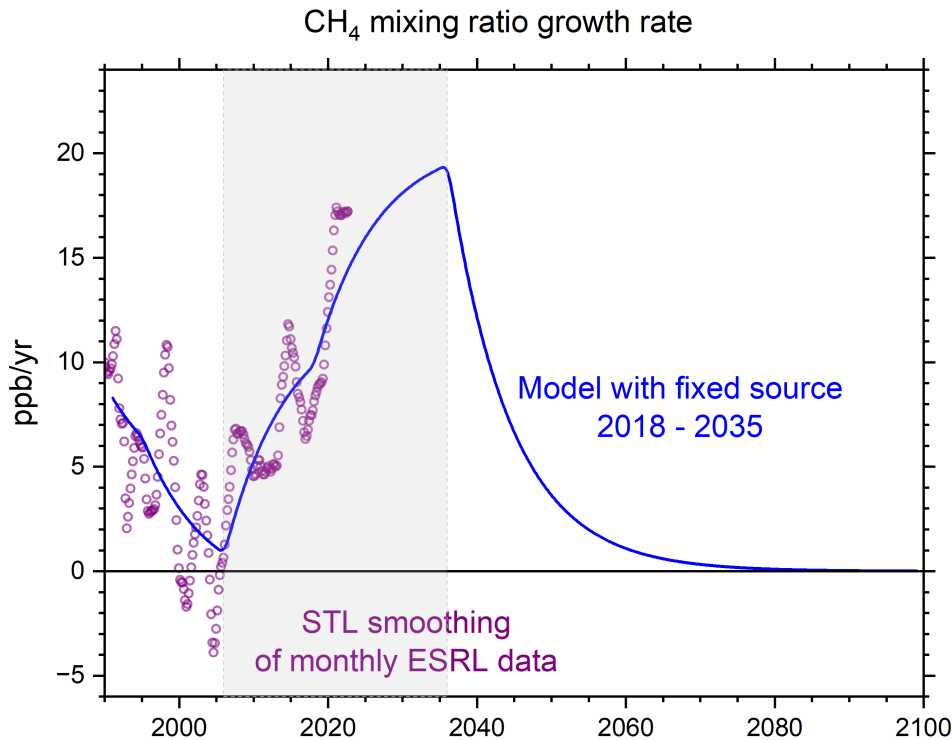
1033



1034

1035 *Figure 12b. Observed methane growth rate in ppb/yr from the ESRL data and from the*  
 1036 *model using a fixed source strength up to 2037, as shown in Fig 11. The measurement-based*

1037 growth rate determination uses the Seasonal Trend Loess (STL) analysis of Cleveland et al  
 1038 (1990) to separate a changing seasonal cycle from a changing trend. Compare with Fig. 10b.  
 1039



1040 This analysis successfully tracks the observed inflexion and then decrease in atmospheric  
 1041  $\delta^{13}\text{C}_{\text{CH}_4}$  (see Fig. 4 and green circles on red curve in Fig 12a), observed until 2022. In the  
 1042 projection part of the model analysis, the global mean  $\text{CH}_4$  mixing ratio reaches 2348 ppb  
 1043 and stabilises around the year 2055. The budget analysis also follows the observed decrease  
 1044 in  $\delta^{13}\text{C}_\text{M}$ , which reaches a minimum in the year 2040 followed by some recovery.  
 1045 Stabilisation of  $\delta^{13}\text{C}_\text{M}$  takes longer than for the mixing ratio because of the Tans effect, with  
 1046  $\delta^{13}\text{C}_{\text{CH}_4}$  eventually reaching a minimum in 2040, followed by some limited recovery as the  
 1047 burden equilibrates, while the global mean  $\delta^{13}\text{C}_\text{s}$  of source emissions decreases from -  
 1048 54.3‰ in 2006 to -55.2‰ in 2099.

1049 Our modelling suggests that the modern pulse of new biogenic methane, despite ongoing  
 1050 anthropogenic fossil fuel inputs with relatively positive  $\delta^{13}\text{C}_{\text{CH}_4}$ , is capable of shifting the  
 1051  $\delta^{13}\text{C}_{\text{CH}_4}$  of the much larger whole modern atmospheric burden by, say, -1.1‰ over the full  
 1052 30 year period 2007-2037. That includes inputs of equatorial methane with little isotopic  
 1053 leverage, outer seasonal tropical methane with some isotopic leverage, and boreal/Arctic  
 1054 methane with strong isotopic leverage. In the real record of the contemporary modern  
 1055 atmosphere, prior to the onset of growth in 2006, the mean atmospheric methane burden  
 1056 was slightly over 4900 Tg. In 2022, the mean burden had risen to 5300 Tg, a net increase of  
 1057 roughly 400 Tg during 2006-2022 inclusive. The accompanying  $\delta^{13}\text{C}_{\text{CH}_4}$  shift of about -0.55‰  
 1058 includes a 'positive' isotopic input from thermogenic sources such as anthropogenic fossil  
 1059 fuel emissions and biomass burning with isotopic signatures more  $^{13}\text{C}$  rich than the bulk  
 1060 atmospheric source. Had there been no such positive leverage, the total biogenic-driven  
 1061  $\delta^{13}\text{C}_{\text{CH}_4}$  shift over 2007-2022 that we would now be measuring would have been perhaps -

1062 0.7‰. Note that this shift has occurred despite the new emissions being diluted into a  
 1063 global burden five times larger than in glacial periods. A comparable pulse into the glacial air  
 1064 would shift  $\delta^{13}\text{C}_{\text{CH}_4}$  by 3 to 4‰ over a complete termination, including turn-on of boreal  
 1065 sources.

1066 To conclude: If methane emissions, primarily from biogenic methane sources, continue to  
 1067 rise at a rate similar to the one observed in recent years, the modern rise since 2006 would  
 1068 be large enough to be identified as the first part of a 'termination-scale' event in the ice core  
 1069 record of atmospheric methane. The conclusion also holds if only 85% of the current growth  
 1070 is considered, given that 15% of the ongoing rise is likely from fossil emissions that may be  
 1071 mitigated in the near future. Even if livestock emissions growth as fast as 1.4 Tg/yr/yr (Zhang  
 1072 et al., 2022: see above) is deducted, the remaining 'non-fossil fuel, non-livestock' growth  
 1073 rate still bears comparison with abrupt growth in a termination-scale event, the more so  
 1074 because the productivity of tropical livestock depends on vegetation growth that in turn  
 1075 follows climate-driven rain and warmth.

1076

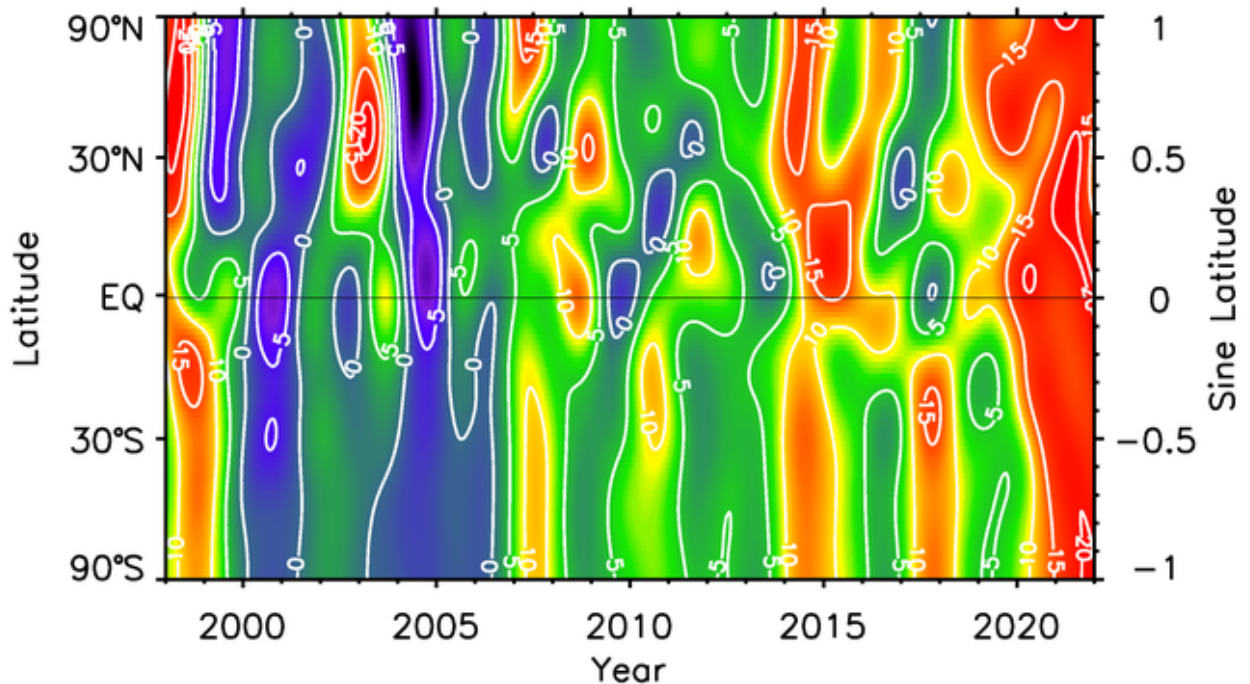
## 1077 **10. Discussion of Comparison**

1078 To summarize, methane's mole fraction growth in the past 15 years is comparable to growth  
 1079 in termination events, and it is likely that ongoing changes in methane emissions from  
 1080 present day wetlands are comparable to feedbacks during the past global change events.  
 1081 Even if only 85% of modern methane growth is biogenic, and part of that biogenic growth is  
 1082 due to anthropogenic inputs like increased cattle populations and more use of nitrogen  
 1083 fertilisers, methane's non-anthropogenic growth in the past 15 years has been at least  
 1084 comparable to growth in past climate change events. Allowing for the difference in the mass  
 1085 of the pre-transition burden, the associated isotopic shift is also comparable to shifts  
 1086 recorded (Fig. 8) across whole termination events (i.e. after the boreal wetlands had  
 1087 become fully active).

1088 It remains unclear how much the biogenic changes to the methane budget in recent  
 1089 decades are within the natural range of responses to decadal or centennial-scale climate  
 1090 variability.

1091 The current methane growth event started in late 2006 in both northern and southern high  
 1092 latitudes (Fig. 13). In Arctic summer, southerly winds blew high-methane air poleward from  
 1093 boreal zones. From then on, the tropics became the main zone of methane growth,  
 1094 especially in 2014/5, but with marked growth in the northern temperate zone in 2014 and in  
 1095 the southern outer tropics around in 2018 (e.g. Pantanal wetland). Then came the  
 1096 extraordinary ongoing growth surge of 2019-2022. The sine-latitude-time methane map in  
 1097 Figure 13 (updated from Lan et al. 2021b) reflects this history, though with the obvious  
 1098 caveat that changes in natural sources and sinks are added to by changes in human  
 1099 emissions from the fossil fuel industry, agriculture and waste.

1100 *Figure 13 –Methane growth rate averaged by latitudinal zone, from 2000 through 2021,*  
 1101 *updated from NOAA data. Red 'warm' colours – growth. Blue 'cool' colours – decline. The*  
 1102 *vertical axis denotes the sine of latitude, which weights each latitude band by its*  
 1103 *atmospheric mass. The ITCZ migrates seasonally from roughly 30°N to 30°S (sine latitude 0.5*  
 1104 *to -0.5), while the Arctic zone is the band north of sine latitude 0.91. The current growth*  
 1105 *event began in late 2006. Note the remarkable growth since 2020.*



1106  
1107

1108 Although the ongoing increase in global biogenic methane emission might be within the  
1109 multi-century range of historic emissions variability (Fig. 3) (Ferretti et al. 2005, Mischler et  
1110 al. 2009), the speed-of-change of the modern trend is extreme, much more rapid than  
1111 methane's medieval changes or the post-1800 rise driven by fossil fuel use. The inference is  
1112 that the biogenic component of methane's current (2007-2022) change is indeed likely  
1113 outside the range of natural variability.

1114 Methane's modern growth, in ppb/yr, and isotopic shift are more rapid than in glacial-  
1115 interglacial terminations (Table 3), though not necessarily faster than the maximum decadal  
1116 change rates during some terminations. Thus there is evident similarity between the past  
1117 increases in tropical biogenic sources that drove the glacial-interglacial terminations and the  
1118 present-day biogenic inputs driving the current 2006-2022 rise in methane emissions.  
1119 Though the events are very different, in the 15 years of growth to date the modern rise does  
1120 indeed bear comparison with the scale and speed of the abrupt phase of a termination  
1121 event.

1122 Previous orbitally driven natural transitions from cold glacial periods to warmer interglacial  
1123 periods took place in the presence of large ice caps and widespread sea ice. In contrast, the  
1124 modern climate change is from a warm Holocene (i.e. with widespread northern wetlands)  
1125 to a new, presumably even warmer future. The comparison between modern growth and  
1126 past analogues should not be taken too far. A modern 'termination-style' event marking the  
1127 reorganisation from a Holocene warm climate to some new post-Holocene yet-warmer  
1128 climate will be very different from any of the end-glacial events of the past half-million  
1129 years.

1130 Moreover, today's transition is anthropogenically driven, in an atmosphere where CO<sub>2</sub> is  
1131 much higher and rapidly growing, and where crop wastes and fertilizer run-off are

1132 widespread. Thus it is possible that the wetland response today has already surpassed the  
1133 wetland response in past glacial interglacial terminations.

1134 Yet it is indeed possible to imagine a new, modern step-change reorganisation of the  
1135 planetary climate in a global 'termination-scale' event – this could include marked ocean  
1136 warming and expansion of the ITCZ, and changes in the behaviour of the Indian Ocean  
1137 Dipole as the Hadley circulation expands coupled with alteration in the strength and  
1138 frequency of ENSO variations. Such changes could be accompanied by rapid Arctic land-  
1139 surface warming and sustained ocean circulation responses, including changes in the  
1140 Atlantic Meridional Overturning Circulation, on centennial-level timescales (Matsumoto,  
1141 2007).

1142 Compared to the 'natural' CO<sub>2</sub> budget, which has a major component in the deciduous  
1143 vegetation of the temperate northern hemisphere, changes in the biogenic methane signal  
1144 reflect more global distribution of sources and sinks. In past palaeo-climate transitions, large  
1145 changes occurred in the CO<sub>2</sub> budget, in response to changing latitude distribution of  
1146 insolation or meteorology and warming oceans. But such feedback-related changes in CO<sub>2</sub>  
1147 are hard to identify. In the present-day record there is not yet clear evidence for sustained  
1148 changes in the CO<sub>2</sub> burden that directly relate to climate change feedbacks and which  
1149 cannot be explained within the uncertainty of quantifying anthropogenic fossil fuel  
1150 emissions and land use changes. In contrast, given methane's lifetime, it can serve as a  
1151 'tallying-together' of ongoing climate change impacts, a representative bellwether.

1152 Methane is a good integrative signal of the state of global wetlands, and methane's global  
1153 budget – its growth or decline when the burden in the air is not in equilibrium with the net  
1154 flux from sources and sinks – sums the changing breath of the whole land biosphere. This  
1155 includes not only changing outputs from biogenic sources (nearly all terrestrial or coastal,  
1156 not oceanic) such as tropical and boreal wetlands, grass and tree growth for ruminants, and  
1157 growth in biomass fire fuel loads, but also changes in the meteorologically sensitive  
1158 oxidative capacity of the atmosphere involving [OH] Cl, and soil uptake. All natural sources  
1159 and sinks are highly variable with climate fluctuation. Wetland and ruminant emissions vary  
1160 with plant growth, rapidly changing as precipitation and temperature shift in ENSO and  
1161 Indian Ocean Dipole cycles, and as CO<sub>2</sub> varies. Methane removal by [OH] (especially in the  
1162 tropical mid-troposphere) and Cl fluctuates with the intensity of the Inter-Tropical  
1163 Convergence and the trade winds in the ENSO cycles. Hydroxyl is also sensitive to  
1164 atmospheric NO<sub>x</sub>, that historically came from dry season fires, usually human-lit. Soil sinks in  
1165 aerated soils, capable of breathing as pressure fluctuates under frontal passage are climate-  
1166 dependent, as bacterial methanotrophy needs the right conditions, neither too dry nor too  
1167 wet.

1168 If the climate is constant, then the methane burden equilibrates and is steady. When the  
1169 climate changes, natural methane sources and sinks respond and there is consequent  
1170 disequilibrium in the methane budget (i.e. growth or decline of the burden). Sustained  
1171 disequilibrium in the methane burden thus signals ongoing change in the biological  
1172 productivity of the entire planet's land surface. With the isotopic spin-up taking several  
1173 decades, a long-sustained growth or decline indicates a multi-decade change that is outside  
1174 decadal variability.

1175 The abruptness, power and global scale of past glacial/interglacial terminations provide  
1176 palaeoclimatological standards for comparison with what is taking place today (Tzedakis et

1177 al. 2009). The Eemian interglacial (130-115 kaBP, Marine Isotopic Stage 5, initiated by  
 1178 Termination II) was warmest around 125,000 years ago, with sea level perhaps 6 to 9 m  
 1179 above present-day level, implying significant melting both in Greenland and Antarctica  
 1180 compared to today (Dutton and Lambeck, 2012). The Eemian 'green Sahara' had abundant  
 1181 wetlands and great lakes (Larrasoana et al. 2013), very different from the current climate.  
 1182 However, the Eemian may be a poor guide to the future. Such past records may give little  
 1183 predictive help: the driving force today is anthropogenic, the speed of growth in CO<sub>2</sub> and  
 1184 CH<sub>4</sub> burdens is unprecedented, as is global land use change, so what is to come may be  
 1185 warmer than recent interglacials, even the Eemian.

1186 The model growth curve in Figures 12 a,b assumes growth that may be below what will  
 1187 occur in the next decade if both natural and anthropogenic emissions rise strongly.  
 1188 However, assuming the emission growth rates in the model, the increased radiative forcing  
 1189 of the climate from this extra methane input from the years 2021-2036 can be estimated at  
 1190 roughly 0.17 W/m<sup>2</sup>. To put this in context, that is about equivalent to five years of present-  
 1191 day growth in CO<sub>2</sub> forcing. There are important consequences for climate modellers. Using a  
 1192 methane-enabled Earth System Model, Kleinen et al. (2021) found methane mixing ratios  
 1193 and hence radiative forcing substantially higher than assumed in the scenarios used for the  
 1194 Coupled Model Intercomparison Project (CMIP6); assuming methane growth is only due to  
 1195 anthropogenic causes may lead to underestimation of future change.

1196 The question remains open. The observed post-2006 CH<sub>4</sub> growth (Fig. 1) is comparable to  
 1197 growth during the abrupt phase of a termination. Top-down and bottom-up estimates of  
 1198 modern emission growth rates are comparable to or greater than growth in termination  
 1199 events. Modelling shows that the modern record is comparable to termination events both  
 1200 for the change in CH<sub>4</sub> abundance driven by natural sources and that there are parallels  
 1201 between the observed modern  $\delta^{13}\text{C}_{\text{CH}_4}$  record and the isotopic records during full  
 1202 terminations.

1203 Methane's unexpected rise means achieving the Paris Agreement's targets will be very  
 1204 difficult (Mikaloff-Fletcher and Schaefer 2019, Nisbet et al. 2020) and will likely demand  
 1205 accelerated switching from fossil fuels to renewable energy sources, in addition to rapid  
 1206 elimination of methane emissions from fossil fuel use. Reducing the methane burden to its  
 1207 pre-industrial size would have beneficial impacts not only on climate, but also on air quality,  
 1208 increasing the oxidising capacity of the atmosphere (Staniaszek et al. 2022). Shooting the  
 1209 methane messenger will not eliminate methane's message. But it would help.

1210 A casual coincidence is not necessarily a causal connection. That we are in the midst of an  
 1211 rapid methane growth event, substantially driven by natural sources, does not necessarily  
 1212 mean the onset of global climate change. There is still the possibility that we are simply  
 1213 experiencing decadal- or centennial-scale variability. But past decadal- and centennial- scale  
 1214 Holocene variability, while significant, is smaller and much less abrupt than the typical  
 1215 abrupt climate change. Moreover, rapid growth in natural methane emissions does not  
 1216 happen unless climate is changing also: thus methane may indeed be the bellwether, the  
 1217 first indicator, the messenger of climate change.

1218 There are limits to comparison. Applying the designation 'termination' to current changes is  
 1219 not strictly correct in the modern usage of Terminations IX to I. Yet Broecker and Denton  
 1220 (1990) originally recognised terminations in the wider sense as "massive and abrupt  
 1221 reorganizations of the ocean-atmosphere system". In this sense, such an event may indeed

1222 be taking place. The remarkable shifts in the biogenic methane budget since the end of 2006  
 1223 may indeed be a first indicator of a large-scale reorganisation of the climate system on a  
 1224 scale that matches past great changes. Any current or near-future warming transition will  
 1225 differ greatly from the past glacial-interglacial Terminations IX to I. There is no Roman  
 1226 number zero. But then, zero is different from all other numbers. The question is valid: have  
 1227 we already entered Termination Zero?

1228

## 1229 **Acknowledgements**

1230 EGN, DL, REF, JLF and the Royal Holloway laboratory thank the UK Met Office for three  
 1231 decades of support on Ascension Island, and NILU-Norway, IUP Heidelberg, and  
 1232 Environment Canada for sampling at Zeppelin, Svalbard and Alert, Canada. EGN thanks the  
 1233 UK Natural Environment Research Council for grants NE/S00159X/1 ZWAMPS Quantifying  
 1234 Methane Emissions in remote tropical settings: a new 3D approach and NE/N016238/1  
 1235 MOYA: The Global Methane Budget, and colleagues involved with the UNEP International  
 1236 Methane Emissions Observatory for discussions and insight. REF thanks NERC for grant  
 1237 NE/V000780/1 Methane D/H Discovering reasons for global atmospheric methane growth  
 1238 using deuterium isotopes. PIP acknowledges support from the UK National Centre for Earth  
 1239 Observation funded by the National Environment Research Council (NE/R016518/1). TR's  
 1240 laboratory was supported in part by the European Union's Marie Curie project MEMO<sup>2</sup>  
 1241 (Methane goes Mobile – Measurements and Modeling).

1242

## 1243 **Contributions**

1244 EJD, XL, SEM, DL, REF, JLF, TR, JS and EGN collected samples, made primary measurements,  
 1245 participated in development of the study and edited the manuscript. SEM performed  $\delta^{13}\text{C}_{\text{CH}_4}$   
 1246 measurements. MRM carried out the modelling in Section 9 and he and PP had input on  
 1247 meteorological and modelling discussion, especially in the tropics. XL and HDvdG estimated  
 1248 emissions growth from EDGAR data. JS and MND guided the input on ice core records and  
 1249 past terminations. Figures, including updates and modifications: 1 EJD,XL,(NOAA), EGN; 2  
 1250 PIP; 3 JS, MRM; 4 SEM,MRM,GD, TB; 5 SEM,MRM,GD, TB; 6 XL, HDvdG; 7 JS; 8 EJD; 9, 10,  
 1251 11 MRM; 12 JLF with input from TR and SEM; 13 EJD, XL; SI 1 SEM, EJD, SI 2,3,4 MRM, GB,TB  
 1252 SI 5 XL and HDvdG,. Table 1 EGN; Table 2 HDvdG; Table 3 EGN; Table 4 MRM.  
 1253 Conceptualisation and manuscript preparation mainly by EGN, MRM and EJD, with input  
 1254 from all authors. This paper and all methane papers depend on the impeccable quality of  
 1255 NOAA data (EJD, XL, SEM). Eric Wolff and Mark Lunt, and especially Vas Petrenko are  
 1256 thanked for their thoughtful, critical, and extremely helpful comments. We thank the most  
 1257 helpful anonymous reviewers and the editor for their kind and perceptive assistance over  
 1258 this very long and demanding study.

1259

## 1260 **References**

- 1261 Abram, N.J., Hargreaves, J.A., Wright, N.M., Thirumalai, K., Ummenhofer, C.C. and England,  
 1262 M.H., (2020). Palaeoclimate perspectives on the Indian Ocean dipole. *Quaternary Science*  
 1263 *Reviews*, 237, p.106302.
- 1264 Ackerman, D., Millet, D. B., & Chen, X. (2019). Global estimates of inorganic nitrogen  
 1265 deposition across four decades. *Global Biogeochemical Cycles*,33, 100–107.
- 1266 Barker, P.A., Allen, G., Gallagher, M., Pitt, J.R., Fisher, R.E., Bannan, T., Nisbet, E.G.,  
 1267 Bauguitte, S.J.B., Pasternak, D., Cliff, S. and Schimpf, M.B. (2020). Airborne measurements

- 1268 of fire emission factors for African biomass burning sampled during the MOYA campaign.  
 1269 *Atmospheric Chemistry and Physics*, 20, 15443-15459.
- 1270 Basu, S., Lan, X., Dlugokencky, E., Michel, S., Schwietzke, S., Miller, J. B., Bruhwiler, L., Oh, Y.,  
 1271 Tans, P. P., Apadula, F., Gatti, L. V., Jordan, A., Necki, J., Sasakawa, M., Morimoto, S., Di  
 1272 Iorio, T., Lee, H., Arduini, J., and Manca, G. (2022) Estimating emissions of methane  
 1273 consistent with atmospheric measurements of methane and  $\delta^{13}\text{C}$  of methane, *Atmos.*  
 1274 *Chem. Phys.*, 22, 15351–15377, <https://doi.org/10.5194/acp-22-15351-2022>.
- 1275 Bereiter, B.; Eggleston, S.; Schmitt, J.; Nehrbass-Ahles, C.; Stocker, T. F.; Fischer,  
 1276 H.; Kipfstuhl, S.; Chappellaz, J. (2015) Revision of the EPICA Dome C CO<sub>2</sub> record from 800  
 1277 to 600 kyr before present. *Geophys. Res. Lett.* 42, 542-549.
- 1278 Berner, L.T., Massey, R., Jantz, P., Forbes, B.C., Macias-Fauria, M., Myers-Smith, I., Kumpula,  
 1279 T., Gauthier, G., Andreu-Hayles, L., Gaglioti, B.V. and Burns, P., (2020). Summer warming  
 1280 explains widespread but not uniform greening in the Arctic tundra biome. *Nature*  
 1281 *Communications*, 11, pp.1-12.
- 1282 Bock, M., Schmitt, J., Beck, J., Seth, B., Chappellaz, J. and Fischer, H. (2017)  
 1283 Glacial/interglacial wetland, biomass burning, and geologic methane emissions  
 1284 constrained by dual stable isotopic CH<sub>4</sub> ice core records. *Proc. Natl. Acad. Sci. USA.* 114,  
 1285 E5778-E5786.
- 1286 Boers N., Ghil M., and Rousseau D.D. (2018) Ocean circulation, ice shelf, and sea ice  
 1287 interactions explain Dansgaard–Oeschger cycles. *Proceedings of the National Academy of*  
 1288 *Sciences.* 115, E11005-14.
- 1289 Bonnet, R., Swingedouw, D., Gastineau, G., Boucher, O., Deshayes, J., Hourdin, F., Mignot, J.,  
 1290 Servonnat, J. and Sima, A., 2021. Increased risk of near term global warming due to a  
 1291 recent AMOC weakening. *Nature communications*, 12(1), pp.1-9.
- 1292 Brierley, C., Thirumalai, K., Grindrod, E., and Barnsley, J.: Indian Ocean variability changes in  
 1293 the Paleoclimate Modelling Intercomparison Project, *Clim. Past*, 19, 681–701,  
 1294 <https://doi.org/10.5194/cp-19-681-2023>, 2023.
- 1295 Broecker, W. S., & Denton, G. H. (1990). The role of ocean-atmosphere reorganizations in  
 1296 glacial cycles. *Quaternary science reviews*, 9, 305-341.
- 1297 Broecker, W.S. & Van Donk, J., 1970. Insolation changes, ice volumes, and the O18 record in  
 1298 deep-sea cores. *Reviews of Geophysics*, 8(1), pp.169-198.
- 1299 Brownlow, R., Lowry, D., Fisher, R. E., France, J. L., Lanoisellé, M., White, B., Wooster, M.J.,  
 1300 Zhang, T., and Nisbet, E. G. (2017). Isotopic ratios of tropical methane emissions by atmo-  
 1301 spheric measurement. *Global Biogeochemical Cycles*, 31, 1408–1419.
- 1302 Cai, W., Wu, L., Lengaigne, M., Li, T., McGregor, S., Kug, J.S., Yu, J.Y., Stuecker, M.F., Santoso,  
 1303 A., Li, X. and Ham, Y.G. (2019) Pantropical climate interactions. *Science*, 363, p.eaav4236.
- 1304 Cantrell, C.A., Shetter, R.E., McDaniel, A.H., Calvert, J.G., Davidson, J.A., Lowe, D.C., Tyler,  
 1305 S.C., Cicerone, R.J. and Greenberg, J.P., 1990. Carbon kinetic isotope effect in the oxidation  
 1306 of methane by the hydroxyl radical. *Journal of Geophysical Research: Atmospheres*, 95,  
 1307 22455-22462.
- 1308 Capron, E., Rasmussen, S.O., Popp, T.J., Erhardt, T., Fischer, H., Landais, A., Pedro, J.B.,  
 1309 Vettoretti, G., Grinsted, A., Gkinis, V. and Vaughn, B. (2021) The anatomy of past abrupt  
 1310 warmings recorded in Greenland ice. *Nature Communications*, 12, 2106.
- 1311 Chang, J., Peng, S., Ciais, P. et al. (2019) Revisiting enteric methane emissions from domestic  
 1312 ruminants and their  $\delta^{13}\text{C}_{\text{CH}_4}$  source signature. *Nat Commun* 10, 3420.  
 1313 <https://doi.org/10.1038/s41467-019-11066-3>

- 1314 Chang, K.Y., Riley, W.J., Collier, N., McNicol, G., Fluet-Chouinard, E., Knox, S.H., Delwiche,  
 1315 K.B., Jackson, R.B., Poulter, B., Saunois, M. and Chandra, N. (2023) Observational  
 1316 constraints reduce model spread but not uncertainty in global wetland methane emission  
 1317 estimates. *Global Change Biology*.
- 1318 Cheng, H., Edwards, R.L., Broecker, W.S., Denton, G.H., Kong, X., Wang, Y., Zhang, R. and  
 1319 Wang, X. (2009) Ice age terminations. *Science*, 326, 248-252.
- 1320 Cheng, H., Zhang, H., Spötl, C., Baker, J., Sinha, A., Li, H., Bartolomé, M., Moreno, A.,  
 1321 Kathayat, G., Zhao, J. and Dong, X. (2020). Timing and structure of the Younger Dryas event  
 1322 and its underlying climate dynamics. *Proc. Natl. Acad. Sci. USA*, 117, 23408-23417.
- 1323 Cheng, L. J., and Coauthors, 2023: Another year of record heat for the oceans. *Adv. Atmos.*  
 1324 *Sci.*, <https://doi.org/10.1007/s00376-023-2385-2>.
- 1325 Cheng, W., Bitz, C.M. and Chiang, J.C., 2007. Adjustment of the global climate to an abrupt  
 1326 slowdown of the Atlantic meridional overturning circulation. *Geophysical Monograph-*  
 1327 *American Geophysical Union*, 173, 295
- 1328 Cleveland, R.B., Cleveland, W.S., McRae, J.E. and Terpenning, I. (1990) STL: A seasonal-trend  
 1329 decomposition. *J. Off. Stat*, 6, 3-73.
- 1330 Craig, H., Chou, C. C., Welhan, J. A., Stevens, C. M., & Engelkemeir, A. (1988). The isotopic  
 1331 composition of methane in polar ice cores. *Science*, 242, 1535-1539.
- 1332 Clauss, M., Dittmann, M.T., Vendl, C., Hagen, K.B., Frei, S., Ortmann, S., Müller, D.W.,  
 1333 Hammer, S., Munn, A.J., Schwarm, A. and Kreuzer, M. (2020). Comparative methane  
 1334 production in mammalian herbivores. *Animal*, 14, s113-s123.
- 1335 Crippa, M., Guizzardi, D., Solazzo, E., Muntean, M., Schaaf, E., Monforti-Ferrario, F., Banja,  
 1336 M., Olivier, J.G.J., Grassi, G., Rossi, S., Vignati, E., GHG emissions of all world countries -  
 1337 2021 Report, EUR 30831 EN, Publications Office of the European Union, Luxembourg,  
 1338 2021, ISBN 978-92-76-41547-3, doi:10.2760/173513, JRC126363
- 1339 Cooper, M. J., Martin, R. V., Hammer, M. S., Levelt, P. F., Veefkind, P., Lamsal, L. N., Krotkov,  
 1340 N. A., Brook, J. R., and McLinden, C. A. (2022) Global fine-scale changes in ambient NO<sub>2</sub>  
 1341 during COVID-19 lockdowns, *Nature*, 601, 380–387.
- 1342 Curry, C. L. (2007). Modeling the soil consumption of atmospheric methane at the global  
 1343 scale. *Global Biogeochemical Cycles*, 21, GB4012. <https://doi.org/10.1029/2006GB002818>
- 1344 Dangal, S.R., Tian, H., Xu, R., Chang, J., Canadell, J.G., Ciais, P., Pan, S., Yang, J. and Zhang, B.  
 1345 (2019) Global nitrous oxide emissions from pasturelands and rangelands: magnitude,  
 1346 spatiotemporal patterns, and attribution. *Global Biogeochemical Cycles*, 33(2), pp.200-222.
- 1347 Dean, J.F., Middelburg, J.J., Röckmann, T., Aerts, R., Blauw, L.G., Egger, M., Jetten, M.S.M.,  
 1348 Jong, A.E.E.d., Meisel, O.H., Rasigraf, O., Slomp, C.P., Zandt, M.H.i.t., and Dolman, A.J.,  
 1349 (2018) Methane feedbacks to the global climate system in a warmer world. *Rev. Geophys*,  
 1350 56, 207-250.
- 1351 Denton, G. H., Anderson, R. F., Toggweiler, J. R., Edwards, R. L., Schaefer, J. M., & Putnam, A.  
 1352 E. (2010). The last glacial termination. *Science*, 328, 1652-1656.
- 1353 Dlugokencky EJ, Masarie KA, Lang PM, Tans PP, Steele LP, & Nisbet EG. A dramatic decrease  
 1354 in the growth rate of atmospheric methane in the northern hemisphere during 1992  
 1355 (1994) *Geophysical Research Letters*. 1994 Jan 1;21(1):45-8.
- 1356 Dlugokencky EJ, Masarie KA, Lang PM, & Tans PP (1998) Continuing decline in the growth  
 1357 rate of the atmospheric methane burden. *Nature*. 393, 447-50.
- 1358 Dlugokencky, E.J., Houweling, S., Bruhwiler, L., Masarie, K.A., Lang, P.M., Miller, J.B. and  
 1359 Tans, P.P. (2003) Atmospheric methane levels off: Temporary pause or a new steady-  
 1360 state? *Geophysical Research Letters*, 30 (19).

- 1361 Dlugokencky, E.J., Nisbet, E.G., Fisher, R. & Lowry, D. (2011) Global atmospheric methane:  
 1362 budget, changes and dangers. *Philosophical Transactions of the Royal Society A:*  
 1363 *Mathematical, Physical and Engineering Sciences*, 369, 2058-2072.
- 1364 Dutton, A. and Lambeck, K., (2012). Ice volume and sea level during the last interglacial.  
 1365 *Science*, 337, 216-219.
- 1366 Drinkwater, A., Palmer, P., Feng, L., Arnold, T., Lan, X., Michel, S., Parker, R. and Boesch, H.,  
 1367 (2022) Atmospheric data support a multi-decadal shift in the global methane budget  
 1368 towards natural tropical emissions. *Atmospheric Chemistry and Physics Discussions*, 1-35.
- 1369 EDGAR (2023) Global Greenhouse Emissions. Emissions Database for Global Atmospheric  
 1370 Research V7.0. [https://edgar.jrc.ec.europa.eu/dataset\\_ghg70](https://edgar.jrc.ec.europa.eu/dataset_ghg70) accessed at various dates up  
 1371 to 15/01/2023
- 1372 Ehhalt, D.H. (1974). The atmospheric cycle of methane. *Tellus*, 26, 58-70.
- 1373 Etheridge DM, Steele L, Francey RJ, Langenfelds RL. Atmospheric methane between 1000 AD  
 1374 and present: Evidence of anthropogenic emissions and climatic variability (1998). *Journal*  
 1375 *of Geophysical Research: Atmospheres*. 103, 15979-93.
- 1376 FAO (2017) World fertilizer trends and outlook to 2020  
 1377 <https://www.fao.org/3/i6895e/i6895e.pdf>
- 1378 Feng, L., Palmer, P.I., Zhu, S., Parker, R.J. and Liu, Y. (2022) Tropical methane emissions  
 1379 explain large fraction of recent changes in global atmospheric methane growth rate.  
 1380 *Nature communications*, 13, pp.1-8.
- 1381 Feng, L., Palmer, P.I., Parker, R.J., Lunt, M.F. and Bösch, H. (2023) Methane emissions are  
 1382 predominantly responsible for record-breaking atmospheric methane growth rates in 2020  
 1383 and 2021. *Atmospheric Chemistry and Physics*, 23, 4863-4880..
- 1384 Ferretti DF, Miller JB, White JW, Etheridge DM, Lassey KR, Lowe DC, Meure CM, Dreier MF,  
 1385 Trudinger CM, Van Ommen TD, Langenfelds RL. (2005) Unexpected changes to the global  
 1386 methane budget over the past 2000 years. *Science*, 309, 1714-7.
- 1387 Fischer, H., Behrens, M., Bock, M., Richter, U., Schmitt, J., Loulergue, L., Chappellaz, J.,  
 1388 Spahni, R., Blunier, T., Leuenberger, M. and Stocker, T.F. (2008). Changing boreal methane  
 1389 sources and constant biomass burning during the last termination. *Nature*, 452(7189),  
 1390 pp.864-867.
- 1391 Fowler, D., Coyle, M., Skiba, U., Sutton, M.A., Cape, J.N., Reis, S., Sheppard, L.J., Jenkins, A.,  
 1392 Grizzetti, B., Galloway, J.N. and Vitousek, P. (2013). The global nitrogen cycle in the twenty-  
 1393 first century. *Philosophical Transactions of the Royal Society B: Biological Sciences*, 368,  
 1394 p.20130164.
- 1395 France J.L., Fisher, R.E., Lowry, D., Lanoisellé, M., Nisbet-Jones, P.B.R., Andrade, M., Moreno,  
 1396 I., Forster, G., Orams, D., Gondwe, M., Skiba, U., Stephens, M., Broderick, T., Hoyt, A.,  
 1397 Gondwe, M., Jones, A.E., & Nisbet, E.G. (2021)  $\delta^{13}\text{C}$  methane source signatures from  
 1398 tropical wetland and rice field emissions. *Phil. Trans. R. Soc. A* 20200449.  
 1399 10.1098/rsta.2020.0449
- 1400 France, J.L., Lunt, M.F., Andrade, M., Moreno, I., Ganesan, A.L., Lachlan-Cope, T., Fisher,  
 1401 R.E., Lowry, D., Parker, R.J., Nisbet, E.G. and Jones, A.E. (2022). Very large fluxes of  
 1402 methane measured above Bolivian seasonal wetlands. *Proceedings of the National*  
 1403 *Academy of Sciences*, 119(32), p.e2206345119.
- 1404 Ganesan, A.L., Stell, A.C., Gedney, N., Comyn-Platt, E., Hayman, G., Rigby, M., Poulter, B. and  
 1405 Hornibrook, E.R.C. (2018). Spatially resolved isotopic source signatures of wetland  
 1406 methane emissions. *Geophysical Research Letters*, 45(8), pp.3737-3745.

- 1407 Gauci, V., Fowler, D., Chapman, S.J. *et al.* Sulfate deposition and temperature controls on  
 1408 methane emission and sulfur forms in peat. *Biogeochemistry* **71**, 141–162 (2005).  
 1409 <https://doi.org/10.1007/s10533-005-0681-9>
- 1410 Geng, T., Cai, W., Wu, L., Santoso, A., Wang, G., Jing, Z., Gan, B., Yang, Y., Li, S., Wang, S. and  
 1411 Chen, Z. (2022) Emergence of changing Central-Pacific and Eastern-Pacific El Niño-  
 1412 Southern Oscillation in a warming climate. *Nature Communications*, **13**, 1-11.
- 1413 Gloor, M., Gatti, L. V., Wilson, C., Parker, R. J., Boesch, H., Popa, E., et al. (2021). Large  
 1414 methane emissions from the Pantanal during rising water-levels revealed by regularly  
 1415 measured lower troposphere CH<sub>4</sub> profiles. *Global Biogeochemical Cycles*, **35**,  
 1416 e2021GB006964. <https://doi.org/10.1029/2021GB006964>
- 1417 Gorbatenko, V.P., Pustovalov, K.N. and Konstantinova, D.A. (2020). Convective potential of  
 1418 the atmosphere of Western Siberia amid global climate change. In *IOP Conference Series:  
 1419 Earth and Environmental Science* (Vol. 611, No. 1, p. 012001). IOP Publishing.
- 1420 Graven, H.D., Keeling, R.F., Piper, S.C., Patra, P.K., Stephens, B.B., Wofsy, S.C., Welp, L.R.,  
 1421 Sweeney, C., Tans, P.P., Kelley, J.J. and Daube, B.C. (2013). Enhanced seasonal exchange of  
 1422 CO<sub>2</sub> by northern ecosystems since 1960. *Science*, **341**, 1085-1089.
- 1423 Grise, K.M., Davis, S.M., Simpson, I.R., Waugh, D.W., Fu, Q., Allen, R.J., Rosenlof, K.H.,  
 1424 Ummenhofer, C.C., Karnauskas, K.B., Maycock, A.C. and Quan, X.W. (2019) Recent tropical  
 1425 expansion: natural variability or forced response?. *Journal of Climate*, **32**, 1551-1571.
- 1426 Hasan NA, Chikamoto Y & McPhaden MJ (2022) The influence of tropical basin interactions  
 1427 on the 2020–2022 double-dip La Niña. *Front. Clim.* **4**:1001174. doi:  
 1428 10.3389/fclim.2022.1001174
- 1429 Haverd, V., Smith, B., Canadell, J.G., Cuntz, M., Mikaloff-Fletcher, S., Farquhar, G.,  
 1430 Woodgate, W., Briggs, P.R. and Trudinger, C.M., 2020. Higher than expected CO<sub>2</sub>  
 1431 fertilization inferred from leaf to global observations. *Global change biology*, **26**(4),  
 1432 pp.2390-2402.
- 1433 He, J., Naik, V., Horowitz, L.W., Dlugokencky, E. and Thoning, K. (2020). Investigation of the  
 1434 global methane budget over 1980–2017 using GFDL-AM4. 1. *Atmospheric Chemistry and  
 1435 Physics*, **20**, 805-827.
- 1436 Holden, P.B., Edwards, N.R., Gerten, D. and Schaphoff, S. (2013) A model-based constraint  
 1437 on CO<sub>2</sub> fertilisation. *Biogeosciences*, **10**, pp.339-355.
- 1438 Hossaini, R., Chipperfield, M. P., Saiz-Lopez, A., Fernandez, R., Monks, S., Feng, W., et al.  
 1439 (2016). A global model of tropospheric chlorine chemistry: Organic versus inorganic  
 1440 sources and impact on methane oxidation. *Journal of Geophysical Research: Atmospheres*,  
 1441 **121**, 14,271–14,297. <https://doi.org/10.1002/2016JD025756>
- 1442 Howarth, R. W.: Ideas and perspectives: is shale gas a major driver of recent increase in  
 1443 global atmospheric methane?(2019) *Biogeosciences*, **16**, 3033–3046,  
 1444 <https://doi.org/10.5194/bg-16-3033-2019>.
- 1445 Huntingford, C., Burke, E.J., Jones, C.D., Jeffers, E.S. and Wiltshire, A.J. (2022) Nitrogen cycle  
 1446 impacts on CO<sub>2</sub> fertilisation and climate forcing of land carbon stores. *Environmental  
 1447 Research Letters*, **17**, p.044072.
- 1448 IEA (2022) [https://www.iea.org/data-and-statistics/charts/global-methane-emissions-from-  
 1449 the-energy-sector-over-time-2000-2021](https://www.iea.org/data-and-statistics/charts/global-methane-emissions-from-the-energy-sector-over-time-2000-2021).
- 1450 IFAsat (2022) International Fertilizer Association database 1.1. Fertilizer Consumption -  
 1451 Historical Trends by Country or Region. [https://www.ifastat.org/databases/graph/1\\_1](https://www.ifastat.org/databases/graph/1_1)
- 1452 IPCC (2021) Figure 8.11, Chapter 8. In *Climate Change 2021: The Physical Science Basis.  
 1453 Contribution of Working Group I to the Sixth Assessment Report of the Intergovernmental*

- 1454 *Panel on Climate Change*. Cambridge University Press, Cambridge, United Kingdom and  
 1455 New York, NY, USA, 1055–1210, doi: [10.1017/9781009157896.010](https://doi.org/10.1017/9781009157896.010).]
- 1456 Jo, H-S., Ham, Y-G., Kug, J-S., Li, T., Kim, J-H., Kim, J-G., and Kim, H. (2022) Southern Indian  
 1457 Ocean Dipole as a trigger for Central Pacific El Niño since the 2000s. *Nature*  
 1458 *Communications* **13**, 6965. <https://doi.org/10.1038/s41467-022-34721-8>
- 1459 Kim, YH., Min, SK., Gillett, N.P. *et al.* (2023) Observationally-constrained projections of an  
 1460 ice-free Arctic even under a low emission scenario. *Nat Commun* **14**, 3139  
 1461 <https://doi.org/10.1038/s41467-023-38511-8>
- 1462 Kleinen, T., Gromov, S., Steil, B. and Brovkin, V. (2021). Atmospheric methane  
 1463 underestimated in future climate projections. *Environmental Research Letters*, *16*, 094006.
- 1464 Lan, X., Basu, S., Schwietzke, S., Bruhwiler, L.M., Dlugokencky, E.J., Michel, S.E., Sherwood,  
 1465 O.A., Tans, P.P., Thoning, K., Etiope, G. and Zhuang, Q., (2021a) Improved constraints on  
 1466 global methane emissions and sinks using  $\delta^{13}\text{C}\text{-CH}_4$ . *Global biogeochemical cycles*, *35*(6),  
 1467 p.e2021GB007000
- 1468 Lan, X., Nisbet, E. G., Dlugokencky, E. J., & Michel, S. E. (2021b). What do we know about the  
 1469 global methane budget? Results from four decades of atmospheric CH<sub>4</sub> observations and  
 1470 the way forward. *Phil. Trans. Royal Soc. A*, *379*, 20200440.
- 1471 Lan, X., E.J. Dlugokencky, J.W. Mund, A.M. Crotwell, M.J. Crotwell, E. Moglia, M. Madronich,  
 1472 D. Neff and K.W. Thoning (2022), Atmospheric Methane Dry Air Mole Fractions from the  
 1473 NOAA GML Carbon Cycle Cooperative Global Air Sampling Network, 1983-2021, Version:  
 1474 2022-11-21, <https://doi.org/10.15138/VNCZ-M766>
- 1475 Lan, X., K.W. Thoning, and E.J. Dlugokencky (2023) Trends in globally-averaged CH<sub>4</sub>, N<sub>2</sub>O,  
 1476 and SF<sub>6</sub> determined from NOAA Global Monitoring Laboratory measurements. Version  
 1477 2022-11, <https://doi.org/10.15138/P8XG-AA10>.  
 1478 [https://gml.noaa.gov/webdata/ccgg/trends/ch4/ch4\\_annmean\\_gl.txt](https://gml.noaa.gov/webdata/ccgg/trends/ch4/ch4_annmean_gl.txt)
- 1479 Lang, N. and Wolff, E.W. (2011) Interglacial and glacial variability from the last 800 ka in  
 1480 marine, ice and terrestrial archives. *Climate of the Past*, *7*, 361-380.
- 1481 Larrasoana J.C., Roberts A.P., and Rohling E.J. (2013) Dynamics of Green Sahara Periods and  
 1482 Their Role in Hominin Evolution. *PLoS ONE* *8*: e76514.  
 1483 doi:10.1371/journal.pone.0076514
- 1484 Lassey, K.R., Lowe, D.C. and Smith, A.M., 2007. The atmospheric cycling of radiomethane  
 1485 and the " fossil fraction" of the methane source. *Atmospheric Chemistry and Physics*, *7*,  
 1486 2141-2149.
- 1487 Laughner, J.L., Neu, J.L., Schimel, D., Wennberg, P.O., Barsanti, K., Bowman, K.W.,  
 1488 Chatterjee, A., Croes, B.E., Fitzmaurice, H.L., Henze, D.K. and Kim, J., 2021. Societal shifts  
 1489 due to COVID-19 reveal large-scale complexities and feedbacks between atmospheric  
 1490 chemistry and climate change. *Proceedings of the National Academy of Sciences*, *118*(46),  
 1491 p.e2109481118.
- 1492 Leitner, S., Carbonell, V., Butterbach-Bahl, K., Barthel, M., Mhindu, R. L., Mutuo, P.,  
 1493 Buchmann, N., and Merbold, L.(2023) Traditional livestock enclosures are greenhouse gas  
 1494 hotspots in the African savanna landscape: The case of a rangeland in Kenya, EGU General  
 1495 Assembly 2023, Vienna, Austria, 24-28 Apr 2023, EGU23-14773, [https://doi.org](https://doi.org/10.5194/egusphere-egu23-14773)  
 1496 [/10.5194/egusphere-egu23-14773](https://doi.org/10.5194/egusphere-egu23-14773).
- 1497 Lelieveld, J., Gromov, S., Pozzer, A., and Taraborrelli, D.: Global tropospheric hydroxyl  
 1498 distribution, budget and reactivity, *Atmos. Chem. Phys.*, *16*, 12477–12493,  
 1499 <https://doi.org/10.5194/acp-16-12477-2016>, 2016.

- 1500 Levin, I., Veidt, C., Vaughn, B.H., Brailsford, G., Bromley, T., Heinz, R., Lowe, D., Miller, J.B.,  
 1501 Poß, C., and White, J.W.C. (2012) No inter-hemispheric  $\delta^{13}\text{CH}_4$  trend observed. *Nature*,  
 1502 486, E3-E4.
- 1503 Liu, J., Wu, D., Xu, X., Ji, M., Chen, Q. and Wang, X. (2021). Projection of extreme  
 1504 precipitation induced by Arctic amplification over the Northern Hemisphere.  
 1505 *Environmental Research Letters*, 16, p.074012.
- 1506 Lobell, D.B. and Field, C.B. (2008). Estimation of the carbon dioxide (CO<sub>2</sub>) fertilization effect  
 1507 using growth rate anomalies of CO<sub>2</sub> and crop yields since 1961. *Global Change Biology*, 14,  
 1508 39-45.
- 1509 Loulergue, L.; Schilt, A.; Spahni, R.; Masson-Delmotte, V.; Blunier, T.; Lemieux,  
 1510 B.; Barnola, J.-M.; Raynaud, D.; Stocker, T. F.; Chappellaz, J. (2008) Orbital and millennial-  
 1511 scale features of atmospheric CH<sub>4</sub> over the past 800,000 years. *Nature*, 453, 383-386.
- 1512 Lowe, D.C., Brenninkmeijer, C.A., Manning, M.R., Sparks, R. and Wallace, G. (1988)  
 1513 Radiocarbon determination of atmospheric methane at Baring Head, New Zealand. *Nature*,  
 1514 332, 522-525.
- 1515 Lowe, D.C., Brenninkmeijer, C.A., Tyler, S.C. and Dlugokencky, E.J. (1991). Determination of  
 1516 the isotopic composition of atmospheric methane and its application in the Antarctic.  
 1517 *Journal of Geophysical Research: Atmospheres*, 96, 15455-15467.
- 1518 Lowe, D.C., Brenninkmeijer, C.A., Brailsford, G.W., Lassey, K.R., Gomez, A.J. and Nisbet, E.G.,  
 1519 (1994). Concentration and <sup>13</sup>C records of atmospheric methane in New Zealand and  
 1520 Antarctica: Evidence for changes in methane sources. *Journal of Geophysical Research:*  
 1521 *Atmospheres*, 99, 16913-16925.
- 1522 Ludemann, C.I., Gruere, A., Heffer, P. & Dobermann, A., (2022). Global data on fertilizer use  
 1523 by crop and by country. *Scientific data*, 9, pp.1-8.
- 1524 Lunt, M. F., Palmer, P. I., Feng, L., Taylor, C. M., Boesch, H., and Parker, R. J.(2019) An  
 1525 increase in methane emissions from tropical Africa between 2010 and 2016 inferred from  
 1526 satellite data, *Atmos. Chem. Phys.*, 19, 14721–14740.
- 1527 Lunt, M. F., Palmer, P. I., Lorente, A., Borsdorff, T., Landgraf, J., Parker, R. J., & Boesch, H.  
 1528 (2021). Rain-fed pulses of methane from East Africa during 2018–2019 contributed to  
 1529 atmospheric growth rate. *Environmental Research Letters*, 16, 024021.
- 1530 Łupikasza, E. B. & Cielecka-Nowak, K. (2020) Changing probabilities of days with snow and  
 1531 rain in the Atlantic sector of the Arctic under the current warming trend. *J. Clim.* 33, 2509–  
 1532 2532.
- 1533 McPhaden, M. J., Hasan, N., & Chikamoto, Y.(2023) Causes and Consequences of the  
 1534 Prolonged 2020-2023 La Niña , EGU General Assembly 2023, Vienna, Austria, 24–28 Apr  
 1535 2023, EGU23-10801, <https://doi.org/10.5194/egusphere-egu23-10801>, 2023.
- 1536 Matsumoto, K. (2007) Radiocarbon-based circulation age of the world oceans. *Journal of*  
 1537 *Geophysical Research: Oceans*, 112.
- 1538 Matthews, H.D. (2007) Implications of CO<sub>2</sub> fertilization for future climate change in a  
 1539 coupled climate–carbon model. *Global Change Biology*, 13, 1068-1078.
- 1540 Melton, J. R., Schaefer, H., & Whiticar, M. J. (2012). Enrichment in <sup>13</sup>C of atmospheric CH<sub>4</sub>  
 1541 during the Younger Dryas termination. *Climate of the Past*, 8, 1177-1197.
- 1542 Menoud, M., Van Der Veen, C., Lowry, D., Fernandez, J.M., Bakkaloglu, S., France, J.L.,  
 1543 Fisher, R.E., Maazallahi, H., Stanisavljević, M., Nečki, J. and Vinkovic, K. (2022) New  
 1544 contributions of measurements in Europe to the global inventory of the stable isotopic  
 1545 composition of methane. *Earth System Science Data*, 14, 4365-4386.
- 1546 Michel, S.E., Clark, J.R., Vaughn, B.H., Crotwell, M., Madronich, M., Moglia, E., Neff, D.,  
 1547 Mund, J. (2022), University of Colorado, Institute of Arctic and Alpine Research (INSTAAR).

- 1548 Stable Isotopic Composition of Atmospheric Methane (13C) from the NOAA GML Carbon  
 1549 Cycle Cooperative Global Air Sampling Network, 1998-2021. Version: 2022-12-  
 1550 15 <https://doi.org/10.15138/9p89-1x02>
- 1551 Mikaloff-Fletcher, S.E. and Schaefer, H. (2019). Rising methane: A new climate challenge.  
 1552 *Science*, 364, pp.932-933.
- 1553 Milkov, A.V., Schwietzke, S., Allen, G. *et al.* (2020) Using global isotopic data to constrain the  
 1554 role of shale gas production in recent increases in atmospheric methane. *Sci Rep* 10, 4199  
 1555 (2020). <https://doi.org/10.1038/s41598-020-61035-w>
- 1556 Mischler, J.A., Sowers, T.A., Alley, R.B., Battle, M., McConnell, J.R., Mitchell, L., Popp, T.,  
 1557 Sofen, E. and Spencer, M.K., (2009). Carbon and hydrogen isotopic composition of  
 1558 methane over the last 1000 years. *Global Biogeochemical Cycles*, 23.
- 1559 Möller, L., Sowers, T., Bock, M., Spahni, R., Behrens, M., Schmitt, J., Miller, H. and Fischer,  
 1560 H., 2013. Independent variations of CH<sub>4</sub> emissions and isotopic composition over the past  
 1561 160,000 years. *Nature Geoscience*, 6, 885-890.
- 1562 Moseley, G.E., Spötl, C., Cheng, H., Boch, R., Min, A. and Edwards, R.L. (2015) Termination-II  
 1563 interstadial/stadial climate change recorded in two stalagmites from the north European  
 1564 Alps. *Quaternary Science Reviews*, 127, 229-239.
- 1565 MOYA/ZWAMPS Team (2021) Nisbet, E.G., Allen, G., Fisher, R.E., France, J.L., Lee, J.D.,  
 1566 Lowry, D., Andrade, M.F., Bannan, T.J., Barker, P. and Bateson, P. (2021). Isotopic  
 1567 signatures of methane emissions from tropical fires, agriculture and wetlands: the MOYA  
 1568 and ZWAMPS flights. *Philosophical Transactions of the Royal Society A*, 380, p.20210112.
- 1569 Myhre, G., Shindell, D., Bréon, F.M., Collins, W., Fuglestedt, J., Huang, J., Koch, D.,  
 1570 Lamarque, J.F., Lee, D., Mendoza, B. and Nakajima, T. (2013). Climate change 2013: the  
 1571 physical science basis. Contribution of Working Group I to the Fifth Assessment Report of  
 1572 the Intergovernmental Panel on Climate Change. Anthropogenic and Natural Radiative  
 1573 Forcing. Cambridge, UK and New York, NY: Cambridge University Press.
- 1574 Nicely, J. M., Canty, T. P., Manyin, M., Oman, L. D., Salawitch, R. J., Steenrod, S. D., et al.  
 1575 (2018). Changes in global tropospheric OH expected as a result of climate change over the  
 1576 last several decades. *Journal of Geophysical Research: Atmospheres*, 123, 10,774–10,795.  
 1577 <https://doi.org/10.1029/2018JD028388>
- 1578 Nicholson, S.E., 2015. Long-term variability of the East African ‘short rains’ and its links to  
 1579 large-scale factors. *International Journal of Climatology*, 35(13), pp.3979-3990.
- 1580 Nicholson, S.E., Fink, A.H., Funk, C., Klotter, D.A. and Satheesh, A.R. (2022) Meteorological  
 1581 causes of the catastrophic rains of October/November 2019 in equatorial Africa. *Global  
 1582 and Planetary Change*, 208, 103687.
- 1583 Nisbet, E. G. (1990). The end of the ice age. *Canadian Journal of Earth Sciences*, 27, 148-157.
- 1584 Nisbet, E. G., & Chappellaz, J. (2009). Shifting gear, quickly. *Science*, 324, 477-478.
- 1585 Nisbet, E.G., Dlugokencky, E.J. and Bousquet, P. (2014) Methane on the rise—again. *Science*,  
 1586 343, 493-495.
- 1587 Nisbet, E.G., Dlugokencky, E.J., Manning, M.R., Lowry, D., Fisher, R.E., France, J.L., Michel,  
 1588 S.E., Miller, J.B., White, J.W.C., Vaughn, B. and Bousquet, P. (2016) Rising atmospheric  
 1589 methane: 2007–2014 growth and isotopic shift. *Global Biogeochemical Cycles*, 30,  
 1590 pp.1356-1370.
- 1591 Nisbet, E. G., Manning, M. R., Dlugokencky, E. J., Fisher, R. E., Lowry, D., Michel, S. E., ... &  
 1592 Brownlow, R. (2019). Very strong atmospheric methane growth in the 4 years 2014–2017:  
 1593 Implications for the Paris Agreement. *Global Biogeochemical Cycles*, 33, 318-342.

- 1594 Nisbet, E.G., Fisher, R.E., Lowry, D., France, J.L., Allen, G., Bakkaloglu, S., Broderick, T.J., Cain,  
 1595 M., Coleman, M., Fernandez, J. and Forster, G. (2020) Methane mitigation: methods to  
 1596 reduce emissions, on the path to the Paris agreement. *Reviews of Geophysics*, *58*,  
 1597 p.e2019RG000675.
- 1598 Nisbet E.G., Dlugokencky E.J., Fisher R.E., France J.L., Lowry D., Manning M.R., Michel S.E., &  
 1599 Warwick N.J. (2021) Atmospheric methane and nitrous oxide: challenges along the path to  
 1600 Net Zero. *Phil. Trans. R. Soc. A* **379**:20200457.
- 1601 Nisbet, E.G. (2022) Methane's unknowns better known. *Nature Geoscience*, *15*, 861-862.
- 1602 Nisbet, E.G. (2023 in press) Climate change feedback on methane emissions from global  
 1603 wetlands. *Nature Climate Change*.
- 1604 NOAA (2023a) [https://gml.noaa.gov/webdata/ccgg/trends/ch4/ch4\\_annmean\\_gl.txt](https://gml.noaa.gov/webdata/ccgg/trends/ch4/ch4_annmean_gl.txt)
- 1605 NOAA (2023b) <https://www.cpc.ncep.noaa.gov/data/indices/soi>
- 1606 Oh, Y., Zhuang, Q., Welp, L.R., Liu, L., Lan, X., Basu, S., Dlugokencky, E.J., Bruhwiler, L., Miller,  
 1607 J.B., Michel, S.E. and Schwietzke, S. (2022). Improved global wetland carbon isotopic  
 1608 signatures support post-2006 microbial methane emission increase. *Communications Earth*  
 1609 *& Environment*, *3*, 159, 1-12.
- 1610 Osland, M.J., Stevens, P.W., Lamont, M.M., Brusca, R.C., Hart, K.M., Waddle, J.H., Langtimm,  
 1611 C.A., Williams, C.M., Keim, B.D., Terando, A.J. and Reyier, E.A., 2021. Tropicalization of  
 1612 temperate ecosystems in North America: The northward range expansion of tropical  
 1613 organisms in response to warming winter temperatures. *Global Change Biology*, *27*(13),  
 1614 pp.3009-3034.
- 1615 Palmer PI, Wainwright CM, Dong B, Maidment RI, Wheeler KG, Gedney N, Hickman JE,  
 1616 Madani N, Folwell SS, Abdo G, Allan RP. (2023). Drivers and impacts of Eastern African  
 1617 rainfall variability. *Nature Reviews Earth & Environment*. *4*, 254–270  
 1618 <https://doi.org/10.1038/s43017-023-00397-x>
- 1619 Pandey, S., Houweling, S., Krol, M., Aben, I., Monteil, G., Nechita-Banda, N., Dlugokencky,  
 1620 E.J., Detmers, R., Hasekamp, O., Xu, X. and Riley, W.J. (2017) Enhanced methane emissions  
 1621 from tropical wetlands during the 2011 La Niña. *Scientific reports*, *7*, 1-8.
- 1622 Pandey, S., Houweling, S., Krol, M., Aben, I., Nechita-Banda, N., Thoning, K., Röckmann, T.,  
 1623 Yin, Y., Segers, A. and Dlugokencky, E.J. (2019) Influence of atmospheric transport on  
 1624 estimates of variability in the global methane burden. *Geophysical Research Letters*, *46*,  
 1625 2302-2311.
- 1626 Peng, S., Lin, X., Thompson, R.L., Xi, Y., Liu, G., Hauglustaine, D., Lan, X., Poulter, B.,  
 1627 Ramonet, M., Saunois, M., Yin, Y., Zhang, Z., Zheng, B., and Ciais, P. (2022). Wetland  
 1628 emission and atmospheric sink changes explain methane growth in 2020. *Nature*, *612*,  
 1629 477-482.
- 1630 Prather MJ, Holmes CD, Hsu J. 2012 Reactive greenhouse gas scenarios: systematic  
 1631 exploration of uncertainties and the role of atmospheric chemistry. *Geophys. Res. Lett.* *39*,  
 1632 L09803.
- 1633 Previdi, M., Smith, K.L. and Polvani, L.M. (2021) Arctic amplification of climate change: a  
 1634 review of underlying mechanisms. *Environmental Research Letters*, *16*, 093003.
- 1635 Qu, Z., Jacob, D.J., Zhang, Y., Shen, L., Varon, D.J., Lu, X., Scarpelli, T., Bloom, A., Worden, J.  
 1636 and Parker, R.J. (2022) Attribution of the 2020 surge in atmospheric methane by inverse  
 1637 analysis of GOSAT observations. *Environmental Research Letters*, *17*, 094003.
- 1638 Quay, P.D., King, S.L., Lansdown, J.M. and Wilbur, D.O. (1988) Isotopic composition of  
 1639 methane released from wetlands: implications for the increase in atmospheric methane.  
 1640 *Global Biogeochemical Cycles*, *2*, 385-397.

- 1641 Quay, P.D., King, S.L., Stutsman, J., Wilbur, D.O., Steele, L.P., Fung, I., Gammon, R.H., Brown,  
 1642 T.A., Farwell, G.W., Grootes, P.M., and Schmidt, F.H. (1991) Carbon isotopic composition of  
 1643 atmospheric CH<sub>4</sub>: fossil and biomass burning source strengths. *Global Biogeochem. Cycles*,  
 1644 5, 25-47.
- 1645 Raymo, M.E., (1997) The timing of major climate terminations. *Paleoceanography*, 12, 577-  
 1646 585.
- 1647 Rhodes, R.H., Brook, E.J., Chiang, J.C., Blunier, T., Maselli, O.J., McConnell, J.R., Romanini, D.  
 1648 and Severinghaus, J.P. (2015) Enhanced tropical methane production in response to  
 1649 iceberg discharge in the North Atlantic. *Science*, 348, 1016-1019.
- 1650 Riddell-Young, B., Rosen, J., Brook, E., Buizert, C., Martin, K., Lee, J., Edwards, J., Mühl, M.,  
 1651 Schmitt, J., Fischer, H., and Blunier, T. (2023 submitted) Tropical sources dominated  
 1652 methane changes of the last glacial maximum and deglaciation.  
 1653 <https://doi.org/10.21203/rs.3.rs-2522042/v1>
- 1654 Ringeval, B., Houweling, S., Van Bodegom, P.M., Spahni, R., Van Beek, R., Joos, F. and  
 1655 Röckmann, T. (2014). Methane emissions from floodplains in the Amazon Basin: challenges  
 1656 in developing a process-based model for global applications. *Biogeosciences*, 11, pp.1519-  
 1657 1558.
- 1658 Rosentreter, J.A., Borges, A.V., Deemer, B.R., Holgerson, M.A., Liu, S., Song, C., Melack, J.,  
 1659 Raymond, P.A., Duarte, C.M., Allen, G.H., Olefeldt, D., et al. (2021) Half of global methane  
 1660 emissions come from highly variable aquatic ecosystem sources. *Nature Geoscience*, 14,  
 1661 225-230.
- 1662 Rubino, M., Etheridge, D. M., Thornton, D. P., Howden, R., Allison, C. E., Francey, R. J.,  
 1663 Langenfelds, R. L., Steele, L. P., Trudinger, C. M., Spencer, D. A., Curran, M. A. J., van  
 1664 Ommen, T. D., and Smith, A. M. (2019) Revised records of atmospheric trace gases CO<sub>2</sub>,  
 1665 CH<sub>4</sub>, N<sub>2</sub>O, and  $\delta^{13}\text{C-CO}_2$  over the last 2000 years from Law Dome, Antarctica, *Earth Syst.*  
 1666 *Sci. Data*, 11, 473–492, <https://doi.org/10.5194/essd-11-473-2019>.
- 1667 Sapart, C.J., Monteil, G., Prokopiou, M., van de Wal, R.S., Kaplan, J.O., Sperlich, P.,  
 1668 Krumhardt, K.M., Van der Veen, C., Houweling, S., Krol, M.C. and Blunier, T. (2012) Natural  
 1669 and anthropogenic variations in methane sources during the past two millennia. *Nature*,  
 1670 490, 85-88.
- 1671 Saunio, M., Stavert, A.R., Poulter, B., Bousquet, P., Canadell, J.G., Jackson, R.B., Raymond,  
 1672 P.A., Dlugokencky, E.J., Houweling, S., Patra, P.K. and Ciais, P. (2020) The global methane  
 1673 budget 2000–2017. *Earth System Science Data*, 12, 1561-1623.
- 1674 Schaefer, H., Whiticar, M.J., Brook, E.J., Petrenko, V.V., Ferretti, D.F. and Severinghaus, J.P.  
 1675 (2006) Ice record of  $\delta^{13}\text{C}$  for atmospheric CH<sub>4</sub> across the Younger Dryas-Preboreal  
 1676 transition. *Science*, 313, 1109-1112.
- 1677 Schaefer, H., Fletcher, S.E.M., Veidt, C., Lassey, K.R., Brailsford, G.W., Bromley, T.M.,  
 1678 Dlugokencky, E.J., Michel, S.E., Miller, J.B., Levin, I. and Lowe, D.C. (2016) A 21st-century  
 1679 shift from fossil-fuel to biogenic methane emissions indicated by <sup>13</sup>CH<sub>4</sub>. *Science*, 352, 80-  
 1680 84.
- 1681 Schmitt, J., Schneider, R., Elsig, J., Leuenberger, D., Lourantou, A., Chappellaz, J., Köhler, P.,  
 1682 Joos, F., Stocker, T.F., Leuenberger, M. and Fischer, H., (2012). Carbon isotope constraints  
 1683 on the deglacial CO<sub>2</sub> rise from ice cores. *Science*, 336, 711-714.
- 1684 Sharmila, S. and Walsh, K.J.E., 2018. Recent poleward shift of tropical cyclone formation  
 1685 linked to Hadley cell expansion. *Nature Climate Change*, 8(8), pp.730-736.
- 1686 Severinghaus, J. P., & Brook, E. J. (1999). Abrupt climate change at the end of the last glacial  
 1687 period inferred from trapped air in polar ice. *science*, 286, 930-934.

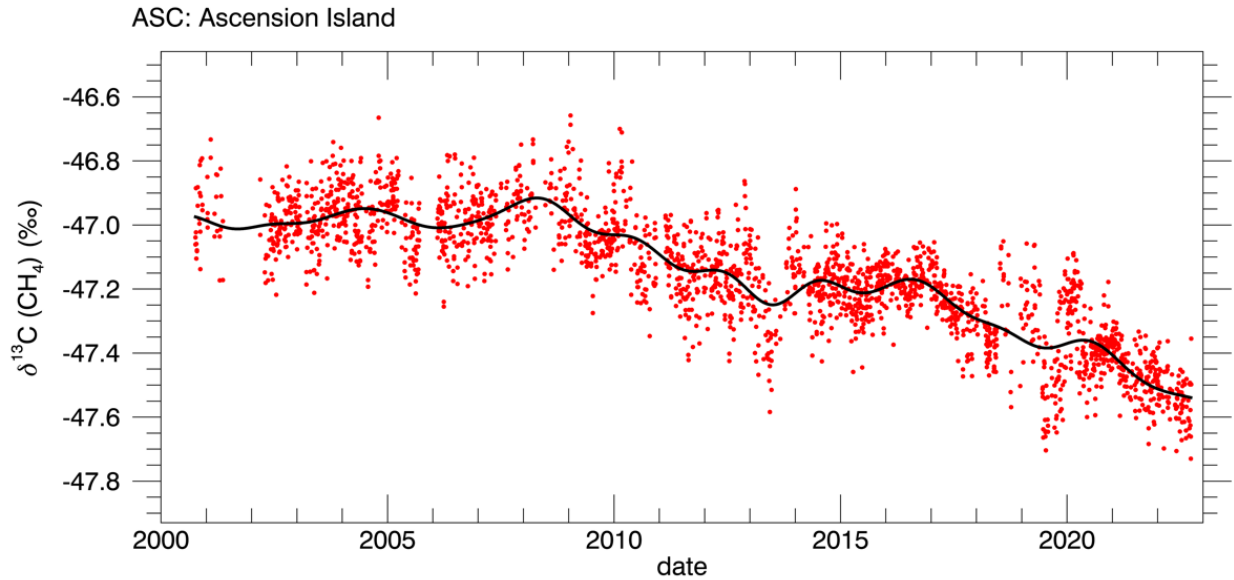
- 1688 Severinghaus, J. P., Sowers, T., Brook, E. J., Alley, R. B., & Bender, M. L. (1998). Timing of  
 1689 abrupt climate change at the end of the Younger Dryas interval from thermally  
 1690 fractionated gases in polar ice. *Nature*, *391*, 141-146.
- 1691 Shaw, J.T., Allen, G., Barker, P., Pitt, J.R., Pasternak, D., Bauguitte, S.J.B., Lee, J., Bower, K.N.,  
 1692 Daly, M.C., Lunt, M.F. & Ganesan, A.L. (2022). Large Methane Emission Fluxes Observed  
 1693 from Tropical Wetlands in Zambia. *Global Biogeochemical Cycles*, *36*, p.e2021GB007261.
- 1694 Sherwood, O. A., Schwietzke, S., Arling, V. A., & Etiope, G. (2017, 2021). Global inventory of  
 1695 gas geochemistry data from fossil fuel, microbial and burning sources,. *Earth System*  
 1696 *Science Data*, *9*, 639-656. version 2021 <https://gml.noaa.gov/ccgg/arc/?id=13>
- 1697 Spahni, R., Chappellaz, J., Stocker, T.F., Loulergue, L., Hausammann, G., Kawamura, K.,  
 1698 Fluckiger, J., Schwander, J., Raynaud, D., Masson-Delmotte, V. and Jouzel, J. (2005).  
 1699 Atmospheric methane and nitrous oxide of the late Pleistocene from Antarctic ice cores.  
 1700 *Science*, *310*(5752), pp.1317-1321.
- 1701 Spivakovsky, C. M., Logan, J. A., Montzka, S. A., Balkanski, Y. J., Foreman-Fowler, M., Jones,  
 1702 D. B. A., et al. (2000). Three dimensional climatological distribution of tropospheric OH:  
 1703 Update and evaluation. *Journal of Geophysical Research*, *105*(D7), 8931–8980. <https://doi.org/10.1029/1999JD901006>
- 1705 Staniaszek, Z., Griffiths, P. T., Folberth, G. A., O'Connor Fiona, M., Luke, A. N., & Archibald, A.  
 1706 T. (2022). The role of future anthropogenic methane emissions in air quality and climate.  
 1707 *NPJ Climate and Atmospheric Science*, *5*(1).
- 1708 Staten, P.W., Grise, K.M., Davis, S.M., Karnauskas, K.B., Waugh, D.W., Maycock, A.C., Fu, Q.,  
 1709 Cook, K., Adam, O., Simpson, I.R. & Allen, R.J., (2020) Tropical widening: From global  
 1710 variations to regional impacts. *Bulletin of the American Meteorological Society*, *101*, E897-  
 1711 E904.
- 1712 Steele, L.P., Dlugokencky, E.J., Lang, P.M., Tans, P.P., Martin, R.C. and Masarie, K.A. (1992).  
 1713 Slowing down of the global accumulation of atmospheric methane during the 1980s.  
 1714 *Nature*, *358*, 313-316.
- 1715 Strode SA, Wang JS, Manyin M, Duncan B, Hossaini R, Keller CA, Michel SE, & White JW  
 1716 (2020). Strong sensitivity of the isotopic composition of methane to the plausible range of  
 1717 tropospheric chlorine. *Atmospheric Chemistry and Physics*. *20*, 8405-19.
- 1718 Studholme, J., Fedorov, A.V., Gulev, S.K., Emanuel, K. & Hodges, K. (2022). Poleward  
 1719 expansion of tropical cyclone latitudes in warming climates. *Nature Geoscience*, *15*(1),  
 1720 pp.14-28.
- 1721 Sun, S., Fang, Y., Zu, Y., Liu, L. & Li, K. (2022) Increased occurrences of early Indian Ocean  
 1722 Dipole under global warming. *Science Advances*, *8*, p.eadd6025.
- 1723 Tans, P. P. (1997). A note on isotopic ratios and the global atmospheric methane budget.  
 1724 *Global Biogeochemical Cycles*, *11*, 77-81.
- 1725 Taylor, R.D. & Walker, B.H. (1978) Comparisons of Vegetation Use and Herbivore Biomass  
 1726 on a Rhodesian Game and Cattle Ranch. *Journal of Applied Ecology* , *15*, 565-581,  
 1727 <https://www.jstor.org/stable/2402611>
- 1728 Thanwerdas, J., Saunois, M., Berchet, A., Pison, I., Vaughn, B.H., Michel, S.E. & Bousquet, P.  
 1729 (2022). Variational inverse modeling within the Community Inversion Framework v1. 1 to  
 1730 assimilate  $\delta^{13}\text{C}$  (CH<sub>4</sub>) and CH<sub>4</sub>: a case study with model LMDz-SACS. *Geoscientific Model*  
 1731 *Development*, *15*, 4831-4851.
- 1732 Thompson, R. L., Nisbet, E. G., Pisso, I., Stohl, A., Blake, D., Dlugokencky, E. J., Helmig, D.,  
 1733 and White, J. W. C. (2018) Variability in Atmospheric Methane From Fossil Fuel and

- 1734 Microbial Sources Over the Last Three Decades, *Geophys. Res. Lett.*, 45, 11499– 11508,  
 1735 <https://doi.org/10.1029/2018GL078127>.
- 1736 Tzedakis, P.C., Raynaud, D., McManus, J.F., Berger, A., Brovkin, V. & Kiefer, T. (2009)  
 1737 Interglacial diversity. *Nature Geoscience*, 2, 751-755.
- 1738 Uddin S, Löw M, Parvin S, Fitzgerald GJ, Tausz-Posch S, Armstrong R, et al. (2018) Elevated  
 1739 CO<sub>2</sub> mitigates the effect of surface drought by stimulating root growth to access sub-soil  
 1740 water. *PLoS ONE* 13, e0198928. <https://doi.org/10.1371/journal.pone.0198928>
- 1741 Umezawa, T., Brenninkmeijer, C. A., Röckmann, T., Van Der Veen, C., Tyler, S. C., Fujita, R., ...  
 1742 & Levin, I. (2018). Interlaboratory comparison of  $\delta^{13}\text{C}$  and  $\delta\text{D}$  measurements of  
 1743 atmospheric CH<sub>4</sub> for combined use of data sets from different laboratories. *Atmospheric*  
 1744 *Measurement Techniques*, 11, 1207-1231.
- 1745 Voigt, A., Albern, N., Ceppi, P., Grise, K., Li, Y. & Medeiros, B. (2021) Clouds, radiation, and  
 1746 atmospheric circulation in the present-day climate and under climate change. *Wiley*  
 1747 *Interdisciplinary Reviews: Climate Change*, 12, e694.
- 1748 von Schuckmann, K., Minière, A., Gues, F., Cuesta-Valero, F. J., Kirchengast, G., Adusumilli,  
 1749 S., Straneo, F., Ablain, M., Allan, R. P., Barker, P. M., Beltrami, H., Blazquez, A., Boyer, T.,  
 1750 Cheng, L., Church, J., Desbruyeres, D., Dolman, H., Domingues, C. M., García-García, A.,  
 1751 Giglio, D., Gilson, J. E., Gorfer, M., Haimberger, L., Hakuba, M. Z., Hendricks, S., Hosoda, S.,  
 1752 Johnson, G. C., Killick, R., King, B., Kolodziejczyk, N., Korosov, A., Krinner, G., Kuusela, M.,  
 1753 Landerer, F. W., Langer, M., Lavergne, T., Lawrence, I., Li, Y., Lyman, J., Marti, F., Marzeion,  
 1754 B., Mayer, M., MacDougall, A. H., McDougall, T., Monselesan, D. P., Nitzbon, J., Ootosaka, I.,  
 1755 Peng, J., Purkey, S., Roemmich, D., Sato, K., Sato, K., Savita, A., Schweiger, A., Shepherd, A.,  
 1756 Seneviratne, S. I., Simons, L., Slater, D. A., Slater, T., Steiner, A. K., Suga, T., Szekely, T.,  
 1757 Thiery, W., Timmermans, M.-L., Vanderkelen, I., Wjiffels, S. E., Wu, T., and Zemp, M. (2023)  
 1758 Heat stored in the Earth system 1960–2020: where does the energy go?, *Earth Syst. Sci.*  
 1759 *Data*, 15, 1675–1709, <https://doi.org/10.5194/essd-15-1675-2023>.
- 1760 Wanner, H., Beer, J., Bütikofer, J., Crowley, T.J., Cubasch, U., Flückiger, J., Goosse, H. et al.  
 1761 (2008) Mid-to Late Holocene climate change: an overview. *Quaternary Science Reviews* 27,  
 1762 1791-1828.
- 1763 Wang, B., Luo, X., Yang, Y.M., Sun, W., Cane, M.A., Cai, W., Yeh, S.W. & Liu, J. (2019)  
 1764 Historical change of El Niño properties sheds light on future changes of extreme El Niño.  
 1765 *Proceedings of the National Academy of Sciences*, 116, 22512-22517.
- 1766 Wang, P., Huang, Q., Liu, S., Cai, H., Yu, J., Wang, T., Chen, X. & Pozdniakov, S.P., (2022).  
 1767 Recent regional warming across the Siberian lowlands: a comparison between permafrost  
 1768 and non-permafrost areas. *Environmental Research Letters*, 17, 054047.
- 1769 Wang, S., Zhang, Y., Ju, W., Chen, J.M., Ciais, P., Cescatti, A., Sardans, J., Janssens, I.A., Wu,  
 1770 M., Berry, J.A. & Campbell, E., (2020). Recent global decline of CO<sub>2</sub> fertilization effects on  
 1771 vegetation photosynthesis. *Science*, 370, 1295-1300.
- 1772 Wen, X., Unger, V., Jurasinski, G., Koebisch, F., Horn, F., Rehder, G., Sachs, T., Zak, D.,  
 1773 Lischeid, G., Knorr, K.-H., Böttcher, M.E., Winkel, M., Bodelier, P.L.E., and Liebner, S. (2018)  
 1774 Predominance of methanogens over methanotrophs in rewetted fens characterized by  
 1775 high methane emissions. *Biogeosciences*, 15, 6519-6536.
- 1776 Wolff, E.W., Fischer, H. and Röthlisberger, R. (2009) Glacial terminations as southern  
 1777 warmings without northern control. *Nature Geoscience*, 2, 206-209.
- 1778 Wolff, E. W., Chappellaz, J., Blunier, T., Rasmussen, S. O., & Svensson, A. (2010). Millennial-  
 1779 scale variability during the last glacial: The ice core record. *Quaternary Science Reviews*, 29,  
 1780 2828-2838.

- 1781 WMO (2023) WMO Global Annual to Decadal Climate Update (see Appendix)  
1782 [https://hadleyserver.metoffice.gov.uk/wmolc/WMO\\_GADCU\\_2023-2027.pdf](https://hadleyserver.metoffice.gov.uk/wmolc/WMO_GADCU_2023-2027.pdf)
- 1783 Worden, J.R., Bloom, A.A., Pandey, S., Jiang, Z., Worden, H.M., Walker, T.W., Houweling, S.  
1784 and Röckmann, T. (2017) Reduced biomass burning emissions reconcile conflicting  
1785 estimates of the post-2006 atmospheric methane budget. *Nature communications*, *8*,  
1786 2227.
- 1787 Worden, J., Pandey, S., Zhang, Y., Cusworth, D., Zhen, Q., Bloom, A., Ma, S., Maasackers, B.,  
1788 Byrne, B., Duren, R., Crisp, D., Gordon, D., and Jacob, D. (2023) A Bayesian Framework for  
1789 Verifying Methane Inventories and Trends With Atmospheric Methane Data, EGU General  
1790 Assembly 2023, Vienna, Austria, 24–28 Apr 2023, EGU23-17172,  
1791 <https://doi.org/10.5194/egusphere-egu23-17172>.
- 1792 Yin, Y., Chevallier, F., Ciais, P., Bousquet, P., Saunoy, M., Zheng, B., Worden, J., Bloom, A. A.,  
1793 Parker, R. J., Jacob, D. J., Dlugokencky, E. J., and Frankenberg, C. (2021) Accelerating  
1794 methane growth rate from 2010 to 2017: leading contributions from the tropics and East  
1795 Asia, *Atmos. Chem. Phys.*, *21*, 12631–12647, <https://doi.org/10.5194/acp-21-12631-2021>.
- 1796 Zhang, L., Tian, H., Shi, H., Pan, S., Chang, J., Dangal, S.R., Qin, X., Wang, S., Tubiello, F.N.,  
1797 Canadell, J.G. and Jackson, R.B. (2022) A 130-year global inventory of methane emissions  
1798 from livestock: Trends, patterns, and drivers. *Global Change Biology*, *28*, 5142-5158.
- 1799 Zhang, Z., Poulter, B., Knox, S., Stavert, A., McNicol, G., Fluet-Chouinard, E., Feinberg, A.,  
1800 Zhao, Y., Bousquet, P., Canadell, J. G., Ganesan, A., Hugelius, G., Hurtt, G., Jackson, R. B.,  
1801 Patra, P. K., Saunoy, M., Höglund-Isaksson, L., Huang, C., Chatterjee, A., and Li, X. (2021)  
1802 Anthropogenic Emission Is the Main Contributor to the Rise of Atmospheric Methane  
1803 during 1993–2017, *Nat. Sci. Rev.*, *9*, nwab200, <https://doi.org/10.1093/nsr/nwab200>.
- 1804 Zhang Z, Poulter B, Feldman AF, Ying Q, Ciais P, Peng S, Li X. Recent intensification of  
1805 wetland methane feedback. (2023) *Nature Climate Change*. **13**, 430–433
- 1806 Zhao, Y., Saunoy, M., Bousquet, P., Lin, X., Berchet, A., Hegglin, M.I., Canadell, J.G., Jackson,  
1807 R.B., Deushi, M., Jöckel, P. and Kinnison, D. (2020). On the role of trend and variability in  
1808 the hydroxyl radical (OH) in the global methane budget. *Atmospheric Chemistry and*  
1809 *Physics*, *20*, 13011-13022

1810 **Supplementary information**

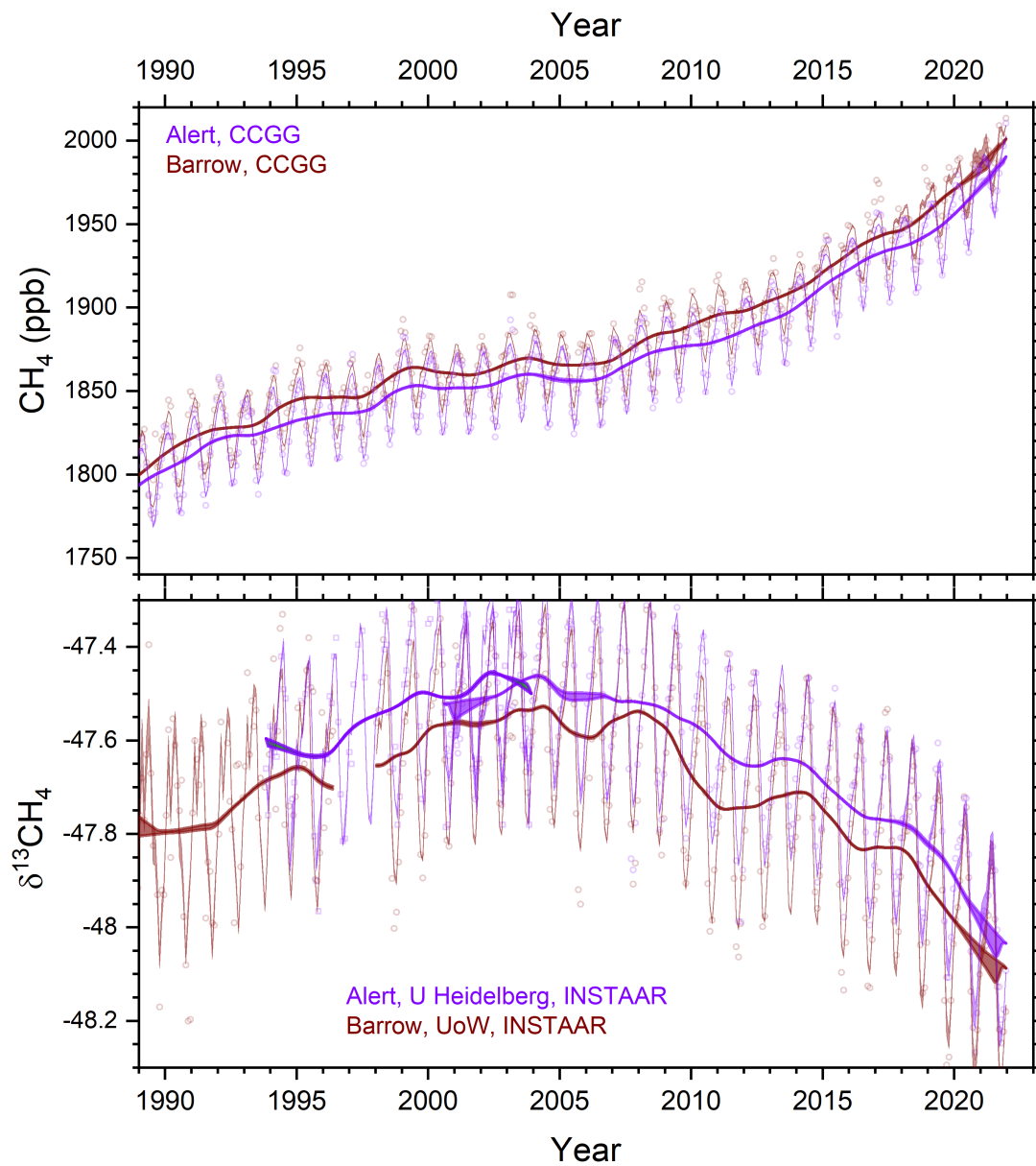
1811 *Figure SI 1. NOAA  $\delta^{13}\text{C}_{\text{CH}_4}$  record 2007-2022 from Ascension Island (8°S in the equatorial*  
1812 *zone). Note variability range of short-term weather changes and sustained negative shift.*  
1813 *Ascension Island is the key monitoring station representing the southern hemisphere Atlantic*  
1814 *tropical and trade wind zones.*



1815

1816

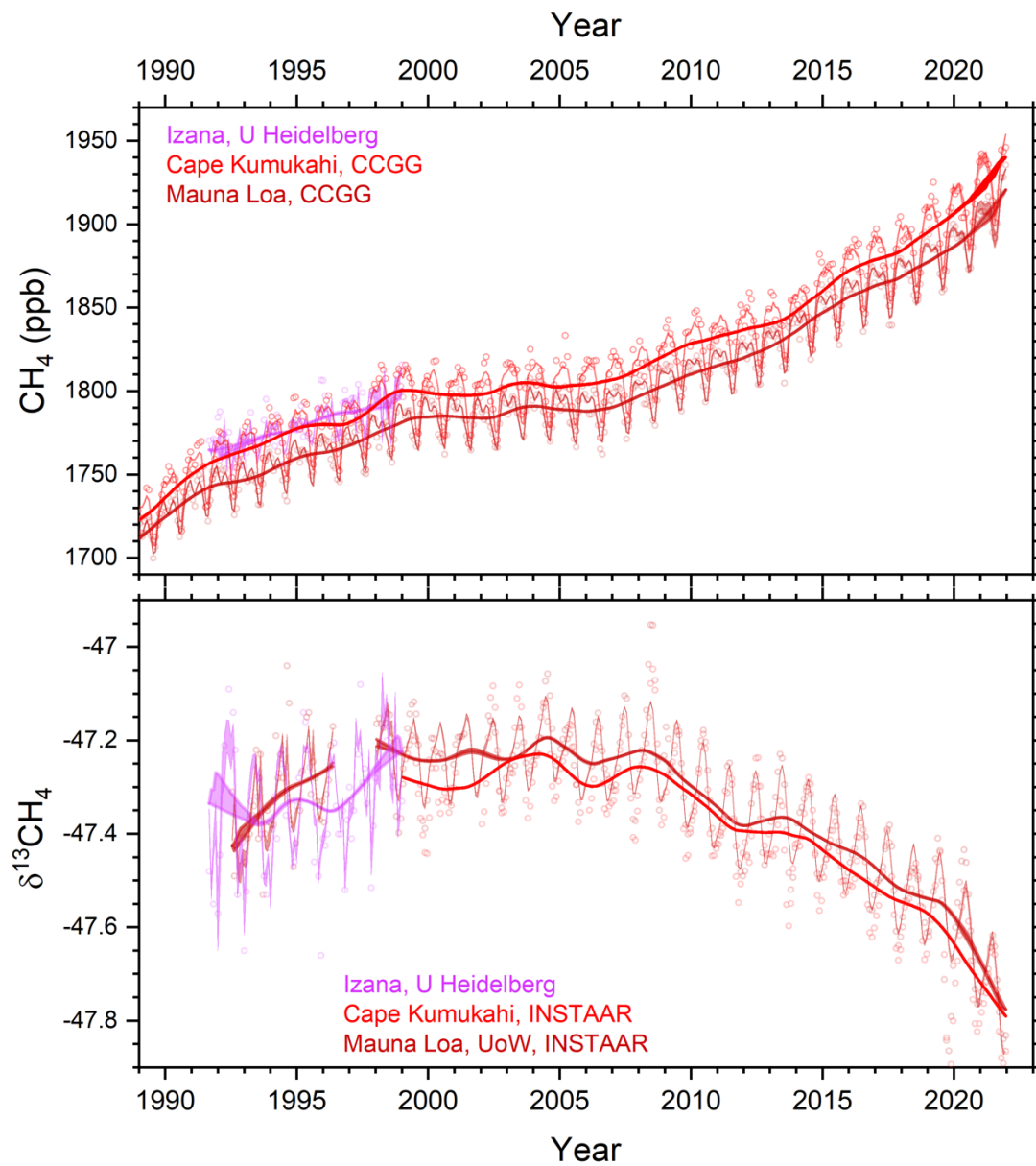
1817 *Figure SI 2 . Polar record for  $\text{CH}_4$  and  $\delta^{13}\text{C}_{\text{CH}_4}$ , Alert and Barrow. NOAA data. See Fig. 4*  
1818 *caption in main text.*



1819

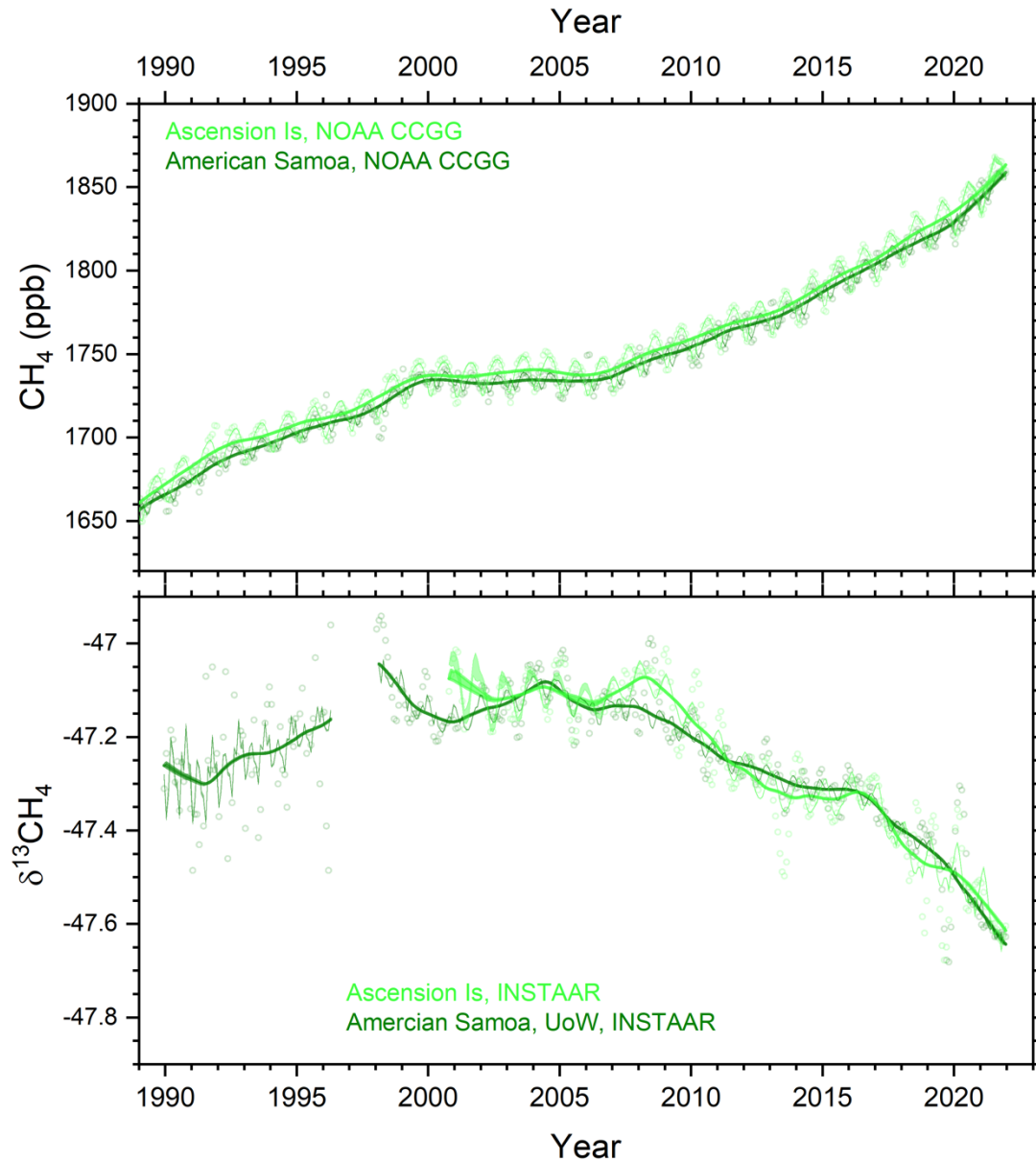
1820

1821 *Figure SI 3 Northern mid-latitude record for CH<sub>4</sub> and  $\delta^{13}\text{C}_{\text{CH}_4}$ . Data from World Data Center*  
1822 *for Greenhouse gases and NOAA (see Fig. 4 caption in main text).*



1823

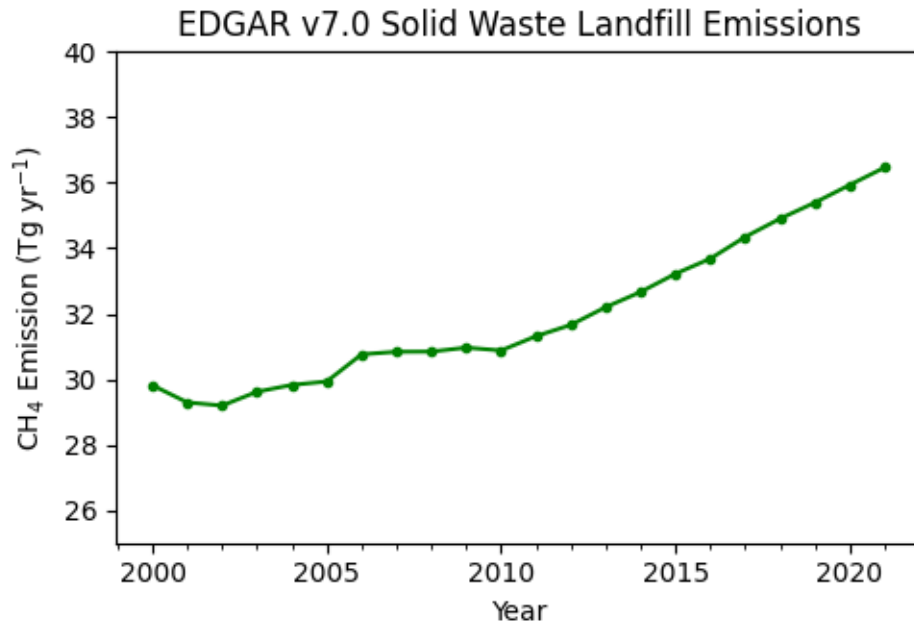
1824 *Figure SI 4. Equatorial record for CH<sub>4</sub> and  $\delta^{13}C_{CH_4}$ , Ascension and American Samoa. NOAA*  
1825 *data. See Fig. 4 caption in main text.*



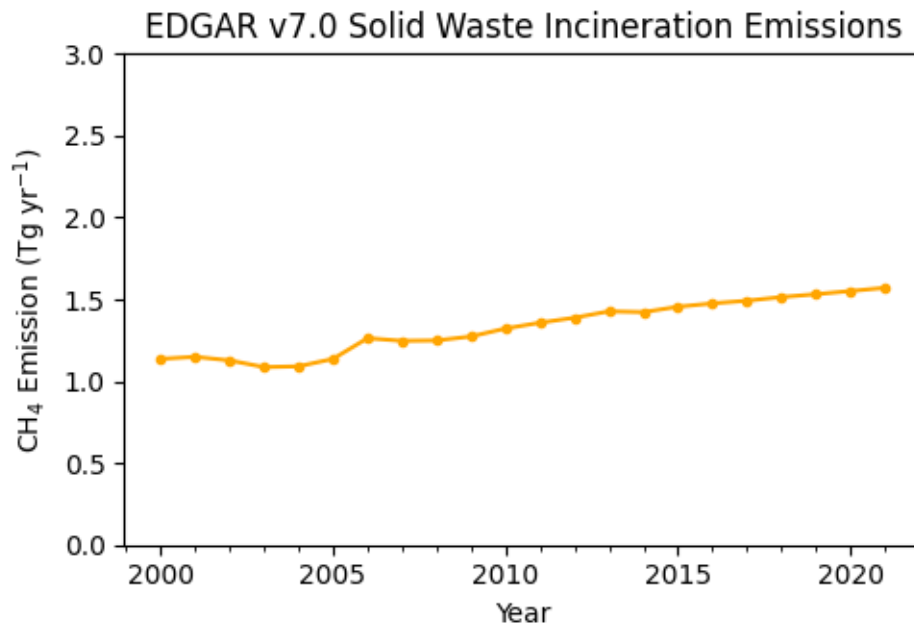
1826 *SI 5 EDGAR v. 7.0 (Emissions Database for Global Atmospheric Research) estimates of*  
1827 *growth in emissions from a) solid waste and landfill; b) solid waste incineration; c) Manure*  
1828 *management; d) Waste water; e) Ricefields.*

1830 *From EDGAR (2023). [https://edgar.jrc.ec.europa.eu/dataset\\_ghg70](https://edgar.jrc.ec.europa.eu/dataset_ghg70)*

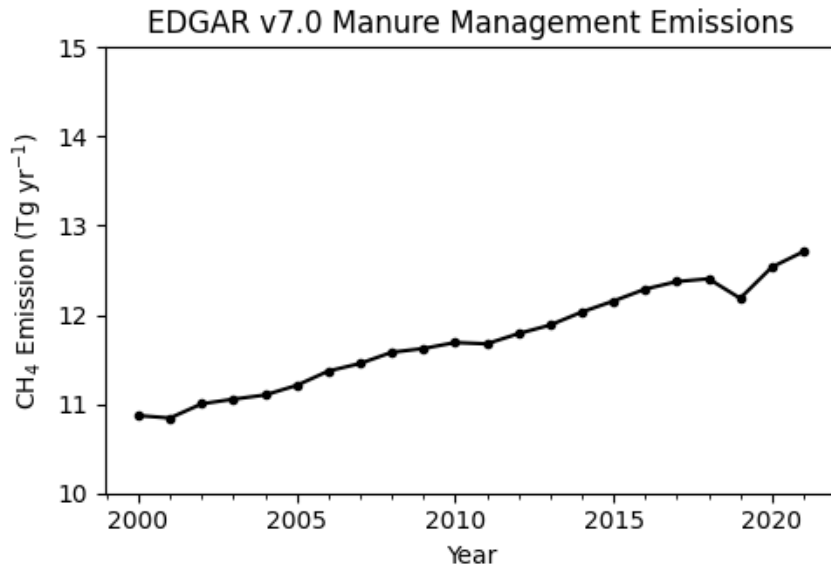
1831



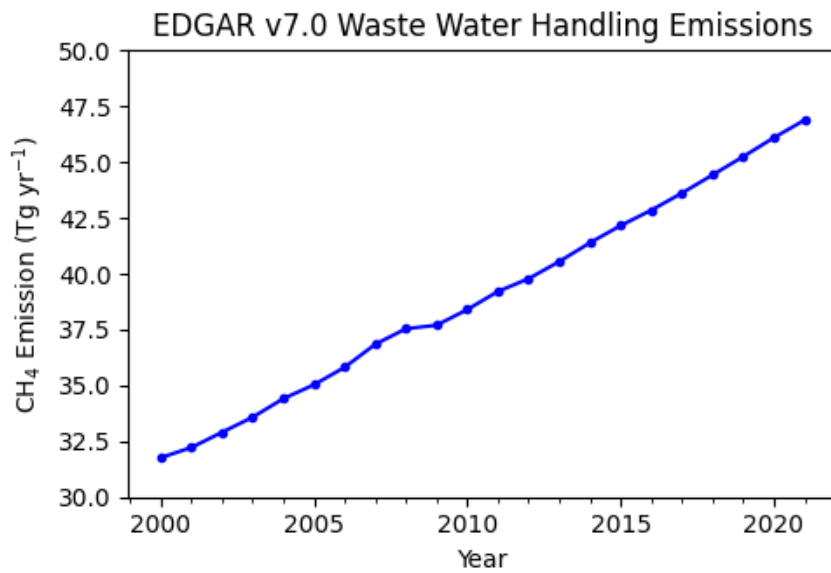
1832



1833



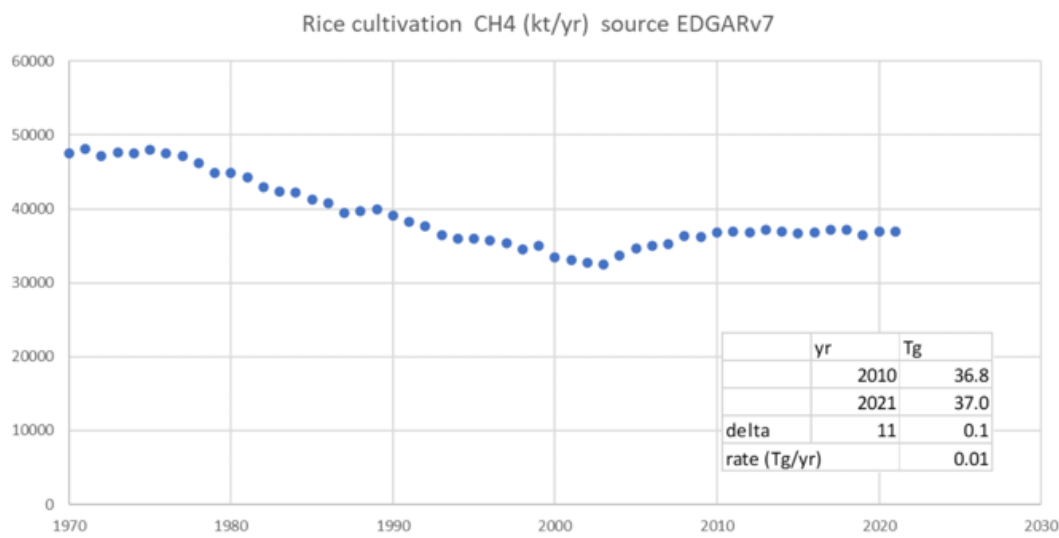
1834



1835

1836

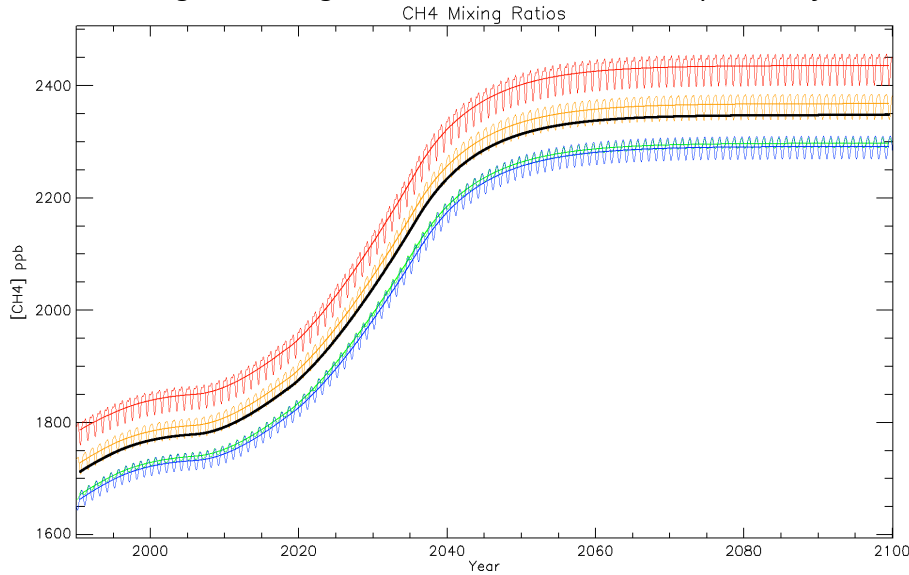
*Fig. SI.5e Methane from rice cultivation: minimal recent (2010-2021) growth rate.*



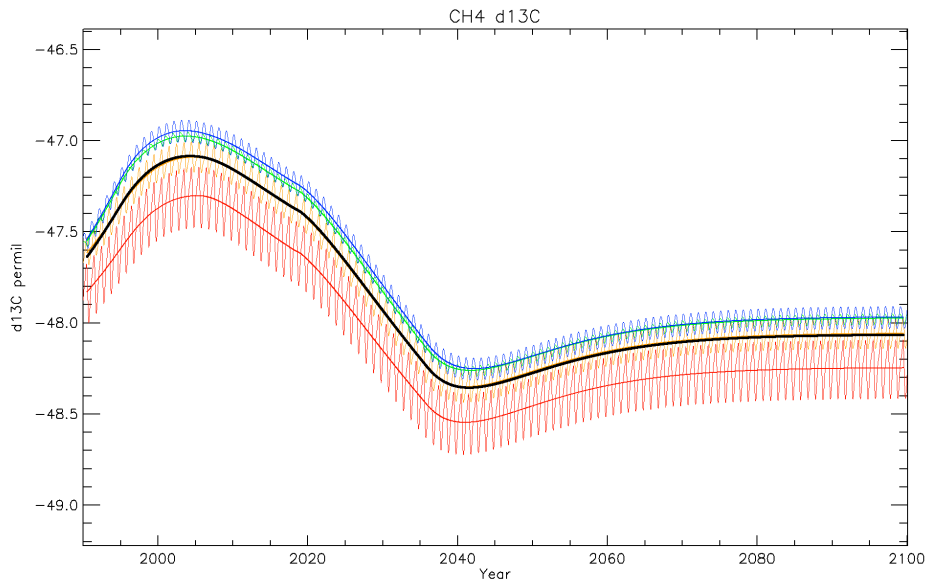
1837

1838

1839 *Fig SI 6. CH<sub>4</sub> mole fraction values in ppb from the 4-box running budget model for sources*  
 1840 *that fit measured values to 2017 and then give 10 ppb/yr growth until 2035. Orange is 0-*  
 1841 *30°N. Black is the global average and overlays the 30-90°N case. Blue is 30-90°S and green 0-*  
 1842 *30°S. Jump in emissions takes place in 2007; equilibration is mostly complete by 2045. Note*  
 1843 *that CH<sub>4</sub> mixing ratio is higher in the 0-30°N semihemisphere before and after this transition.*



1844 *Fig SI 7.  $\delta^{13}C_{CH_4}$  (‰) in the 4 semi-hemispheres for the inputs and colours shown in Fig SI2.*



1845

1846

1847 **Main Text Figures 4 and 5**

1848 Changes in CH<sub>4</sub> mole fraction and  $\delta^{13}C$  have been taken from ten sites and data from the  
 1849 World Data Center for Greenhouse Gases (<https://gaw.kishou.go.jp/>), NOAA, INSTAAR,  
 1850 NIWA, University of Washington and University of Heidelberg (IZO from Levin et al., (2012)).  
 1851 Changing trends in the data have used the Cleveland *et al* STL (Seasonal Trend Loess)  
 1852 method with monthly data for each site. This approach has been extended to deal with  
 1853 missing monthly data values by optimising these to produce a smooth STL fit. Periods where  
 1854 the number of months is not a multiple of 12 are dealt with by merging a series of STL fits

1855 that cover sub-periods that are a multiple of 12 months and retaining the full range of these  
1856 partial fits across common months. The result is a spread in trends at the begin and end of  
1857 the data series and around regions where there are significant groups of missing data.

1858 The same colour code is used in the following plots as in Figure 4 of the main text.

1859 The  $\delta^{13}\text{C}$  values shown have used the recent intercomparison of  $\delta^{13}\text{C}_{\text{CH}_4}$  (Umezawa et al,  
1860 2018) to adjust reported values and make them all consistent with the reference level used  
1861 in that paper. Notably, the degree of agreement between different organisations that is  
1862 shown here demonstrates the great and continuing value of that painstaking study by  
1863 Umezawa *et al.* (2018).

1864

1865

1866